# RHEOLOGY AND PHASE SEPARATION OF POLY(STYRENE-CO-MALEIC ANHYDRIDE)/POLY(METHYL METHACRYLATE) BLENDS

by

DIVYA CHOPRA

B.Tech Chemical Technology (Plastics), Harcourt Butler Technological Institute, 1995

A THESIS SUBMITTED IN PARTIAL FULFILLMENT OF THE REQUIREMENTS FOR THE DEGREE OF MASTER OF APPLIED SCIENCE

In

The Faculty of Graduate Studies
Department of Chemical Engineering

*We accept this thesis as conforming to the required standard*

THE UNIVERSITY OF BRITISH COLUMBIA
June 1998

Department of CHEMICAL ENGINEERING

The University of British Columbia
Vancouver, Canada

Date 30th June 1998

## ABSTRACT

The effects of shear flow on the phase behavior of a polymer blend with high glass transition temperature, $T_g$, constituents and small dynamic asymmetry ($T_g$ contrast) were investigated using shear and capillary rheometry, complemented by differential scanning calorimetry and analysis of the extrudates. This blend is a lower critical solution temperature mixture of a random copolymer of styrene and maleic anhydride, SMA, and poly(methyl methacrylate), PMMA. Both shear-induced mixing, at low and very high shear rates, and shear-induced demixing, at moderate shear rates, were observed. A way to detect and isolate the degradation effects, which are predominant in SMA at high temperatures, and result in opaque but not necessarily phase-separated samples, is also presented. The methodology presented here for the determination of the shear-phase diagram in a flowing polymer blend should be applicable to any industrial mixture, and it is of particular value for assessing the effects of strong shear flow, relevant in processing applications. Furthermore the method of solution preparation, i.e., solution-cast versus melt-mixed samples, did not affect the rheologically determined demixing temperatures. Finally, a simple general thermodynamic model within the framework of Flory's statistical mechanical lattice model is presented for predicting the shear-induced phase changes in polymer fluids. Theoretical predictions of the shear-induced phase diagrams agree reasonably well with selected experiments with the systems polystyrene/dioctyl phthalate and poly(styrene-co-maleic anhydride)/poly(methyl methacrylate).

# TABLE OF CONTENTS

## LIST OF TABLES

## LIST OF FIGURES

# ACKNOWLEDGEMENTS

I wish to express my sincere gratitude to my supervisor Prof. Savvas G. Hatzikiriakos for his skillful guidance, support and encouragement during the course of this work. Also I would like to thank Dr. Dimitris Vlassopoulos for his continuous support and guidance during the course of this work and above all making my stay in Crete productive and memorable. I am thankful to Prof. C.A. Haynes for helping me with the thermodynamic development of the model.

This research was partially supported by the EU (Brite/Euram project BRE2.CT94-0610) and the Natural Sciences and Engineering Research Council of Canada. The polymer samples used were generously donated by ICI (PMMA) and DSM (SMA). I am thankful to Ms. I. Chira for her assistance with the rheological and DSC measurements. I would like to acknowledge Nova Chemicals Ltd., Calgary, Canada, for generously offering their twin screw extruders for the preparation of the melt-mixed samples.

I am thankful to the Foundation for Research & Technology-Hellas (FORTH) for extending their hospitality and making my stay in Heraklion comfortable. Finally, I would like to acknowledge the helpful discussions with my friends Eugene Rosenbaum, Alfonsius B. Ariawan and Igor Kazatchkov in Rheolab at UBC.

# 1. INTRODUCTION

Polymer blends are mixtures of two or more polymers exhibiting enhanced macroscopic (especially mechanical) properties indicative of a single phase. Typical examples include rubber toughened plastics like high impact polystyrene, ABS; teflon inclusions to enhance heat resistance in polymers; compounding to customize the properties of polymers; blending polymers of same chemical composition but different structure to control viscosity and melt strength; engineering thermoplastics like polycarbonate/acrlonitrile butadiene styrene and poly phenylene oxide/polystyrene. Most polymer blends are produced by melt mixing, where they are subjected to high temperature and shear. Therefore understanding the effects of shear flow on the phase behavior of multi-component systems represents a challenge of substantial scientific and industrial significance.

Since the pioneering work of Silberberg and Kuhn (1954, 1952), it has been recognized that the application of shear can lead to structural changes in complex fluids such as polymer solutions or blends [see for example Larson (1992)]. In principle, it can be thought that as a consequence of entropy reduction upon chain deformation due to flow, the phase diagram may be altered both qualitatively and quantitatively. For example, polymer solutions under the application of shear exhibit cloudiness, precipitation of gel-like particles, solid-fiber formation, an increase in nucleation rate, and viscosity changes, suggesting shear-induced demixing [Silberberg *et al.* (1954,1952), Krämer-Lucas *et al.* (1988), Larson (1992), Vrahopoulou-Gilbert *et al.* (1984), Wolf (1980), Schmidt *et al.* (1979), Horst *et al.* (1992, 1997), Horst (1995)]. The various structural changes, such as

formation of aggregates, have been reported in many flow geometries, including cone-and-plate, concentric cylinders, tube flow, and converging extensional flows, whereas their occurrence is quite universal for a variety of both polar and nonpolar polymers of various molecular weights.

Experimental evidence suggests that both shear-induced mixing and shear-induced demixing can occur [Hobbie *et al.* (1994), Larson (1992), Takebe *et al.* (1991), Katsaros *et al.* (1989), Chen *et al.* (1995), Vlassopoulos *et al.* (1996)], depending on the amount of shearing and the molecular characteristics of the polymers (molecular weights, glass transition temperature). For example, Mani *et al.* (1992) carried out step rate measurements in originally homogenous PS/PVME and observed a second overshoot in both shear and normal stresses, which was related to the occurrence of shear induced demixing, as confirmed by simultaneous fluorescence measurements. Fernandez *et al.* (1995) and Hindawi *et al.* (1992) claimed to have observed both mixing and demixing in PS/PVME blends, depending on the magnitude of the storage term in the generalized Gibbs free energy of mixing, which is a function of shear rate. Similar effects were observed in an extensional flow field by Katsaros *et al.* (1989). Soontaranun *et al.* (1996a,b) showed evidence of shear induced mixing in blends of high molecular weight glassy polymers with small $T_g$ contrast, namely poly(styrene-co-acrylonitrile)/poly (methyl methacrylate); they attributed this to the negative deviation of the blend viscosity from the linear mixing rule. Such a deviation was related to the excess stored elastic Gibbs energy. Despite the importance of these results however, these authors did not actually carry out experiments at high shear rates. Their analysis was based entirely on the viscosities of the blend constituents and their phenomenological model. The

mechanism of shear-induced effects was further elucidated by Chen *et al.* (1995) and Remediakis *et al.* (1997) who carried out rheo-optical experiments and pointed out the role of hydrodynamic instabilities in the flow-induced patterns. In this direction, the recent works of Kim *et al.* (1997) and Hashimoto *et al.* (1995) consider the mechanism of shear induced mixing in critical polymer blend solutions of polystyrene and polybutadiene, based on droplet deformation and break-up, much like the situation discussed by Vinckier *et al.* (1996) for nearly inelastic blends of poly(dimethyl siloxane) and polyisobutylene.

The physical mechanism of the flow-induced mixing or demixing is apparently a suppression or enhancement of concentration fluctuations, respectively [Larson (1992), Brochard *et al.* (1977), Nakatani *et al.* (1990)], due to shear. This is essentially the result of coupling of the stress and concentration fluctuations, and dates back to the original development of the two-fluid model [Brochard *et al.* (1977), Brochard (1983)]. More recent theoretical developments [Helfand *et al.* (1989), Doi *et al.* (1990), Milner (1993), van Egmond (1997)] have successfully predicted many aspects of the phenomenon [Larson (1992), Nakatani *et al.* (1990), Hobbie *et al.* (1994), Wu *et al.* (1991), van Egmond *et al.* (1993), Jian *et al.* (1996), Yanase *et al.* (1991), Kume *et al.* (1997)]. In particular, it is noted that van Egmond (1997) was able to predict a second stress overshoot on flow start-up, observed experimentally [Katsaros *et al.* (1989)]. In the general thermodynamic sense, the theoretical understanding of the phase changes in flowing polymer solutions and blends rests on the introduction of the generalized Gibbs energy of mixing, $\Delta G^*_M$. This is the sum of the Gibbs energy of the mixture (solution or

blend) under quiescent conditions, plus the energy the fluid stores while flowing [Wolf (1984)]. The extra storage energy term is essentially responsible for the flow-induced mixing or demixing, observed experimentally, by changing the sign of the second derivative of $\Delta G^*_M$ with respect to the composition from negative to positive (mixing), or vice versa (demixing). Several approaches have been proposed to explain flow-induced effects based on this concept. Most notable and extensive is the work of Wolf and co-workers [Horst *et al.* (1995), Wolf (1980, 1984, 1996), Schmidt *et al.* (1979), Horst *et al.* (1992, 1997), Horst (1995)], who predicted the shear influences in polymer solutions as well as polymer blends of both the upper critical (UCST) and lower critical (LCST) type phase diagrams. In their calculations, the extra energy term, which is essentially stored as the fluid undergoes steady shear flow, is described in terms of a semi-empirical expression [Wolf (1980, 1984, 1996), Schmidt *et al.* (1979), Horst *et al.* (1992, 1997), Horst (1995)], depending on the shear rate, $\dot{\gamma}$, the steady shear compliance, $J_e^0$, and shear viscosity, $\eta$, of the blend. In addition to mixing and demixing, a number of interesting phenomena were predicted as functions of shear rate, such as for example, closed miscibility gaps. These findings were in reasonable agreement with experimental observations [Chen *et al.* (1995), Horst *et al.* (1992)]. Recent extensions of this approach include calculations of the phase diagrams of ternary polymeric systems, i.e., a polymer blend and a copolymeric compatibilizer [Horst *et al.* (1997), Horst (1995)]. Despite its success, however, this theory remains largely phenomenological in the sense that it does not directly connect the stored energy term to the change of macromolecular conformation. Such connection can provide direct information on the mechanism of the shear-induced effects and thus explain the physical parameters controlling the

phenomenon. In contrast, it relates the stored energy directly to macroscopic properties, which are a consequence of the conformational changes, such as shear viscosity and compliance. Actually, in Wolf's development, which is essentially established and used by all subsequent treatments [Soontaranun *et al.* (1996a,b)], all contributions due to flow fields are incorporated into the extra energy storage term. Thus, the question that arises is how to treat the effects of flow. Such effects include deformation of macromolecules, orientation at different length scales, interfacial effects and changes in the contact statistics of segments. Detailed incorporation of these effects requires an elaborate analysis on a microscopic level; thus, these authors have used under various assumptions the semi-empirical approach mentioned above, in which the entropic origin of the model and the universality for different fluids (solutions or blends) are not evident. Yet, with the advancement of experimentation and the availability of fine rheo-optical data on the structural changes during shear [Nakatani *et al.* (1990), Hobbie *et al.* (1994), Wu *et al.* (1991), van Egmond (1993), Jian *et al.* (1996), Yanase *et al.* (1991), Kume *et al.* (1997)], further elucidation of the molecular origin of the stored energy during flow becomes a true challenge. To a first order approximation, Marrucci (1972) had expressed the stored elastic energy of a dumbbell representing a dilute polymer solution in a steady simple shear flow in terms of the trace of the first normal stress difference. Vrahopoulou-Gilbert and McHugh (1984) derived an expression for the free energy change per mole of polymer associated with the application of flow. They assumed that the thermodynamic mixing behavior of a system of random coils under stress would be equivalent to that of a "model" system of semiflexible macromolecules in the absence of applied forces. This analysis predicts the basic shape of the binodal curve if the chain flexibility in the

concentrated phase is assumed to be less than that in the dilute phase. The free energy increase is therefore consumed in creating a flexibility gradient among the chains in the two phases.

Despite the above developments, there are several important issues that have not yet been addressed adequately. These are also necessary for developing a complete phenomenology and thus for gaining a better understanding of the flow-induced phenomena in polymer blends. These are the following: (i) what happens with *real* industrial blends (as compared to model systems) ; (ii) what is the effect of very high shear rates, such as those typically encountered in processing conditions (200 $s^{-1}$ and above) ; (iii) how does the presence of glassy components and the small dynamic asymmetry interplay with the shear influences on the phase characteristics; (iv) How can we correlate various thermodynamic and rheological quantities to model and predict the phase changes observed experimentally.

In this thesis, we address the above issues by investigating the effects of high shear flow on the phase behavior of a polymer blend consisting of a random copolymer of styrene and maleic anhydrite and poly(methyl methacrylate). This is a polymeric mixture of direct industrial use in applications such as car rear lamps, lenses of large diameter and street lamps, where the performance of the SMA/PMMA blend is superior to that of pure PMMA. This is a LCST blend, i.e., it is homogeneous at low temperatures, whereas it phase separates at higher ones [Brannock *et al.* (1991), Feng *et al.* (1995)]. The present study extends the report of Aelmans and Reid (1996) on a SMA/PMMA blend of

different grade, to much higher shear rates, and compliments it with a rigorous analysis of the sheared blends based on the theoretical concepts mentioned above followed by a model to explain the same. The detection of shift of the phase boundary with flow is based on combined information obtained from shear and capillary rheology, differential scanning calorimetry, as well as visual and scanning electron microscopy (SEM) observations. Finally, Marrucci's (1972) approach is generalized, in order to describe the stored free energy during shear flow for any polymer fluid (solution or blend) followed by the implementation of the thus obtained expression to derive a universal expression for the Gibbs free energy of mixing under flow, using Flory's statistical mechanical lattice model [Flory (1953)]. This approach yields a description of shear-induced structural changes based on first principles. The hypothesis that the shear induces a decrease in polymer entropy is used to correlate rheological parameters with the observed thermodynamic changes. Finally, the proposed model is successfully tested for the stress-induced phase diagram for polymer solutions for the system polystyrene (PS)/dioctyl phthalate (DOP). An analogous comparison of theoretical predictions and experimental observations is also carried out for the blend poly(styrene-co-maleic anhydride) (SMA)/poly(methyl methacrylate) (PMMA).

# 2. LITERATURE REVIEW

## 2.1 Thermodynamics of polymer-polymer miscibility

Polymer blends can be characterized as 'miscible' or 'immiscible' with respect to their phase behavior. The term "miscibility of polymer blends" will be used for their dispersal at the molecular level.

The phase behavior of polymer blends comprising amorphous polymers is experimentally well accessible in a "window" the upper bound of which is the thermal decomposition temperature of the polymer components and the lower one is the glass transition temperature of the system (Figure 2.1.). In general, miscible blends display phase separation at elevated temperatures, as shown schematically in Figure 2.1, i.e. Lower Critical Solution Temperature (LCST) behavior can be seen. As a general phenomenon, miscibility of polymers must be coupled with disordering in the systems imposed by mixing. An increase in temperature weakens the specific interaction, which is equivalent to ascending disorder. Hence, an entropy-driven LCST occurs where the blend phase separates upon heating. Some miscible blends exhibit not only LCST behavior but also thermally induced phase separation upon cooling. Cooling causes a decrease in compressibility, which in turn is equivalent to enhanced repulsion between segments exceeding the specific interactions below an Upper Critical Solution Temperature (UCST). Thus, the repulsion between the segments turns out to be unfavorable for order or miscibility below a certain temperature and promotes phase separation. The simultaneous occurence of a LCST or an UCST in blends of high-molar-

mass polymers is considered to be a general phenomenon (Kammer et al., 1989). But usually the UCST shifts far below the glass transition temperature and therefore, is not accessible experimentally. When the glass transition temperature is sufficiently low as in systems containing an elastomer as one of the components, the UCST should be confirmed experimentally besides a LCST [Ougizawa *et al.* (1985, 1986), Saito *et al.* 1987, Cong *et al.* 1986].

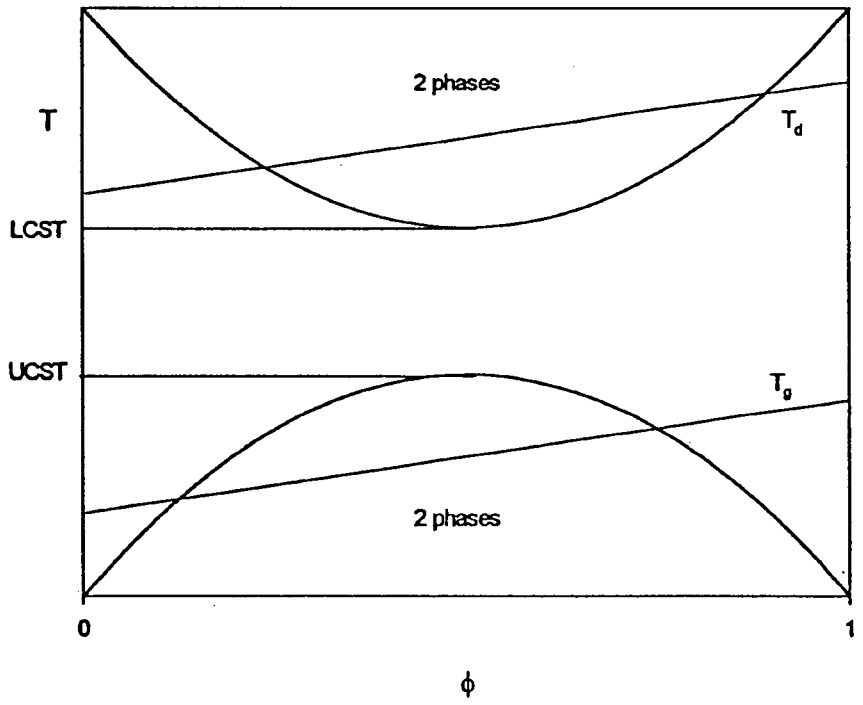


Figure 2.1. The processing window for polymer blends typically lies in-between the glass-transition temperature ($T_g$) and the thermal decomposition temperature ($T_d$).

Molecular architecture plays an important role in determining polymer-polymer phase behavior [Bates (1991)]. Binary homopolymer mixtures at equilibrium consist of either one or two phases (neglecting crystallization). In the event of phase separation, interfacial

tension favors a reduction in surface area that leads to macroscopic segregation. A density gradient also favors this segregation. However polymer melts are extremely viscous so that phase-separated homopolymers rarely reach an equilibrium morphology. Consequently, molecular architecture, which strongly influences polymer mobility, plays an important role in the evolution of phase morphology. Branching in particular disrupts the basic mechanism of polymer motion (known as reptation) and leads to significant increase in polymer viscosity.

The degree of polymerization, i.e. the number of repeat units that make up a polymer chain effects the thermodynamics of the polymer blend [Bates (1991)]. Most thermodynamic theories presume a single repeat unit volume, although in practice chemically different repeat units rarely occupy equal volumes. Therefore it is convenient to define a segment volume $V$ corresponding to either of the repeat unit volumes ($V_1$ or $V_2$), or any suitable mean repeat unit volume. With this definition the number of segments per polymer molecule is $g = M/\rho V N_0$ where $\rho$ and $M$ are the polymer density and molecular weight, and $N_0$ is Avogadro's number. The total number of cells in the lattice is specified as $N$. Based on this convention $\phi_i = g_i/N$ where $\phi_1$ and $\phi_2$ are lattice volume fractions occupied by polymers 1 and 2 and $g_i$ is the degree of polymerization of polymer $i$.

For polymer mixtures with specific interactions the random mixing assumption for the entropy of mixing is no longer valid. In this case, the overall entropy of mixing is usually written as:

$$\Delta S = \Delta S_C + \Delta S_{NC}$$

where $\Delta S_C$ is the combinatorial entropy of mixing for a random orientation. The non combinatorial entropy of mixing $\Delta S_{NC}$ is a correction for cases where some local orientation is important, as in the cases of blends with specific interactions. This orientation decreases the overall entropy of mixing although empirical parameters are often used to describe this effect.

The $\chi_{ij}$ parameter is usually assumed to be a composite term that includes contributions from dispersive forces, specific interactions, non-combinatorial entropy effects and to a lesser extent, compressibility effects. An expression is given to the specific interaction parameter that can include all possible effects (including the above) and explain the experimental data. The choice of particular pair of monomers establishes the sign and the magnitude of the energy of mixing, which can be approximated by the Flory-Huggins interaction parameter $\chi_{ij}$ [Bates (1991)], $\chi_{ij}=A+B/T$ where $T$ represents temperature, and $A$ and $B$ are empirical parameters representing the non-combinatorial entropic term and the enthalpic term respectively. Nearly, 50 years ago Flory [Flory (1953)] and Huggins independently estimated the change in free energy per segment $\Delta G_M$ associated with mixing random walk (Gaussian) polymer chains on an incompressible ($\phi_1+\phi_2 = 1$) lattice,

$$\frac{\Delta G_M}{kT} = \frac{\phi_1}{n_1}\ln\phi_1 + \frac{\phi_2}{n_2}\ln\phi_2 + \phi_1\phi_2\chi_{ij} \qquad (2.1)$$

where $k$ is the Boltzmann constant, T is the absolute temperature and $g_i$ is the number of segments of component $i$ per polymer molecule (the degree of polymerization) .

The first two terms (right hand side) in Eq. (2.1) account for the combinatorial entropy of mixing $\Delta S_C$.. Because mixing increases the systems randomness, it naturally increases $\Delta S_C$ and thereby decreases the free energy of mixing. Large chains can assume fewer mixed configurations than small chains so that $\Delta S_C$ decreases with increasing $n_i$. The third term represents the enthalpy of mixing $\Delta H_M$ and can either decrease or increase $\Delta G_M$ depending on the sign of $\chi_{ij}$. It represents the excess Gibbs energy relative to the combinatorial reference state.

### 2.1.1 Mechanisms of phase separation

Immiscible or partially immiscible (LCST or UCST) homopolymer mixtures can be homogenized by mechanical mixing or temperature changes. Upon shear removal and under certain conditions phase separation will occur. There are two mechanisms of phase separation viz. nucleation and growth and spinodal decomposition. These are illustrated in Figure 2.2 and are discussed below.

Figure 2.2 shows a typical phase diagram for a symmetric polymer mixture exhibiting a LCST. The solid line represents the equilibrium line separating the one phase regime from the two phase regime. The dashed line represents the stability limit. In-between the equilibrium and stability lines lies the metastable region. Inside the equilibrium (solid)

curve, 2 phases exist with compositions $\phi'_A$ and $\phi''_A$. In the metastable region (such as B'), phase separation occurs by a nucleation and growth mechanism, while an unstable mixture (such as A') spontaneously demixes by spinodal decomposition.

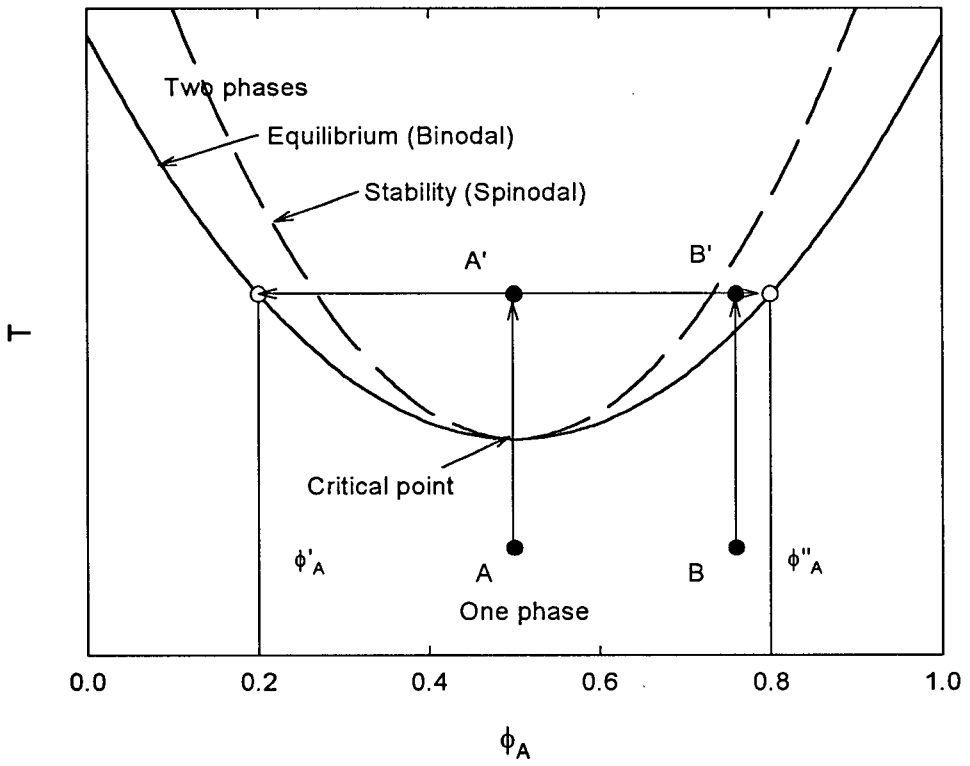


Figure 2. 2.Theoretical phase diagram (mean field) for a symmetric ($n_1=n_2\equiv n$) binary mixture of linear homopolymers [Bates (1991)].

Classical nucleation theory predicts that small droplets of a minority phase develop over time in a homogeous mixture that has been brought into the metastable region of the phase diagram (for example, from point B to B' in Figure 2.2). Initially droplet growth proceeds by diffusion of material from the supersaturated continuum. However, once the composition of the supernatant reaches equilibrium ($\phi_A$ in Figure 2.2), further increases in droplet size occur by droplet coalescence or Ostwald ripening; the latter refers to the

growth of large droplets through the disappearance (evaporation) of smaller ones. Because of the extremely low diffusivity ($D \sim g^{-2}$) and enormous viscosity ($\eta \sim g^{3.4}$) of polymers, the second stage of growth can be extremely slow and may result in unusual particle-size distributions.

In the metastable state, homogenous mixtures must overcome a free energy barrier in order to nucleate a new phase. In the thermodynamically unstable state there is no such barrier, and mixtures phase separate spontaneously (for example , from point A to A' in Figure 2.2). This process which was first described by Cahn (1965) 33 years ago, is known as spinodal decomposition. It results in a disordered bicontinuous two-phase structure that is contrasted in Figure 3 with the morphology associated with the nucleation and growth mechanism. The initial size $d_0$ of the spinodal structure (see Figure 2.3) is controlled by the quench depth; deeper quenches produce finer structures. Almost immediately after the bicontinuous pattern begins to form, interfacial tension drives the system to reduce it's surface area by increasing $d$. In symmetric critical mixtures coarsening does not disrupt the bicontinuous morphology that evolves through a universal, scale invariant form, as depicted in Figure 2.3.

The intricate structures associated with spinodal decomposition lead to a variety of interesting materials applications. These include polymer-based membranes, controlled porous glasses, and certain metal and ceramic alloys. Linear homopolymer mixtures have become one of the most attractive systems for studying spinodal decomposition in recent years.

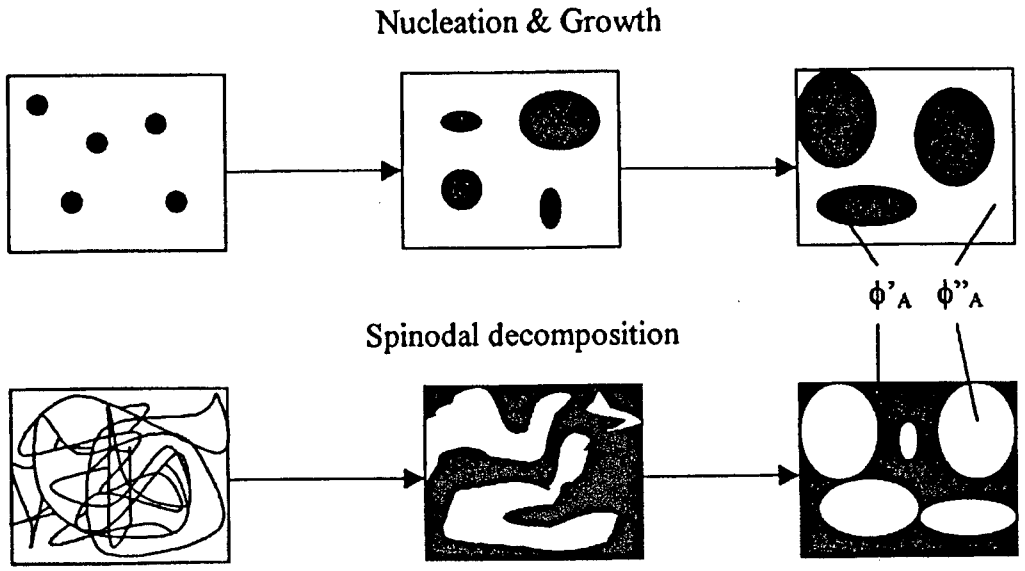


Figure 2.3. Time evolution of structure in phase-separating binary homopolymer mixtures. Nucleation and growth results when a homogenous mixture is thrust into the metastable region of the phase diagram. Spinodal decomposition occurs when a mixture is placed in a thermodynamically unstable state. The driving force behind coarsening in both cases is the minimization of interfacial tension through a reduction in interfacial area [Bates (1991)].

### 2.1.2 Phase equilibrium, phase stability and criticality conditions

The thermodynamic properties of a blend can be evaluated from the Gibbs free energy of mixing [Schwahn (1994), De Gennes (1979)]

$$\Delta G_M = G_M - [\,(1-\phi_b)\,G_a + \phi_b G_b]$$

Which is the difference of the Gibbs free energy of the mixture $G_M$ and of the pure components $G_a$ and $G_b$ weighted by their volume fractions $(1-\phi_b)$ and $\phi_b$, respectively. $\Delta G_M$ is a function of temperature T, volume fraction $\phi_b$ of the polymer *b*, and slightly on pressure P. $\Delta G_M$ is given by

$$\Delta G_M(T, \phi_b) = \Delta H_M(T, \phi_b) - T\Delta S_M(T, \phi_b)$$

$\Delta H_M$ is the enthalpy of mixing and $\Delta S_M$ the entropy of mixing. $\Delta G_M$ must be negative for a miscible system as shown in Figure 2.4. For the discussion of phase stability let's consider the Euler equation [Schwahn (1994)]

$$\Delta G_m = (1- \phi_b)\Delta\mu_a + \phi_b\Delta\mu_b \qquad (2.2)$$

With $\Delta\mu_i = \mu_i - \mu_i^\circ$, the chemical potentials of mixing per unit volume of polymer a and b. $\Delta G_m$ is the molar Gibbs energy of mixing, and $\mu_i$ and $\mu_i^\circ$ are the chemical potentials of the component *i* in the mixed and pure state, respectively.

The region of metastability is bounded by the conditions

$$[\partial(\Delta G_M) / \partial\phi\ ]_{T,P} = 0 \text{ and } [\partial^2(\Delta G_M) / \partial\phi^2\ ]_{T,P} = 0$$

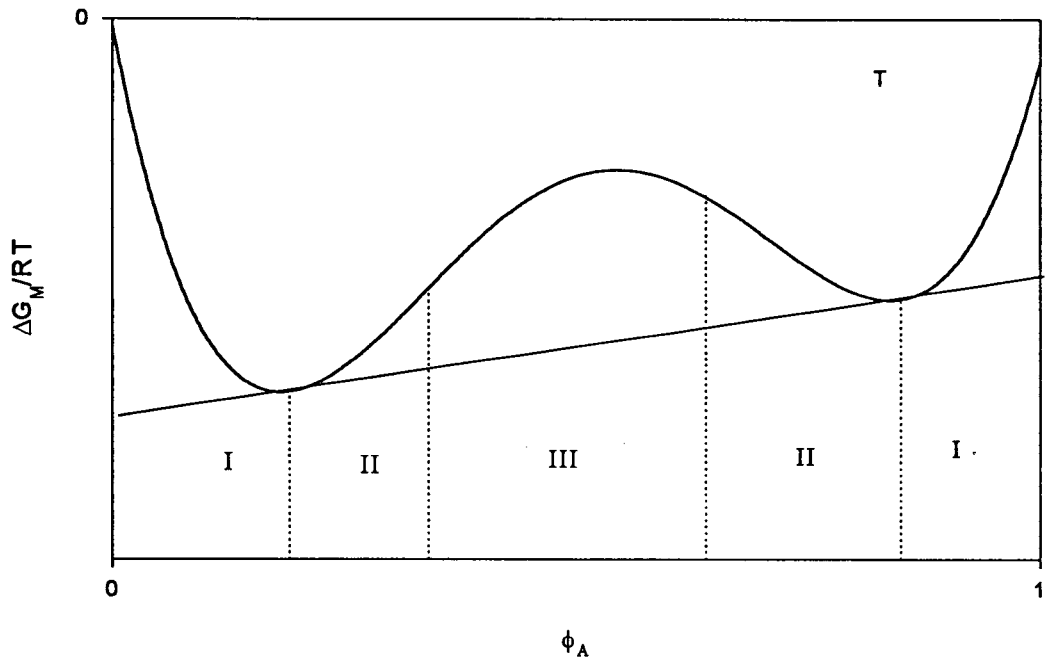


Figure 2.4. Gibbs free energy of mixing at temperature T as a function of composition. The mixture is miscible in region I and decomposes into two phases in region II and III [Schwahn (1994)].

In Figure 2.4, $\Delta G_M$ is plotted versus $\phi_A$ for a partly miscible system. There are the regions I, II, and III which are the stable, metastable ( $[\partial^2(\Delta G_M)/\partial\phi^2]_{T,P} > 0$) and unstable ($[\partial^2(\Delta G_M)/\partial\phi^2]_{T,P} < 0$) ones, respectively. In region I all fluctuations in $\phi$ increase $\Delta G_M$. In region II fluctuations with small amplitudes are stable because of $[\partial^2(\Delta G_M)/\partial\phi^2]_{T,P} > 0$ while fluctuations with sufficient large amplitude become unstable. Finally in region III all long wavelength fluctuations lead to a decrease of $\Delta G_M$ because of $[\partial^2(\Delta G_M)/\partial\phi^2]_{T,P} < 0$. In Figure 2.4, $\Delta G_M$ is plotted together with the Euler relation of Eq. (2.2) as a straight line. According to the tangent rule the phase boundary of the two-phase region or binodal is determined by the intercepts of both curves. According to the equilibrium condition the

chemical potentials of both components must be the same in both phases. In the decomposed state the straight line of the Euler equation gives $\Delta G_M$ of the system, and its difference to $\Delta G_M$ of the mixed state is the driving force of the decomposition process.

The boundary between metastable and unstable region is defined by

$$[\partial^2(\Delta G_M)/\partial\phi^2]_{T,P} = 0 \qquad (2.3)$$

and is called the spinodal. In Figure 2.2 a schematic phase diagram with $T$ and $\phi$ as axes are plotted. The stable, metastable and unstable regions are indicated as in Figure 2.4. Spinodal and binodal touch each other at the critical point, the only point where stable and unstable region are linked together. The following must therefore hold for the critical point

$$[\partial^2(\Delta G_M)/\partial\phi^2]_{T,P} = [\partial^3(\Delta G_M)/\partial\phi^3]_{T,P} = 0$$

For polymer solutions described by Flory-Huggins theory, the critical point is found to be

$$\phi_c = \frac{1}{1+\sqrt{g_P}}, \chi_c = \frac{1}{2}\left(1+\frac{1}{\sqrt{g_P}}\right)^2$$

In case of polymer blends $\chi_c$ is equal to zero. Thus as $g_P$ (degree of polymerization for a single polymer in a monomeric solvent) increases, the critical concentration $\phi_c$ decreases and the critical temperature increases. Such a tendency is indeed observed experimentally

[Doi (1996)]. However, there is no good qualitative agreement between the theoretical and experimental coexistence curves. The reason for the discrepancy is the large concentration fluctuations near the critical point, and to account for such effects, a theory beyond the mean-field theory is required [Doi (1996)].

## 2.2 Shear Rheology: Basic principles

Flow may affect the phase diagram of a polymer in a variety of ways. It may induce either mixing or demixing of multi-component systems. Figure 2.5 depicts characteristic examples of the effect of shear on the phase diagrams of a polymer solution (a) blend (b) as already discussed above (Introduction).

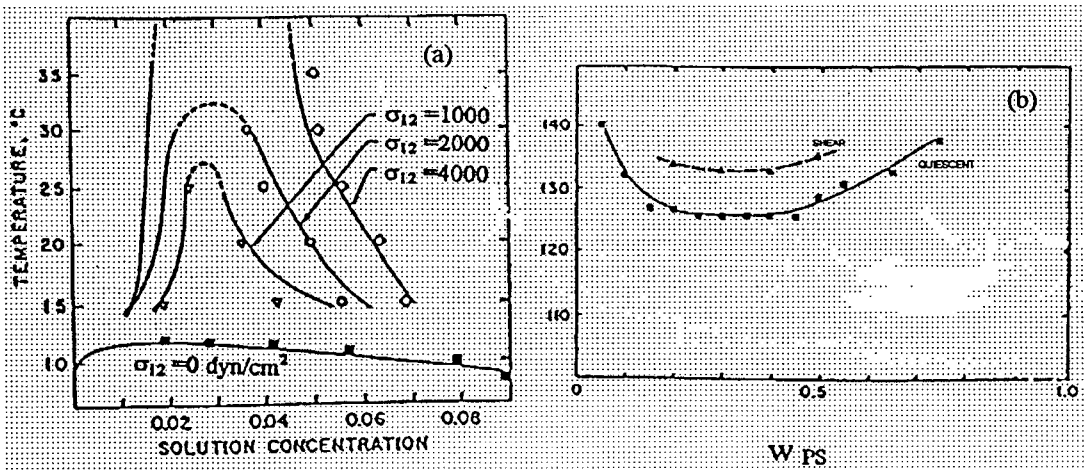


Figure 2.5. Phase diagrams for (a) Polystyrene in dioctyl phthalate at various stress levels [Rangel Nafaile *et al.* (1984)], (b) Polystyrene/Poly vinyl methyl ether blends [Mazich and Carr (1983)].

In order to study the influence of flow on polymer blend miscibility, a convenient way is by means of rheometers which can generate well defined, simple shear and extensional flows. In this section we review some elements of basic rheology, with particular emphasis on shear flows.

### 2.2.1 Simple shear flows

Most rheological data on polymeric liquids of known structure have been obtained by using simple shearing deformations. Consider the flow of a fluid contained between two parallel plates. The upper plate can be freely moved with a constant velocity u and the lower one remains stationary (Figure 2.6).

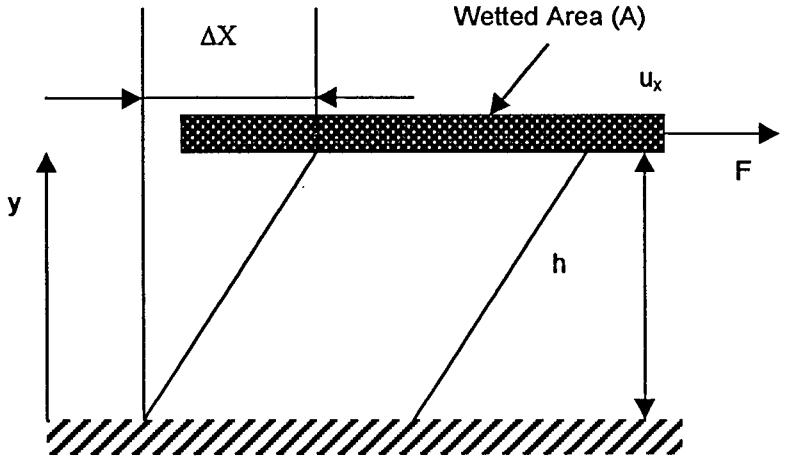


| | |
|---|---|
| *Displacement* | $\Delta X$ |
| *Strain* | $\gamma = \Delta X/h$ |
| *Nominal shear rate* | $\dot{\gamma}_n = u_x/h$ |
| *Shear stress* | $\sigma = F/A$ |

Figure 2.6. Simple shear and related equations.

The velocity profile in the gap is given by [Ferry (1970)]:

$$u_x = \dot{\gamma} y \qquad u_y = 0 \qquad u_z = 0 \tag{2.4}$$

Where $u_x$, $u_y$, $u_z$ are the components of the velocity field. This flow is known as steady simple shear flow; the quantity $\dot{\gamma}$ is called the shear rate and characterizes the intensity of flow field (velocity gradient); for the particular case of molten polymers the current stress depends on the history of shear deformation or strain $\gamma(t)$, which in general is defined as:

$$\gamma(t) = \gamma(0) + \int_0^t \dot{\gamma}(t)dt \tag{2.5}$$

i.e. the values of shear deformation at all previous times. If the orientations of the three planes are chosen to be normal to the coordinate directions of a rectangular Cartesian system (x,y,z or 1,2,3) the Cartesian components of the stress are obtained:

$$\sigma(t) = \begin{bmatrix} \sigma_{11} & \sigma_{12} & \sigma_{13} \\ \sigma_{21} & \sigma_{22} & \sigma_{23} \\ \sigma_{31} & \sigma_{32} & \sigma_{33} \end{bmatrix} \tag{2.6}$$

where $\sigma$ is the stress tensor. This can also be written in terms of the extra stress tensor $\tau$ as:

$$\sigma = -PI + \tau \tag{2.7}$$

where P is the isotropic pressure and I is a unit tensor. Symmetry arguments suffice to show that $\sigma_{13}$ and $\sigma_{23}$ are identically zero in this particular flow and $\sigma_{12}$ is equal to $\sigma_{21}$.

$$\sigma(t) = \begin{bmatrix} \sigma_{11} & \sigma_{12} & 0 \\ \sigma_{21} & \sigma_{22} & 0 \\ 0 & 0 & \sigma_{33} \end{bmatrix} \tag{2.8}$$

From such a flow the shear stress, $\sigma_{12}$ or $\sigma_{21}$ can be measured as,

$$\sigma_{12} = \sigma_{21} = F/A$$

where F is the tangential force acting on the sample and A is the area of sample in contact with the plates.

### 2.2.2 Material functions for polymers

For steady shear flow, the shear rate is constant for all past times. Since deformation history now depends only on the parameter, the stress components become functions of shear rate alone. Since a normal stress by itself cannot induce any deformation to the fluid, in rheology (study of deformation and flow) we are interested in determining normal stress differences [Dealy and Wissbrun (1990)]. The appropriate material functions which are of interest for simple steady shear flow are [Ferry (1970)] :

$$\sigma_{12} = \sigma_{21} \equiv \sigma \equiv \eta(\dot{\gamma})\dot{\gamma} \tag{2.9}$$

$$\sigma_{11} - \sigma_{22} \equiv N_1 \equiv \psi_1(\dot{\gamma})\dot{\gamma}^2 \tag{2.10}$$

$$\sigma_{22} - \sigma_{33} \equiv N_2 \equiv \psi_2(\dot{\gamma})\dot{\gamma}^2 \tag{2.11}$$

where $N_1$ and $N_2$ are the first and second normal stress differences respectively. Symmetry arguments show that the viscosity function $\eta(\dot{\gamma})$ and the first and second normal stress coefficients $\psi_1(\dot{\gamma})$ and $\psi_2(\dot{\gamma})$ are even functions of $\dot{\gamma}$. In the limit of zero shear rate $\eta(\dot{\gamma})$ and the normal stress coefficients $\psi_1(\dot{\gamma})$ and $\psi_2(\dot{\gamma})$ become constants, denoted as $\eta_0$ (zero-shear viscosity), $\psi_{1,0}$ (zero-shear first normal stress coefficient) and $\psi_{2,0}$ (zero-shear second normal stress coefficient).

### 2.2.3 Linear viscoelasticity

The term viscoelasticity is derived from the merger of two terms viz. viscosity and elasticity. Viscosity relates to the "resistance" of material to flow under deformation (or stress). Elasticity relates to the response of an elastic solid like material subject to stress deformation. Viscosity is an energy dissipative process while elasticity is an energy storage process.

The class of materials, which exhibit both viscous and elastic behavior are termed as viscoelastic. Polymeric materials are a typical and common example.

Viscoelastic behavior is classified to linear and non-linear according to the manner by which the stress depends upon the imposed deformation history [Coleman (1961)]. In steady shear flows, for example, the shear rate dependence of viscosity and the normal

stress functions are non-linear properties. Linear viscoelastic behavior is obtained for simple fluids if the deformation is sufficiently small for all past times (infinitesimal deformations) or if it is imposed sufficiently slowly (infinitesimal rate of deformation) [Coleman (1961, 1964)]. The deformation of the polymer specimen is reversible but time dependent and associated with the distortion of polymer chains from their equilibrium conformations through activated segment motion involving rotation about chemical bonds. In shear flow under these circumstances, the normal stress differences are small compared to the shear stress, and the expression for the shear stress reduces to a statement of the Boltzmann superposition principle [Ferry (1970), Gross (1953)].

$$\sigma(t) = \int_{-\infty}^{t} G(t-t')\dot{\gamma}(t')dt' \qquad (2.12)$$

where G(t) is the shear stress relaxation modulus of the fluid in the limit of linear viscoelasticity, and it is a monotonically decreasing function of time, with $G(\infty) = 0$. If the fluid initially at rest is subjected to a small shear deformation $\gamma_0$ at $t = 0$, the shear stress at later times simply becomes:

$$\sigma(t) = \gamma_0 G(t) \qquad (2.13)$$

The value G(0) is called instantaneous modulus, and will be denoted by $G^0$. Whether the behavior being measured does, in fact, lie in the linear viscoelastic region must be judged separately in each system. Generally tests are made at different levels of imposed stress,

strain, or strain rate to establish that the same material function is obtained. In polymer systems the response is usually spread over many more decades of time or frequency than can be covered in a simple isothermal experiment. Typically, the response is measured over a convenient range at several temperatures and the results combined to form a master curve according to the principle of time-temperature superposition.

### 2.2.4 Dynamic Mechanical Measurements

Dynamic mechanical analysis can be used to analyze both elastic and viscous material response simultaneously. In this type of test, a motor is used to apply a sinusoidal strain to a material (either tension, bending, or shear) and the resulting stress is measured with a torque-measuring transducer. The torque is then electronically separated into two components viz. an elastic stress and a viscous stress. Several quantities can be calculated from the measured strain vs. stress relationships. To provide information corresponding to very short times, the strain may be varied periodically, usually with a sinusoidal alteration at a frequency $\omega$. If the viscoelastic behavior is linear, it can be shown that the stress will be a harmonic function but out of phase with respect to the strain (Figure 2.7). Essentially the same behavior can be obtained in a constant-stress controlled rheometer, where the strain is out of phase with respect to the stress. The experiments done in this work have strain as an independent parameter.

The elastic and viscous components of the stress signal are out of phase by 90°. This can be shown from the constitutive equations as follows. Let the shear strain be a sinusoidal function of the frequency $\omega$ [Ferry (1970)]:

$$\gamma = \gamma^0 \sin \omega t \tag{2.14}$$

where $\gamma^0$ is the strain amplitude. Then the shear rate of strain is

$$\dot{\gamma} \equiv \frac{d\gamma}{dt} = \omega\gamma^0 \cos\omega t = \dot{\gamma}^0 \cos\omega t \tag{2.15}$$

where $\dot{\gamma}^0$ is the rate of strain amplitude.

Substituting in Eq. (2.12), and setting s = t-t' we may obtain,

$$\sigma(t) = \int_0^\infty G(s)\omega\gamma^0 \cos[\omega(t-s)]ds$$

$$= \gamma^0[\omega\int_0^\infty G(s)\sin\ \omega s\ ds]\sin\omega t + \gamma^0[\omega\int_0^\infty G(s)\cos\ \omega s\ ds]\cos\omega t \tag{2.16}$$

It is clear that the term in sin ωt is in phase with γ and the term in cos ωt is $90^0$ out of phase; σ is periodic in ω but out of phase with respect to γ to a degree depending on the relative magnitudes of these terms. The quantities in brackets are functions of frequency but not of elapsed time, so Eq. (2.16) can be conveniently written as:

$$\sigma(t) = \gamma^0(G'\sin\omega t + G''\cos\omega t) \tag{2.17}$$

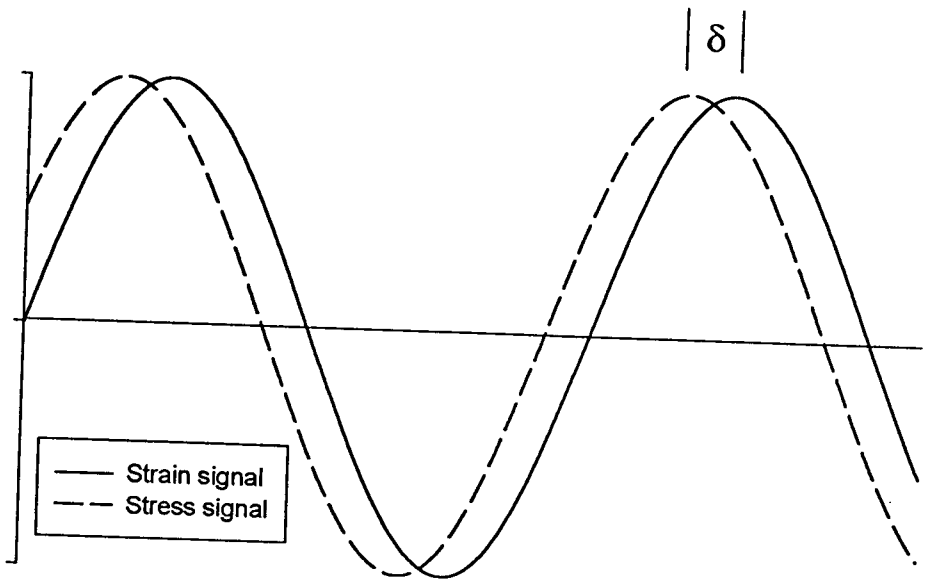


**(a) Stress and Strain signals**

$G' = \tau' / \gamma$

$G'' = \tau'' / \gamma$

$\tan \delta = G'' / G'$

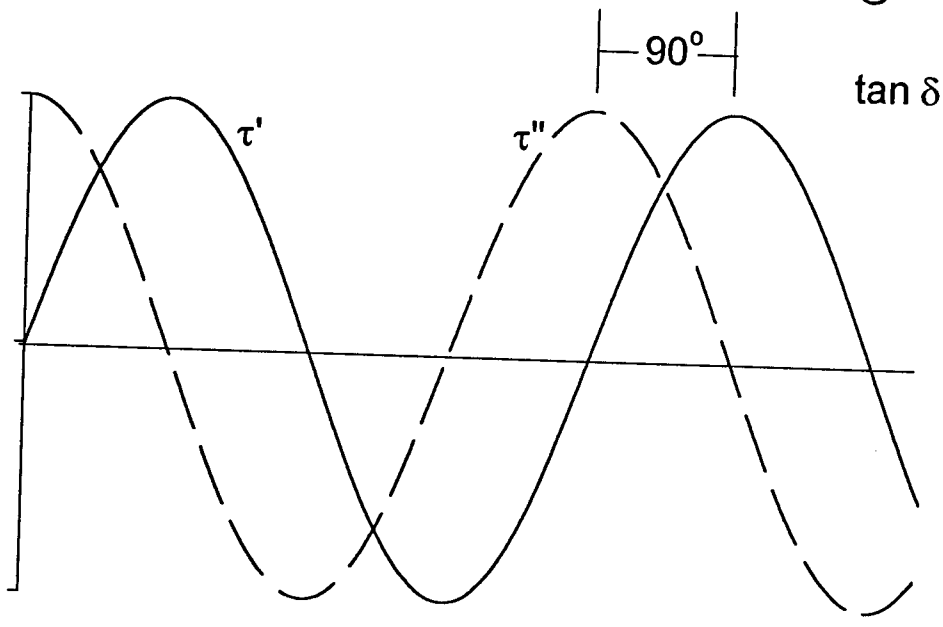


**(b) Elastic and viscous components of stress signal**

Figure 2.7. The angle between stress and strain in viscoelastic materials..

where two frequency-dependent functions i.e. the shear storage modulus G'(ω) and the shear loss modulus G"(ω), have been defined. G'(ω) and G"(ω) in small amplitude sinusoidal deformations are also related to G(t) by:

$$G'(\omega) = \omega \int_0^\infty G(t) \sin \omega t \, dt \tag{2.18}$$

$$G''(\omega) = \omega \int_0^\infty G(t) \cos \omega t \, dt \tag{2.19}$$

The instantaneous modulus is given by:

$$G^0 = \frac{2}{\pi} \int_{-\infty}^{\infty} G''(\omega) \, d\ln \omega \tag{2.20}$$

and the zero shear viscosity by:

$$\eta_0 = \int_0^\infty G(t) \, dt = \lim_{\omega \to 0} \frac{G''(\omega)}{\omega} \tag{2.21}$$

The equivalent expression for the zero shear viscosity in steady state shearing flows is [Coleman (1964)]:

$$\eta_0 = \lim_{\dot{\gamma} \to 0} \eta(\dot{\gamma}) \tag{2.22}$$

The elastic modulus (G') of a material is defined as the ratio of the elastic (in-phase) stress to strain and relates to the material's ability to store energy elastically. Similarly, the loss modulus (G") of a material is the ratio of the viscous (out of phase) component to the strain, and is related to the material's ability to dissipate stress through flow. The ratio of these moduli (G"/G') is defined as tan δ, and indicates the relative degree of viscous to elastic dissipation, or damping, of the material.

In a typical frequency sweep experiment, the rheometer controls three parameters: frequency of oscillation, amplitude of oscillation, and test temperature. A typical test holds two of these parameters constant while varying the third.

### 2.2.5 Capillary rheology : Basic principles

Flow of molten polymer through a tube or a channel under pressure is commonly encountered in polymer processing, for example in an extrusion die or in the runner feeding of an injection mold. This type of flow is also used as the basis of capillary rheometer. A typical schematic is depicted in Figure 2.8. In this work, capillary rheometer was primarily used to extrude various blends at high shear rates. Examining the obtained extrudates by using a variety of methods their phase behavior could be inferred. Therefore in this work the capillary rheometer was used to investigate the thermo-rheological complexity of SMA/PMMA blend. This is extensively discussed in Chapter 4. The present section covers the underlying principles of capillary rheometry.

The capillary rheometer consists of a small tube through which melt is forced to flow by means of a piston capable of moving at a constant speed. The quantities normally measured in such a mode of operation are the flow rate, Q and the driving pressure, $P_d$. The measured piston force, $F_d$, is related to $P_d$ as follows:

$$P_d = F_d / \pi R_b^2 \qquad (2.23)$$

where $R_b$ is the radius of the barrel or reservoir. Alternatively, $P_d$ can be measured by mounting a pressure transducer directly in the barrel.

Capillary rheometers are used primarily to determine the viscosities in the shear rate range of 5 to $1000s^{-1}$ [Dealy and Wissbrun (1990)]. However, in this thesis, shear rates as high as $50{,}625s^{-1}$ were achieved by selecting the appropriate die (smaller dies give higher shear rates for the same $Q$).

To calculate the viscosity, it is necessary to know the wall shear stress and the wall shear rate, and it is therefore necessary to have reliable techniques for evaluating these basic rheological quantities on the basis of experimental data. The wall shear stress is related to the driving pressure by Eq. (2.24).

$$\sigma_w = \frac{P_d}{2(L/R + e)} \qquad (2.24)$$

where $e$ is the Bagley end correction given by $e = \Delta P_{ends} / 2\sigma_w$. Bagley correction can be obtained by measuring the driving pressure ($P_d$) at various values of the flow rate (Q) using a variety of capillaries having different lengths. Alternatively, it can be determined experimentally by using an orifice die (L/D = 0). The driving pressure can thus be plotted for each value of the apparent wall shear rate ($4Q / \pi R^3$). The end correction, $e$, can be obtained by extrapolating the lines corresponding to various values of $\dot{\gamma}$ to the $P_d = 0$ axis as shown in Figure 2.8. This represents the length of the capillary (divided by R) for which fully developed flow would give a pressure drop equal to $\Delta P_{ends}$. Thus, the true wall shear stress can then be calculated by Eq. (2.24) [Dealy and Wissbrun (1990)].

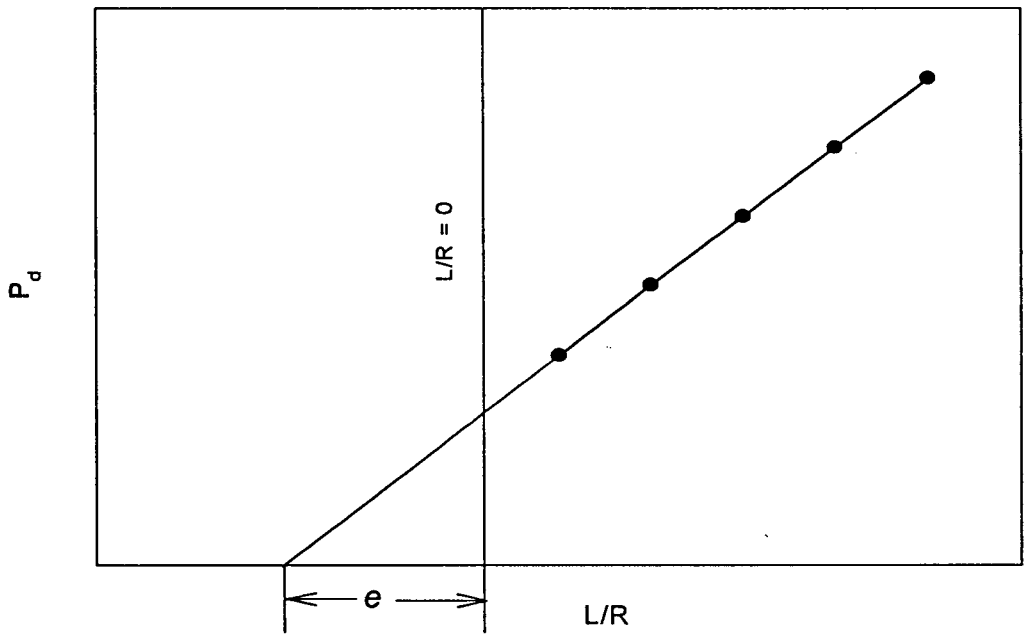


Figure 2.8. Bagley plot for determining the end correction for capillary flow.

The wall shear rate can be determined by using the following equation.

$$\dot{\gamma}_w = \left(\frac{3+b}{4}\right)\dot{\gamma}_A \tag{2.25}$$

where $\dot{\gamma}_A$ is the apparent wall shear rate, $\dot{\gamma}_w$ is the wall shear rate and $b$ is the Rabinowitch correction given by Eq. (2.26).

$$b \equiv \frac{d(\log \dot{\gamma}_A)}{d(\log \sigma_w)} \tag{2.26}$$

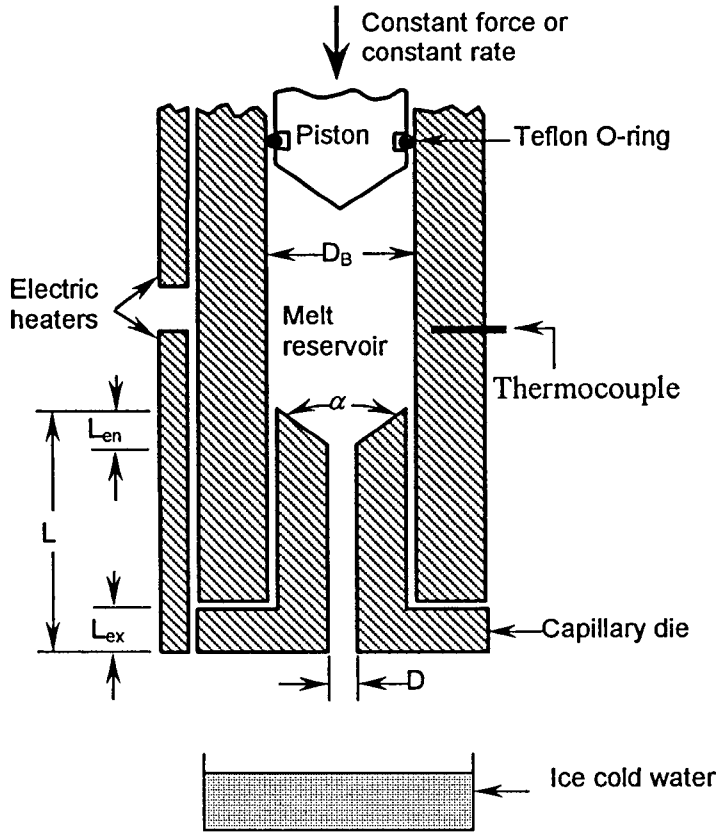


Figure 2.9 Schematic of a capillary rheometer [Baird and Collias (1995)].

# 3. EXPERIMENTAL SECTION

In this section, the complex thermorheological behavior of a blend of high $T_g$ constituents viz. poly(styrene-co-maleic anhydride)/poly(methyl methacrylate) is investigated in a variety of shear rates using capillary and oscillatory shear measurements, especially in the vicinity of phase separation temperature. The extrudates obtained at numerous shear rates are characterized by Differential Scanning Calorimetry and Scanning Electron Microscopy.

## 3.1 MATERIALS

The random copolymer of styrene and maleic anhydride (SMA), containing 32% by weight maleic anhydride was provided by DSM. Poly(methyl methacrylate) (PMMA), incorporating 10 wt% copolymerized ethyl acrylate was provided by ICI; this polymer contains ca. 0.75 wt% of lubricating agent plus ca. 0.25 wt% each of thermal and UV stabilizers. The molecular characteristics of both polymers, along with their zero-shear viscosities at 205 °C (as indicative values for comparison) are presented in Table I below.

| Polymer | $M_w$ | $M_w/M_n$ | $T_g$ (°C) | $\eta_0$ at 205 °C (Pas) |
|---|---|---|---|---|
| SMA | 130,000 | 2-2.5 | 175 | 560,000 |
| PMMA | 100,000 | 2 | 105 | 33,000 |

**Table 3.1:** Molecular characteristics of the homopolymers used for the SMA/PMMA blends.

Before any use, the SMA was dried in a vacuum oven at 80°C for about 12 hours. SMA/PMMA blends, of different weight compositions, varying from 10% SMA (10/90) to 80% SMA (80/20), were prepared by two different methods: (i) solution casting, and (ii) melt mixing. The former procedure involved dissolution of the appropriate amounts of SMA and PMMA in a common solvent butanone (concentration about 10%) and slow evaporation under vacuum, starting from room temperature and increasing the temperature gradually (in order to avoid bubble formation) up to 120°C. The whole procedure lasted about one week. The obtained blends were stored in $N_2$ atmosphere before use, to avoid moisture adsorption due to the hygroscopic nature of SMA. In the latter case, SMA and PMMA were blended in a twin screw extruder. The melt temperature varied between 208°C – 213°C, depending on the composition in order to avoid phase separation. For all compositions prepared by melt mixing, a screw speed of 100 rpm was employed, yielding an output of 8 lb/hr.

## 3.2 METHODS

### 3.2.1. Shear rheometry

A Rheometric Scientific controlled strain rheometer (model ARES, equipped with a dual range force rebalance transducer, 2KFRTN1) and Rheometrics system IV were utilized in the parallel plates geometry (25 mm diameter, 1 mm sample thickness), with air convection temperature control (accuracy ±0.1°C). Measurements were carried out under $N_2$ atmosphere to prevent any adsorption of moisture and/or degradation at high temperatures. Some measurements were also carried out in the cone-and-plate geometry

(25 mm diameter, 0.04 rad cone angle) and yielded identical dynamic results with the parallel plate mode. The small amplitude oscillatory shear measurements performed with each sample included:

(i) Dynamic time sweeps at a given temperature and frequency (from 0.05 rad/s to 10 rad/s), in order to obtain steady state and thus to ensure that measurements were performed under "dynamic equilibrium" conditions;

(ii) Dynamic strain sweeps at a given temperature and frequency (0.01 rad/s to 100 rad/s), in order to determine the limits of linear viscoelasticity (typical strains used were about 5% and never exceeded 20%);

(iii) Isochronal dynamic temperature ramps (at a given low frequency in the terminal regime) by increasing the temperature from the homogeneous to the phase separated regime, at a certain strain in the linear regime (5% to 20%) and heating rate (0.1°C/min to 1°C/min), in order to determine the temperature dependence of the linear viscoelastic properties of the blend in the flow regime with emphasis on the vicinity of phase separation;

(iv) Isothermal dynamic frequency sweeps from 0.01 rad/s to 100 rad/s at a given linear strain (5% to 50%) in order to investigate the linear viscoelastic material functions over the whole accessible frequency range, across the phase diagram.

### 3.2.2. Capillary Rheometry

An Instron piston-driven constant speed capillary rheometer bearing a load cell of 5000 lbs, and a barrel of diameter of 3/8" was used. Circular dies of various diameters (D=0.254, 0.756 and 1.27 mm) and length-to-diameter ratios (L/D=0, 10, 20 and 40) were

used to generate a variety of shear rates for the capillary extrusion experiments. All dies had a 45 degree entrance angle. Before extrusion, all blends were vacuum dried at 80 °C for more than 12 hours, to avoid complications from humidity, since SMA is hygroscopic; the samples were immediately loaded into the barrel to minimize moisture absorption. The time required to reach steady state was determined by the geometric characteristics of the die (D and L/D) as well as from the operating apparent shear rate. Most experiments were conducted with an aspect ratio L/D=10 (D=0.254 mm), so as to generate high shear rates at accessible piston speeds and measurable pressure loads.

Extruded samples corresponding to different temperatures at one shear rate were obtained using the capillary apparatus. The extrudates corresponding to steady state only, were quenched immediately in ice cold water in order to freeze the polymer molecules and consequently to avoid any further morphological changes. The quenched extrudates were subsequently analyzed with morphological and rheological studies. In-between two consecutive shear rates, the piston speed was lowered and the extrudates corresponding to intermediate shear rates were discarded.

### 3.2.3. Differential Scanning Calorimetry

Two calorimeters, one from TA Instruments (model V4.1C) and another from Rheometric Scientific (model PL-DSC) were used at steep temperature ramps (20 °C/min) to capture the glass transition ($T_g$) in the thermograph of various samples examined. The method followed for DSC measurements are as follows; First the sample (10-20mg) was heated

from room temperature to above $T_g$. This temperature was maintained for 3-5 minutes in order to get rid of the thermal history of the sample. Then, the sample (heated cell) was quenched on an ice cube wrapped in aluminum foil. However, quenching was avoided for extrudates in the vicinity of metastable region as it resulted in the loss of phase separation. Before any DSC measurement, all samples were vacuum dried at 80 °C, for a minimum of 8-12 hrs.

### 3.2.4. Scanning Electron Microscopy (SEM)

The extruded blend morphologies were investigated using a Hitachi S-2300 scanning electron microscope, for fractured samples in frozen water and coated with 50/50 gold palladium to avoid charging. A special diamond knife was utilized for cutting smooth sections of the extrudates.

# 4. RESULTS AND DISCUSSION

## 4.1. Glass transition behavior

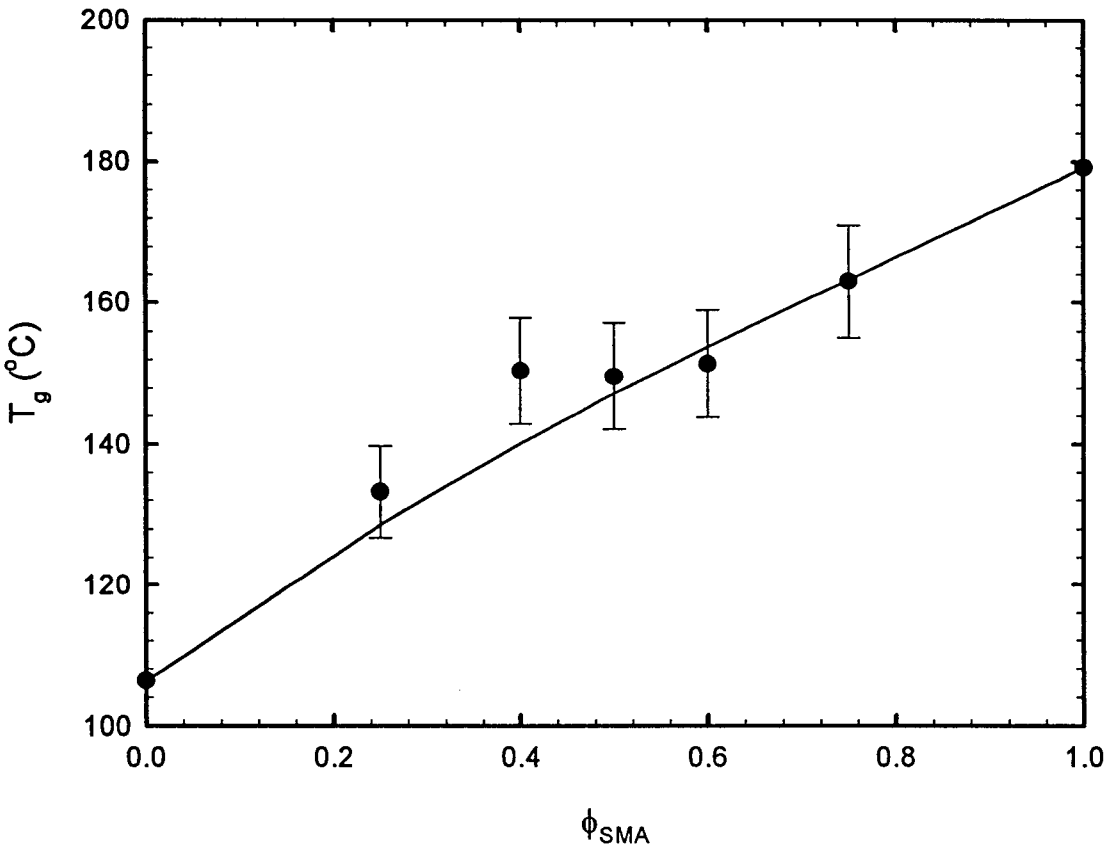


Figure 4.1. Composition dependence of the glass transition of SMA/PMMA (●) The solid line represents the fit with the Gordon-Taylor-Kwei equation (see text).

Since both components of the SMA/PMMA blend exhibit high $T_g$'s, which are actually not very far from the coexistence curve [Vlassopoulos (1996), Vlassopoulos *et al.* (1997), Utracki (1990)], it is important to determine the glass transition of the blend; this was

achieved with DSC measurements. Typically, in the case of single-phase blends DSC yields in a single transition, whereas for phase-separated blends two distinct transitions are observed. Measurements were carried out by quenching to eliminate the effects of thermal history, followed by the application of a steep linear temperature ramp (20°C/min). Given the experimental error, no significant difference between solution cast and melt mixed samples was detected. Figure 4.1 depicts the variation of the blend's glass transition temperature with composition. The meaning of the error bars is to denote the range of $T_g$ rather than the effect of experimental error.

For all compositions, a positive deviation from the linear behavior is observed. The Gordon-Taylor-Kwei empirical equation, shown below, was found to provide a fairly good fit to the data [Utracki (1990)]:

$$T_g = \frac{w_1 T_{g1} + k w_2 T_{g2}}{w_1 + k w_2} + q w_1 w_2 \qquad (1)$$

where the subscripts 1 and 2 refer to the two components, $w_i$ refers to the weight fraction of component i, q is a fitting parameter representing the extent of enthalpic interactions in the blend, and $k \approx T_{g1}/T_{g2}$ . This equation was successfully used to describe the glass transition behavior of polymer mixtures involving glassy components in the past [Utracki (1990), Friedrich *et al.* (1996)]. From Figure 4.1, the fitted value of q is 65 K, for a fixed value of k=1.62; this suggests strong enthalpic interactions (exothermic) in the blend. Strong intermolecular interactions in SMA/PMMA blends arising due to the polar nature of the components have also been reported earlier [Feng *et al.* (1995)].

Figure 4.2 depicts typical DSC thermographs for a homogeneous (a) and a phase-separated (b) blend, both quenched immediately after extrusion to preserve their respective phase state, and indicating one and two glass transitions, respectively. However, as it will be discussed below, DSC alone is not enough of an evidence to detect the phase state of a mixture.

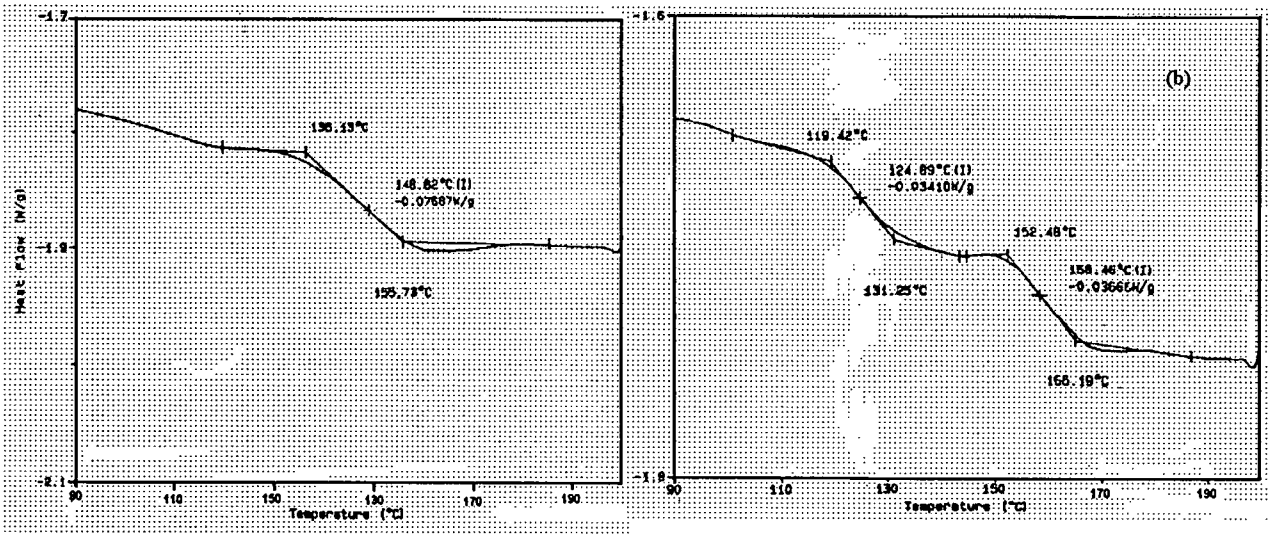


Figure 4.2. Characteristic DSC curves indicating (a) one glass transition or a homogenous SMA/PMMA blend and (b) two glass transitions in the regime of immiscibility.

## 4.2. Shear rheology

### 4.2.1. Time-Temperature Superposition

Rheological properties are usually highly temperature dependent. This means that to obtain a complete picture of the behaviour, experiments must be carried out at several temperatures. It is often found that data taken at several temperatures can be brought

together on a single master curve by means of "time-temperature superposition." This greatly simplifies the description of the effect of temperature. Furthermore, it makes possible the display on a single curve of material behavior covering a much broader range of time or frequency than can ever be measured at a single temperature. Materials whose behaviour can be displayed in this way are said to be "thermorheologically simple" [Dealy and Wissbrun (1990)].

It was found that data for different temperatures can often be superposed by introducing a shift factor, $a_T$, determined empirically. Thus, if one makes a plot of a rheological property versus time, $a_T$ is obtained from the horizontal shift necessary to bring the data for any temperature $T$ onto the same curve as data for temperature $T_0$. For example, flow curves (shear stress vs. shear rate) will be plotted as shear stress versus $\dot{\gamma}\, a_T$. Note that no shift factor is required for quantities not containing units of time. This implies that a plot of one such quantity versus another will be temperature independent.

Despite the marked dependence on molecular structure of the relation between $a_T$ and absolute temperature, nearly general empirical relations have been derived by expressing the temperature for each material in terms of its glass transition temperature $T_g$ or some nearly equivalent reference temperature. Among the most successful of these relations is the Williams-Landel-Ferry (WLF) equation [Williams (1955), Tanner (1985)]:

$$\log(a_T) = \frac{-C_1^0(T - T_0)}{C_2^0 + (T - T_0)}$$

where $C_1^0$ and $C_2^0$ are constants determined at $T_0$ for each material. This equation holds over the temperature range from $T_g$ to about $T_g$ + 100K. The constants are related to free volume [Billmeyer (1984)].

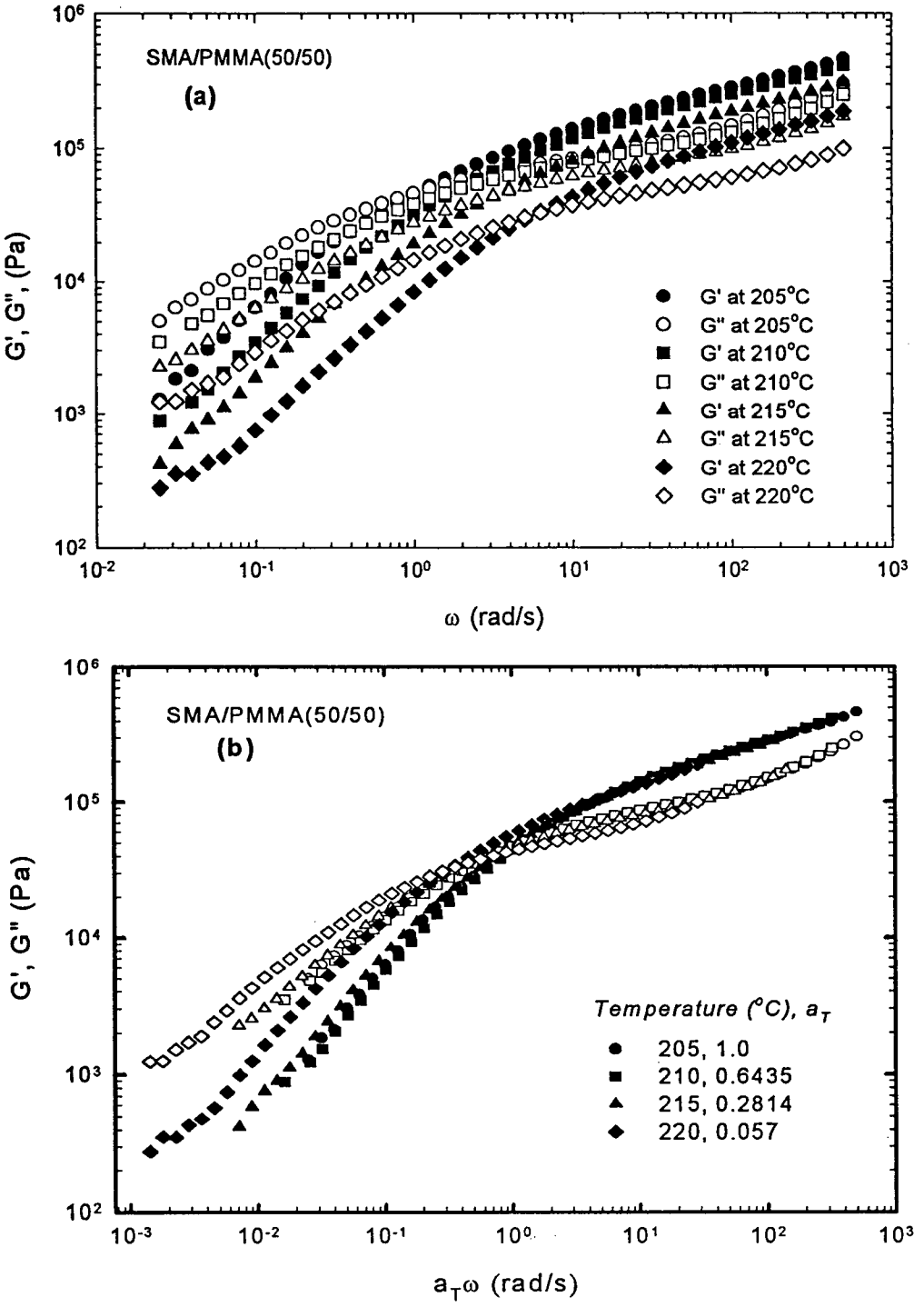


Figure 4.3. (a) Characteristic curves of G' and G'' for a 50/50 SMA/PMMA blend at various temperatures (b) Master curves of G' (closed symbols) and G'' (open) showing a failure of the time-temperature superposition principle.

The data obtained for G' and G" at various temperatures are plotted in Figure 4.3(a). The same data is shifted to obtain the master curve with 205°C as reference temperature in Figure 4.3(b). The failure of time-temperature superposition is usually attributed to morphological changes. The phase separation of SMA and PMMA was associated with the thermorheological complexity of the blend, as already known from several relevant investigations [Vlassopoulos (1996), Vlassopoulos *et al.* (1997), Kapnistos *et al.* (1996a,b)]. A characteristic example is illustrated in Figure 4.3(b), which depicts the master curves of G' and G'' (in the linear viscoelastic region) of a 50/50 SMA/PMMA blend for a wide range of temperature from the well homogeneous (205°C) to the clearly phase separated regimes (220°C); it is clear that in the present case the temperature of 215°C signifies the failure of the time-temperature superposition principle, and relates to the occurrence of the phase separation.

Due to the strong effects of enhanced concentration fluctuations in the homogeneous pretransitional region, the demixing temperature was determined from a combination of the master curves from frequency sweeps and dynamic temperature ramps at low frequencies and very low heating rates (to ensure that the results are independent of the heating rate); an example of the latter is depicted in Figure 4.4 for several blends. It is clear that the observed change of slope in the (more sensitive) G' versus temperature plot occurs at a (heating rate independent) temperature of 215°C, and thus this temperature is taken as the demixing temperature of the 50/50 blend. It has been observed in the past that as the phase separation is approached, there is an increase in G' which is due to

concentration fluctuations effects, i.e. to the formation of dynamic regimes rich in the high-modulus polystyrene component [Kapnistos *et al.* (1996)].

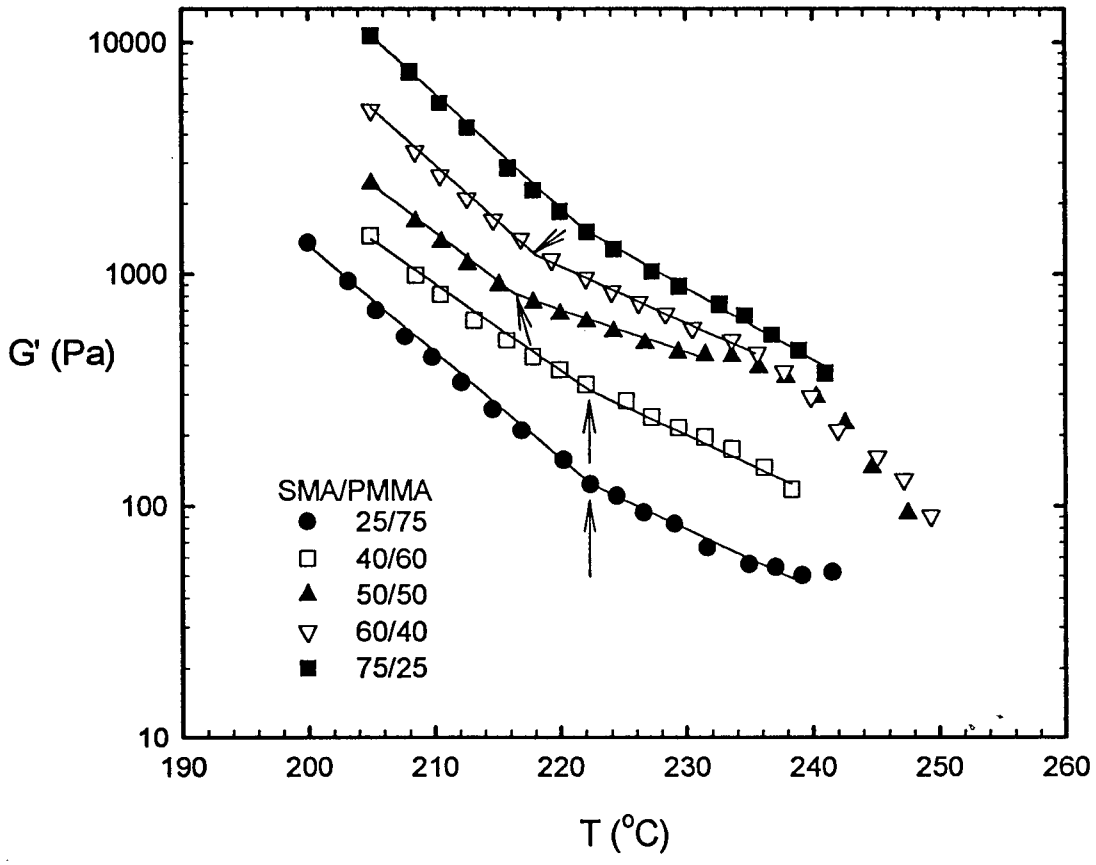


Figure 4.4. Typical dynamic temperature ramps of the storage modulus for the SMA/PMMA blend at different compositions, frequency $\omega$=1 rad/s and strain amplitude 2%. Lines are drawn to guide the eye. Arrows indicate the rheologically determined demixing temperature from the first change of slope, as the blend is heated with a rate of 2°C /min.

By following this procedure for different compositions, it is possible to obtain the phase diagram (coexistence curve) of the blend (Figure 4.5). It is further noted, that the quantitative account of the effects of enhanced pretransitional concentration fluctuations in inducing extra viscoelastic stress, can yield the spinodal curve as well, as already established in the literature [Vlassopoulos (1996), Vlassopoulos *et al.* (1997), Kapnistos *et al.* (1996a,b)]. One issue of importance here is the potential influence of the method of preparation of the blend on the phase behavior; this is due to two main problems: (i) in solution cast samples, even under the best possible methods for solvent evaporation, there is some minute amounts of residual solvent trapped in the polymer molecules, and (ii) in melt mixed samples, and in particular for highly viscous and high-$T_g$ polymers (such as those investigated in this work), the mixing of polymers may not be satisfactory at length scales of the order of the interdiffusion (compared to the solution cast samples).

Using these justifications, several investigations in the literature have reported unambiguous differences in the coexistence curves between the two types of mixtures [Brannock *et al.* (1991)]. In the present case, the viscoelastic moduli exhibited clear differences, i.e., G' for melt-mixed systems was higher than that of solution-cast blends by roughly a factor of 2 (see also Figure 4.10 below); however, the corresponding differences in the rheologically determined demixing temperatures, when observed, were very small, within the experimental error, and thus the method of preparation did not affect the phase diagram of Figure 4.5. On the other hand, there is an unambiguous shift of the moduli G' and G'', under the same measurement conditions, resulting from the different method of sample preparation (seen for example, in Figure 4.10 discussed

below); this suggests that whereas the method of blend preparation influences the viscoelastic moduli, it does not affect their sensitivity to thermodynamics, and thus the rheologically determined phase diagram, within the experimental error of the rheological measurements at least in this high $T_g$ system.

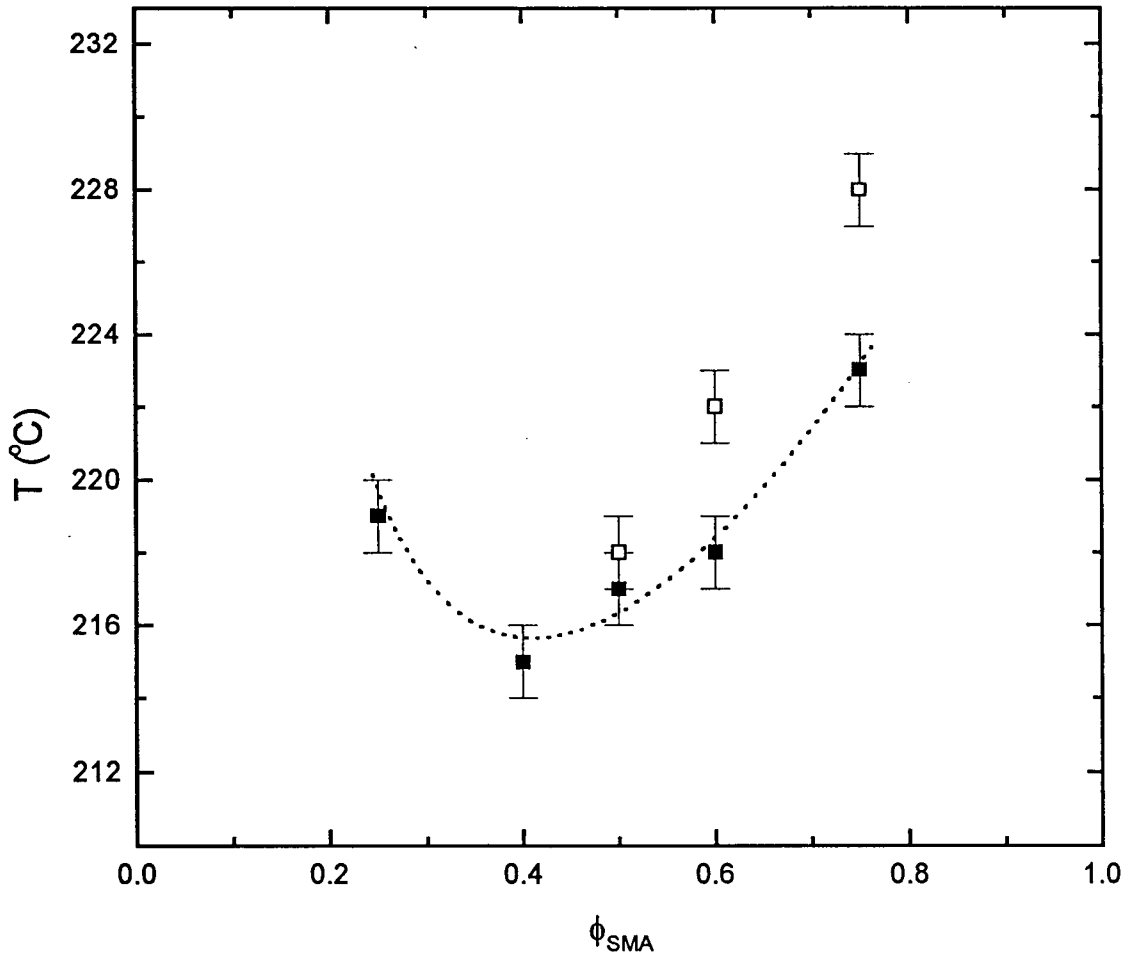


Figure 4.5. Rheologically determined quiescent phase diagram of the SMA/PMMA blend; ■: data points from dynamic temperature ramps and frequency sweeps for melt mix blends; □: for solution cast. Dashed line is drawn to guide the eye.

## 4.3. Capillary rheology

The more thoroughly studied blend is the SMA/PMMA 50/50. This polymer blend, which demixes at about 215°C (see Figure 4.5), has a very high viscosity at 205°C (about $1.5x10^5$ Pas; see also Table 4.1) and it is rather difficult to process it effectively, given the fact that above 240°C significant degradation problems might occur.

The apparent flow curve of this blend obtained from capillary experiments at various temperatures is depicted in Figure 4.6.

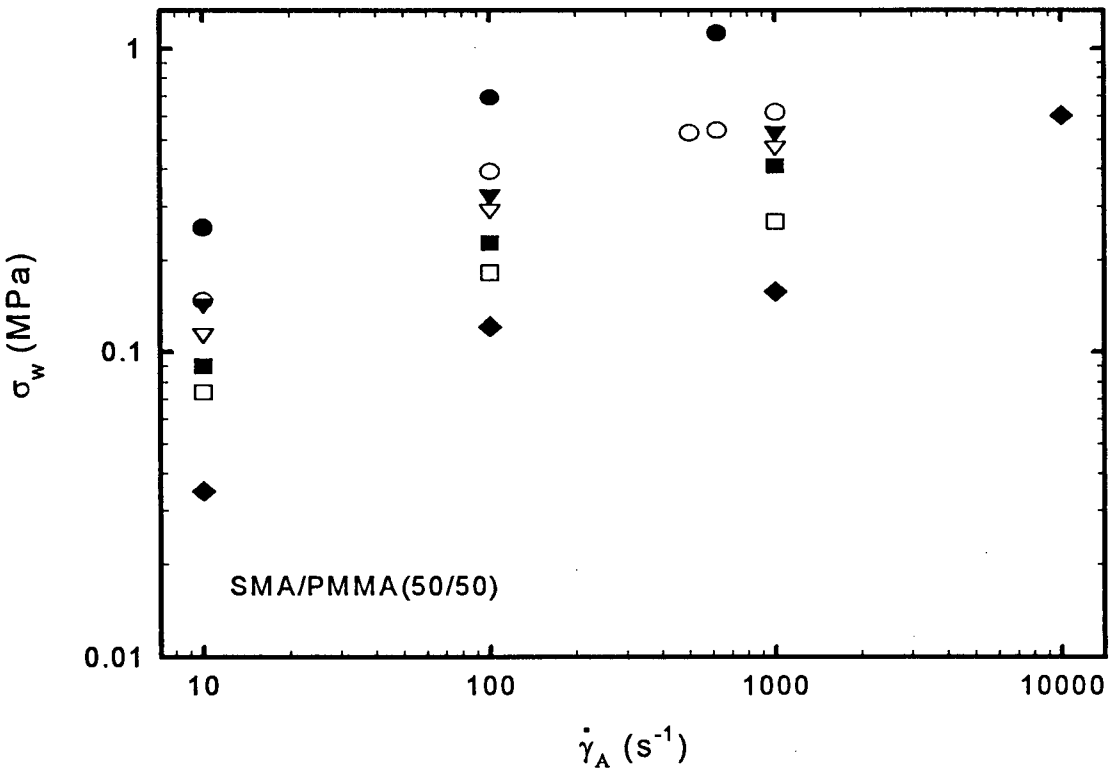


Figure 4.6. Capillary flow curves (shear stress versus apparent shear rate with Bagley correction) of SMA/PMMA 50/50 blend at different temperatures: ●: 200°C ; ○: 210°C; ▼: 215°C ; ▽: 220°C ; ■: 225°C ; ❑: 230°C ; ◆: 240°C.

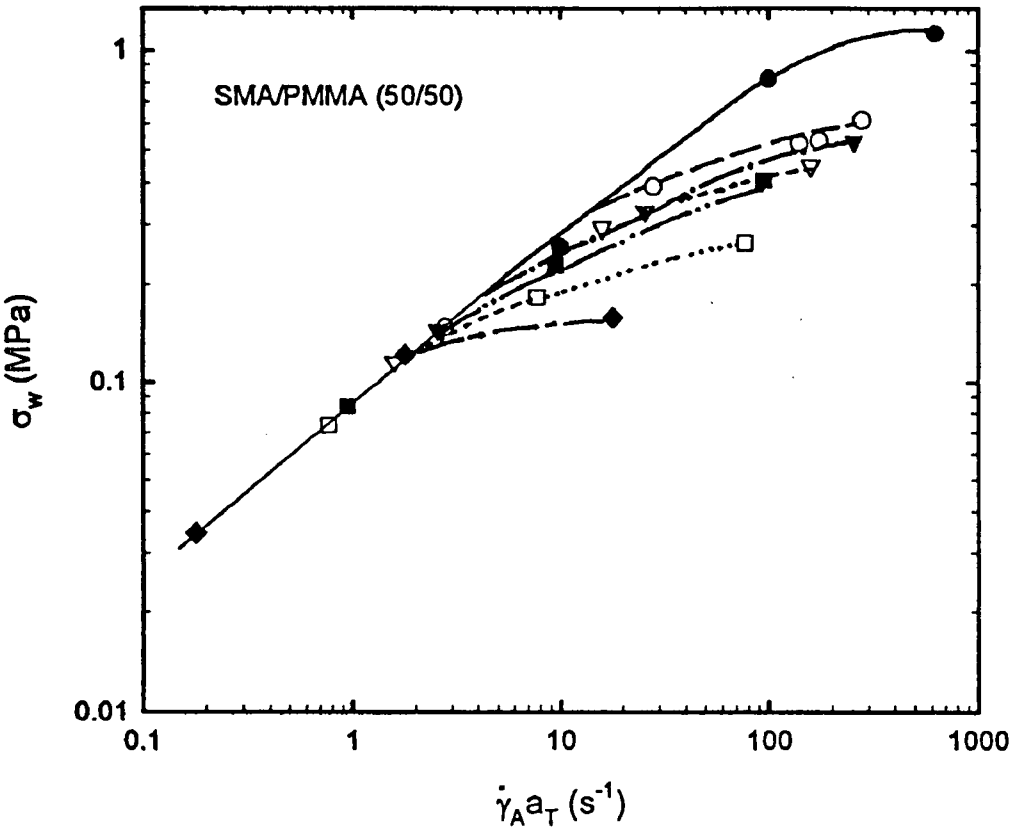


Figure 4.7. Shifted capillary "master" flow curves of SMA/PMMA 50/50 blend of Figure 6, with $T_{ref}$=200°C. Symbols are the same as in Figure 4.6. Solid line in the low shear rate region of perfectly superposed data is drawn to guide the eye.

The shear stress, $\sigma_w$, is defined as $(\Delta P-\Delta P_{End})/(4L/D)$, where $\Delta P$ is the total pressure drop required for capillary flow and $\Delta P_{End}$ represent the pressure drop due to the polymer flow in the entrance and exit regions of the capillary [Dealy and Wissbrun (1990)]. The latter is referred to as Bagley correction and in this study was determined by means of an orifice die (L/D=0). On the other hand, the apparent shear rate, $\dot{\gamma}_A$, is defined as $4Q/\pi D^3$, where

Q is the volumetric flow rate. This quantity represents the true shear rate only for a Newtonian fluid [Dealy and Wissbrun (1990)]. It is noted that on increasing the temperature typically above 215 °C, at high shear rates (typically above 10 $s^{-1}$), there is a deviation from the linear stress-rate relationship (on a log-log scale), associated with fluid-flow nonlinearities and shear thinning.

The superposed data using the principle of time-temperature superposition, much like in shear rheometry, as already discussed by Kazatchkov *et al.* (1995) are presented in Figure 4.7. It is evident from Figure 4.7 that the time-temperature superposition principle fails at higher shear rates (above 10 $s^{-1}$) and temperatures above 215°C. This may be attributed to two reasons. First, to the melt fracture of the blend, which is manifested as visual distortions on the surface of the extrudate [Hatzikiriakos *et al.* (1992)], as well as to the decay in shear stress with time, which becomes more dominant at higher temperatures. Wall slip might also play a role here. It is known that slip increases with temperature and this is the reason that the data corresponding to higher temperature deviate more in Figure 4.7 [Kazatchkov *et al.* (1995)]. The second reason that provides the leading interpretation to the data of Figures 4.6 and 4.7 relates to the phase behavior of the SMA/PMMA blend. Here we have assumed that the change in slope of the flow curve and the lack of superposition observed in figures 4.6 and 4.7 are not primarily due to slip at the wall, but rather to thermodynamic effects; the latter are present and known to influence the rheology of the blend substantially [Vlassopoulos (1996)]. Based on the superposed data of Figure 4.7, this change in slope can clearly be seen to occur in the temperature range

between 210 and 215°C, which is the temperature range associated with phase separation, as detected by the small amplitude oscillatory shear experiments discussed above.

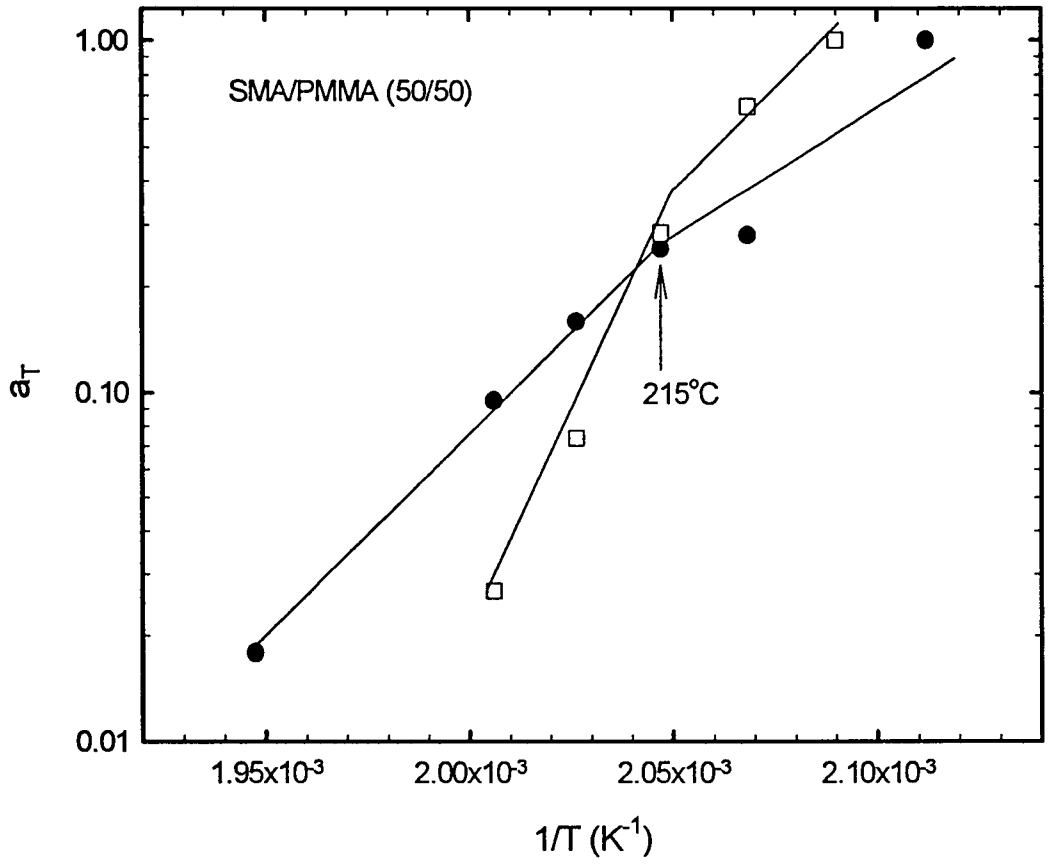


Figure 4.8. Temperature dependence of shift factors for SMA/PMMA 50/50, indicating Arrhenius dependence. Small-amplitude oscillatory shear data ($T_{ref}$=205°C): ❑ ; capillary data with Bagley correction ($T_{ref}$=200°C): ●. The lines are drawn to indicate the slopes (dashed: oscillatory data ; solid: capillary data) in the homogeneous and phase-separated regions. The arrow indicates the temperatures of 215°C, associated with phase changes, as discussed in the text.

The shift factors from both the small-amplitude oscillatory and capillary shear data are depicted in Figure 4.8, and shown to follow Arrhenius behavior in both the homogeneous and phase separated regions. However, the corresponding activation energies in the two regions, as well as in the two sets of experiments (oscillatory and capillary shear), are drastically different. This is apparently due to the fact that in the oscillatory shear data, each shifted frequency sweep curve corresponds to the same phase state of the blend, i.e., equilibrium deformations; on the other hand, this is not the case for each shifted capillary flow curve, where at different shear rates the phase state of the blend might change, as discussed below. However, it is interesting to note that for the specific example of SMA/PMMA 50/50 of Figure 4.8, a change of slope in the Arrhenius shift factor, as the temperature increases, occurs at 215°C in the oscillatory data, which is the quiescent demixing temperature, and in the range of 210-215°C in the capillary data, which is the corresponding range of shear-modified demixing temperature for this blend (see also Figure 4.13 below and relevant discussion).

It is noted that, given the uncertainty due to the limited data available, the slopes (activation energies) are about the same in the homogeneous regime for the oscillatory and capillary shear data, as expected; on the other hand, they are clearly different in the two-phase regime, compared to the homogeneous one, but also different in the two experiments. This is attributed to the phase separation, as well as to the different deformation of the phase-separated morphologies induced by oscillatory or capillary shear.

## 4.4. Extrudate analysis

In order to further elucidate the interplay between capillary flow and thermodynamics, we examined the extrudates from different capillary extrusion runs corresponding to different apparent shear rates. Setting for a moment aside potential complications from flow instabilities (manifested as visual defects, especially at high shear rates) and interfacial phenomena (wall slip), a given extrudate represents the result of a "shear-induced" effect on the SMA/PMMA blend, originally sheared at different rates and temperatures across the phase diagram. Extrudates were analyzed with three different means:

(i) visual observations: Samples resulting from shear-induced mixing were transparent, whereas shear-induced demixing yielded opaque extrudates. There were limiting cases, however, where visual observation alone was not sufficient in order to assess the thermodynamic state of the extrudate, and thus further analysis, as discussed below, was necessary. Additional information was provided by scanning electron microscopy (SEM). Figure 4.9 depicts a typical SEM picture of a sheared SMA/PMMA 50/50 blend at 220°C and 100 $s^{-1}$. The picture in the axial direction of the extrudate, i.e., along the flow direction, is shown in Figure 4.9a, whereas the cross section of the extrudate is depicted in Figure 4.9b. It is clear that for this specific case the flow resulted in phase-separated extrudates (as judged by the dark SMA-rich and bright PMMA-rich regions); moreover, there is unambiguous evidence of domain orientation along the flow direction, i.e., the softer (lower $T_g$) PMMA-rich domains elongate and form large cylinders or filaments (Figure 4.9a), a process which is also helped by the large viscosity difference of SMA and PMMA.

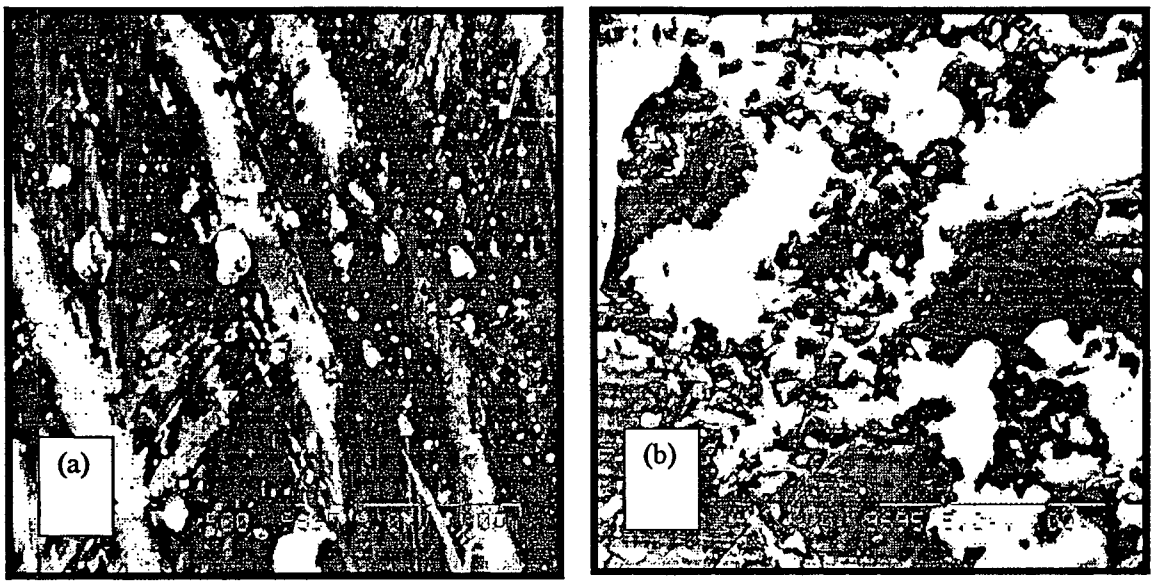


Figure 4.9. SEM images of SMA/PMMA 50/50 samples extruded at 220°C and 100 $s^{-1}$ (a) image of the section cut along the extrudate long axis and the direction of flow ; (b) image of the cross section of the extrudate.

Based on the SEM analysis, and in corroboration with the large viscosities and $T_g$'s of the two phases, there is no evidence whatsoever of a shear mechanism analogous to droplet deformation and break-up, which can describe for instance phase changes in blends of nearly inelastic and low viscosity and $T_g$ polymers [Vinckier *et al.* (1996)]. Instead, the interaction of the elongated filaments with each other and with the matrix seem to determine the final phase state of the sheared blend under certain shear rate and temperature; this kind of shear-induced interdiffusion is significantly affected by the strong intermolecular interactions between the phenyl groups in SMA and the carbonyl groups in PMMA [Feng *et al.* (1995)], which in turn are also affected by the shear. This picture suggests a mechanism for shear-induced structural changes different from the

conventional droplet break-up and coalescence which describes molecular mixtures [Onuki (1989)] and blends of low viscosity inelastic polymers [Vinckier *et al.* (1996)].

(ii) DSC analysis: Extrudates corresponding to the homogeneous regions yielded one $T_g$ when subjected to DSC runs; on the other hand, samples well into the two-phase region (corresponding to shear-induced demixing) were characterized by two distinct $T_g$'s (for example see Figure 4.2). The transitions in the thermographs of blends which were clearly either single-phase or phase-separated (as judged by the full extrudate analysis discussed here) ehxibited nearly the same breadth with those of the pure components. On the other hand, there were cases where DSC analysis alone was insufficient to provide unambiguous information on the phase state of an extruded sample, since it resulted in one broad transition (much broader than either of the pure components [Karatasos *et al.* (1998)]; such cases correspond to blends near their phase boundary, possessing dynamic heterogeneities either in the two-phase or in the single-phase regime [Kumar *et al.* (1996), Meier *et al.* (1998)], and the phase state was determined with additional information from shear rheology and SEM, as discussed below.

(iii) Shear rheology: One complication from cases (i) and (ii) above resulted when opaque samples yielded a single $T_g$. The question raised was whether these samples should be classified as homogeneous or phase-separated blends. This problem was present only in samples sheared at high temperatures, and apparently relates to the degradation taking place above 230°C , especially in the SMA component. The latter is much more susceptible to degradation than PMMA, which is perceived as reasonably stable. Upon

heating above 230°C, SMA turns dark yellow and eventually (with time) brown; besides the change of color, degradation is mainly reflected as a chain scission, with evident implications to dramatic reduction in the viscoelastic moduli. To examine the potential degradation, we carried out dynamic frequency sweeps of the "suspect" extrudates in the linear viscoelastic limit and compared against the results obtained with the "virgin" blend at the same conditions.

Figure 4.10 depicts the G' for four typical cases for the same blend composition and temperature (210°C): (i) "virgin" melt-mixed ; (ii) "virgin" solution-cast ; (iii) no substantial degradation, i.e., sample extruded at 240°C and 11,250 $s^{-1}$ (which was immediately quenched and then measured at 210°C); and (iv) substantial degradation, , i.e., sample extruded at 270 °C and 50,625 $s^{-1}$.

On the other hand, it is worth noting that the extruded quenched samples of the same composition, show all nearly the same sensitivity to thermodynamics, within experimental error, independently of the degree of degradation, as demonstrated with the temperature ramps of the storage modulus, depicted in Figure 4.11; it is clear that despite some differences in the slopes, the unambiguous change of slope (associated with the demixing temperature) occurs at about the same temperature for all samples. Based on these investigations, a slightly turbid extrudate with a single $T_g$, but not broader than the one resulting from the homogeneous virgin blend, and with essentially unchanged linear viscoelastic properties, is classified as marginally homogeneous.

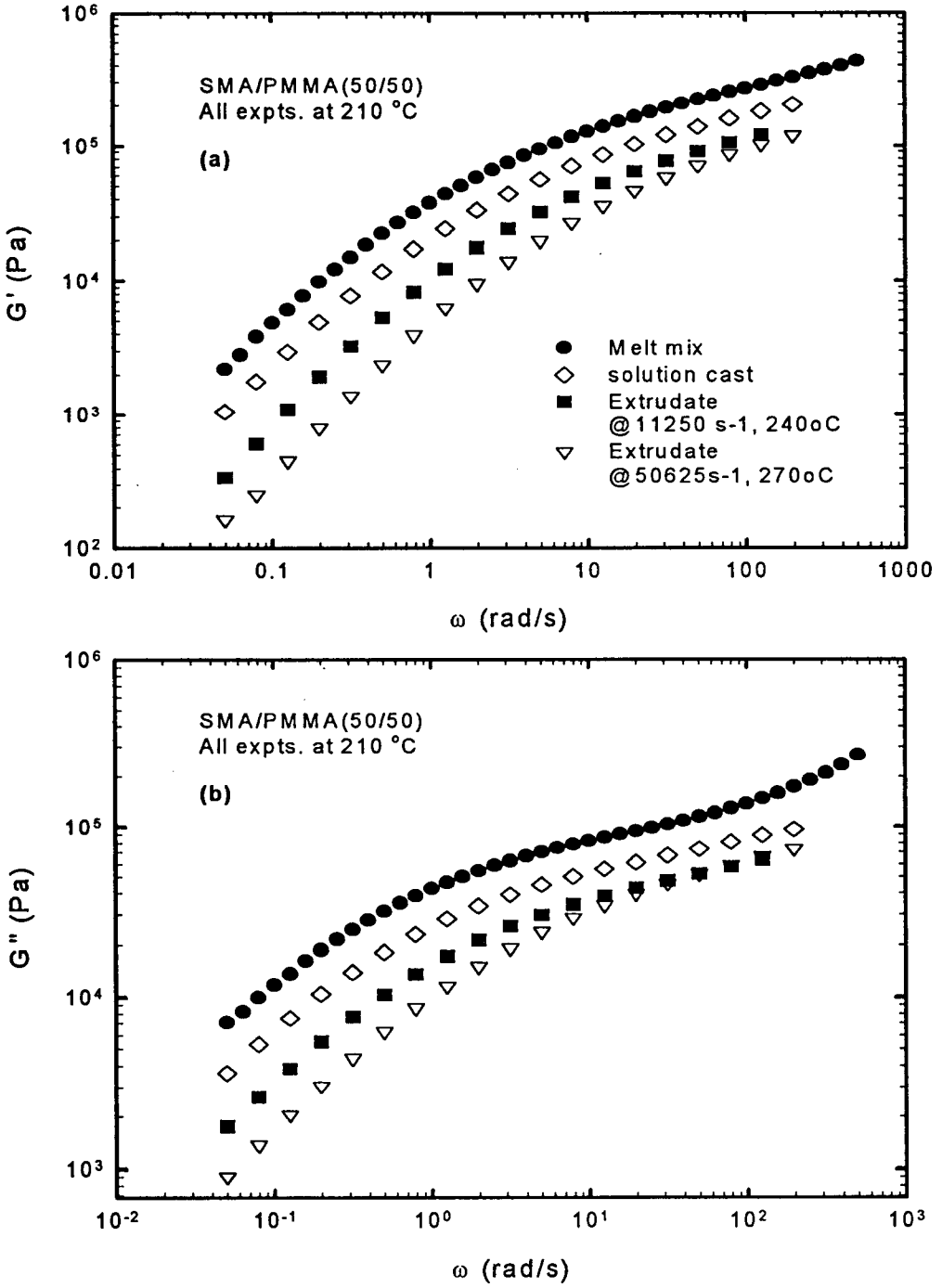


Figure 4.10. Comparison of linear viscoelastic moduli, G' (a) and G'' (b), from dynamic frequency sweeps, for different samples of SMA/PMMA 50/50 at the same temperature (210°C), obtained in different ways.

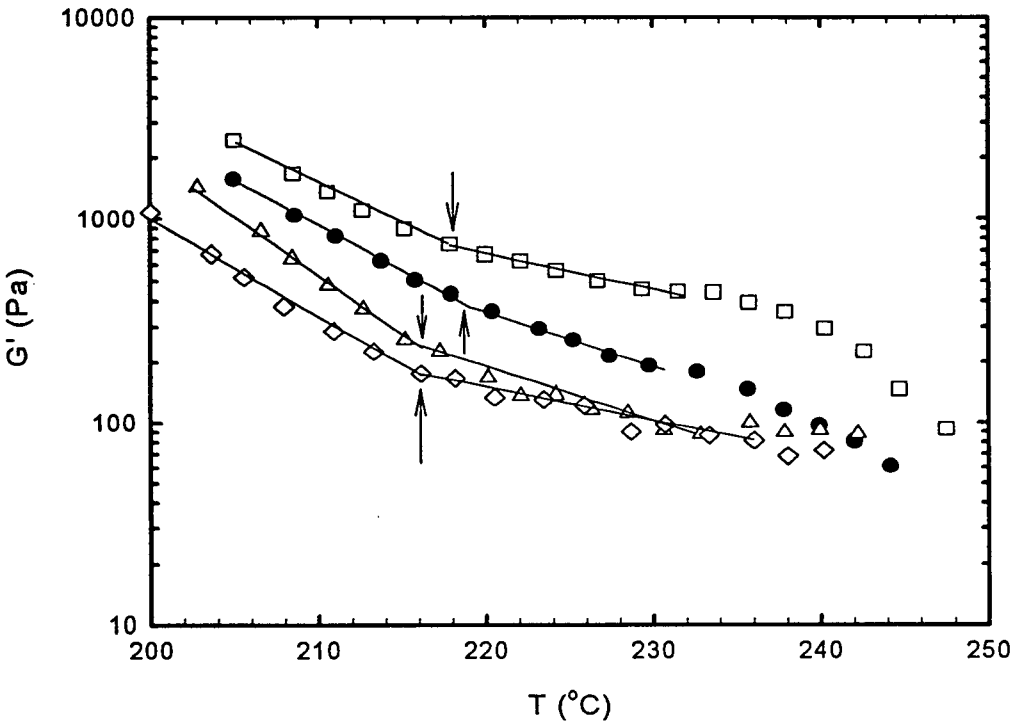


Figure 4.11. Dynamic temperature ramps of G' for various SMA/PMMA 50/50 samples, at 0.5°C/min, 0.05 rad/s and strain amplitude 2%: "virgin" melt-mixed sample: ❑ ; sample extruded at 230°C and 1,000 $s^{-1}$: ●; sample extruded at 240°C and 11,250 $s^{-1}$: Δ; sample extruded at 270°C and 50,625 $s^{-1}$: ◊ .

## 4.5. Shear-induced phase diagrams

Based on the above considerations concerning the characteristics of the extrudates, as well as the dependence of the shear stress on temperature in the capillary studies (seen for instance in Figure 4.12 for various SMA/PMMA compositions, where a clear change of slope is observed at temperatures associated with phase separation) for different shear rates, and in consistency with the DSC and visual observation results, phase diagrams of the SMA/PMMA blend at different shear rates were constructed (Figure 4.13).

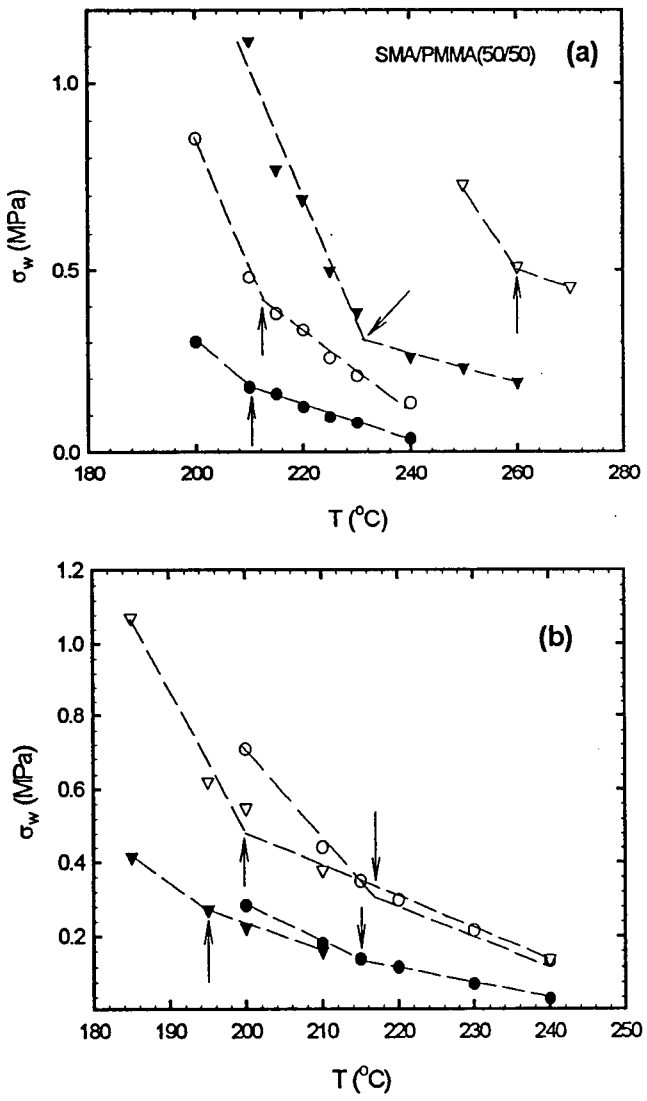


Figure 4.12. Temperature dependence of the shear stress for various shear rates: (a) SMA / PMMA 50/50 (●:10 $s^{-1}$ ; ○: 100 $s^{-1}$; ▼: 1,000 $s^{-1}$; ∇: 10,000 $s^{-1}$) ; (b) SMA/PMMA 40/60 (●:10 $s^{-1}$ ; ○: 100 $s^{-1}$) and SMA/PMMA 25/75 (▼:10 $s^{-1}$ ; ∇: 100 $s^{-1}$). Lines are drawn to guide the eye and indicate the change of slope.

First of all, it is noted that the combination of the DSC analysis of the opaque extrudates with the composition dependence of the $T_g$ of the homogeneous blend in Figure 4.1, yields the coexistence points as follows: each of the two (time-independent) $T_g$'s resulting from the originally 50/50 blend, represents the soft and hard phases, and each of these phases is considered as compositionally homogeneous [Karatasos *et al.* (1998)]. Then, for these SMA-rich and PMMA-rich phases we can back up their composition from Figure 4.1. By following the same procedure for different nominal compositions of SMA/PMMA, it is possible to obtain the coexistence curves of this blend, as shown in Figure 4.13. The fact that the extracted compositions of the SMA-

rich and PMMA-rich phases obey the lever rule of thermodynamics, confirms the validity of this approach. It is evident from Figures 4.12 and 4.13 that the effect of shear on the phase behavior of SMA/PMMA is significant and clearly detected, but on the other hand it is rather complex. As a general trend, at low SMA compositions (typically $\varphi_{SMA}<0.25$), shear-induced mixing takes place, followed by shear-induced demixing at moderate compositions, and finally mixing again at $\varphi_{SMA}>0.65$, depending on the amount of shear.

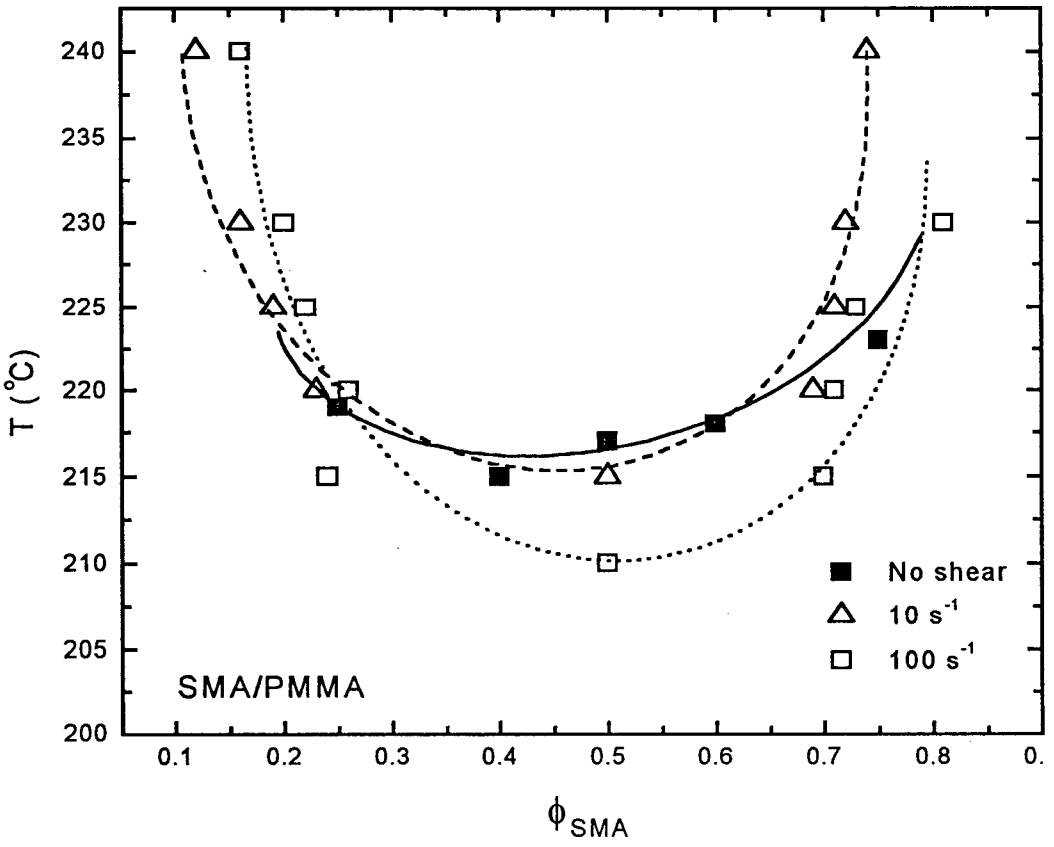


Figure 4.13. Phase diagrams of SMA/PMMA for various shear rates. Lines are drawn to guide the eye.

The nonmonotonicity of shear-induced structural changes is clearly illustrated in Figure 4.14 for a 50/50 SMA/PMMA blend, where based on the above considerations the shear-phase diagram shows both shear-induced demixing at low and moderate shear rates and shear-induced mixing at high shear rates and different temperatures.

It is remarkable to note the very high shear rates reached; thus, these results have direct implications to industrial processing conditions, in which typical deformation rates of 200 $s^{-1}$ and higher are encountered [Utracki (1990), Dealy and Wissbrun (1990)]. It is noted in this respect that most of the limited relevant studies, even with commercial blends, were carried out at rates below 10 $s^{-1}$. The only exception is the work of Aelmans and Reid (1996), who investigated a 20/80 SMA/PMMA blend (of different grade from the present one) at shear rates up to 25,000 $s^{-1}$; although the difference in these commercial blends renders a comparison, even qualitative, ambiguous, it is fair to say that our results are in reasonable qualitative agreement with those reported by Aelmans and Reid (1996), under similar process conditions.

Referring to Figure 4.14(a), the shaded area corresponds to extrudates of different degrees of degradation, as discussed before; although these samples clearly show characteristics of single phase, and seem consistent with the above mentioned analysis of flow-induced structural changes, because of the degradation the data points are not considered as "certain" of the rest, and are therefore shaded with the dotted lines in the plot. Figure 4.14b summarizes the results on the effect of shear on the quiescent demixing

temperature, $T_{d,quiescent}$, for three different SMA/PMMA compositions, namely 50/50, 25/75 and 60/40; the relative deviation $\Delta T/ T_{d,quiescent} = (T_{d,shear} - T_{d,quiescent})/ T_{d,quiescent}$ from the quiescent demixing temperature is plotted against the apparent shear rate, and the shear-induced mixing and demixing is evident.

To explain qualitatively the observed multitude of phenomena presented above, i.e., both shear-induced mixing and shear-induced demixing, one can consider the phenomenological approach based on the generalized Gibbs free energy of mixing, as discussed in detail in Section 5.1.

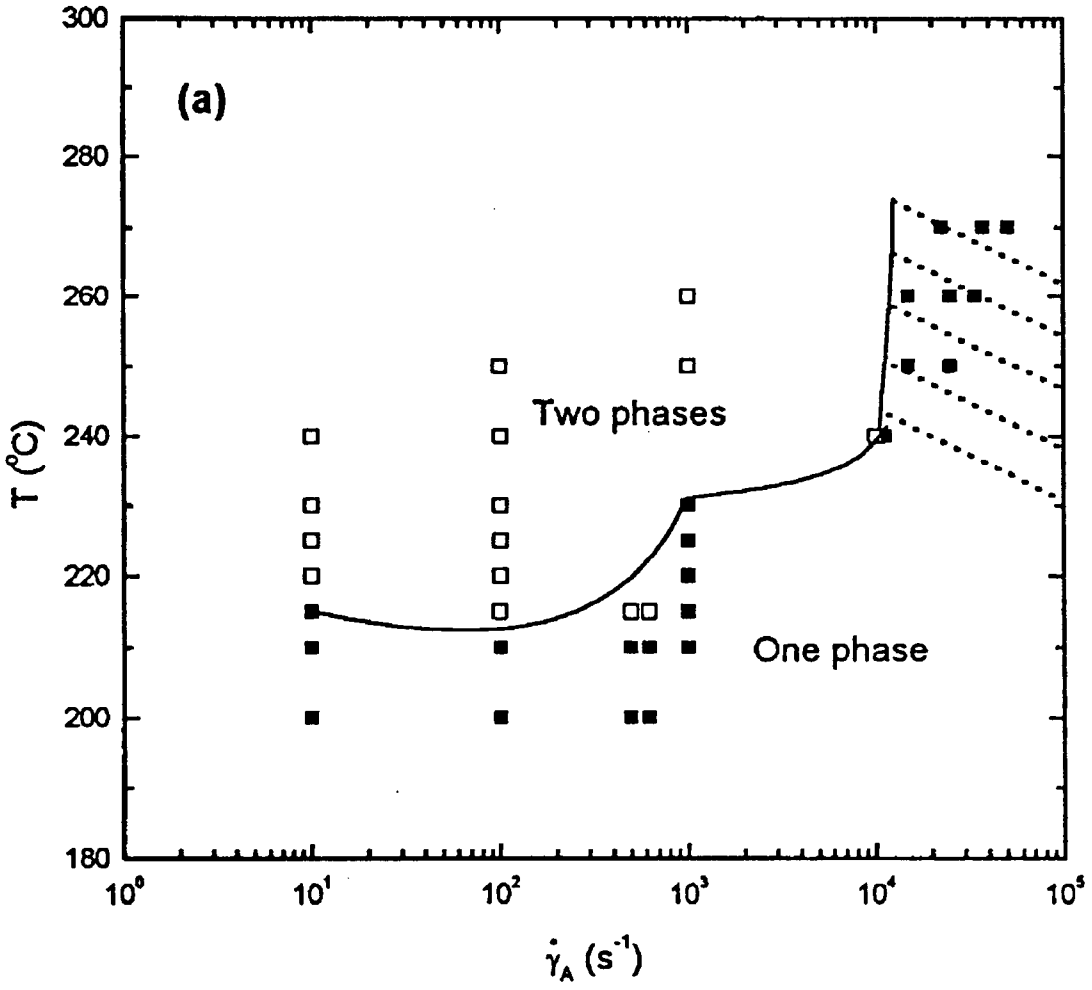

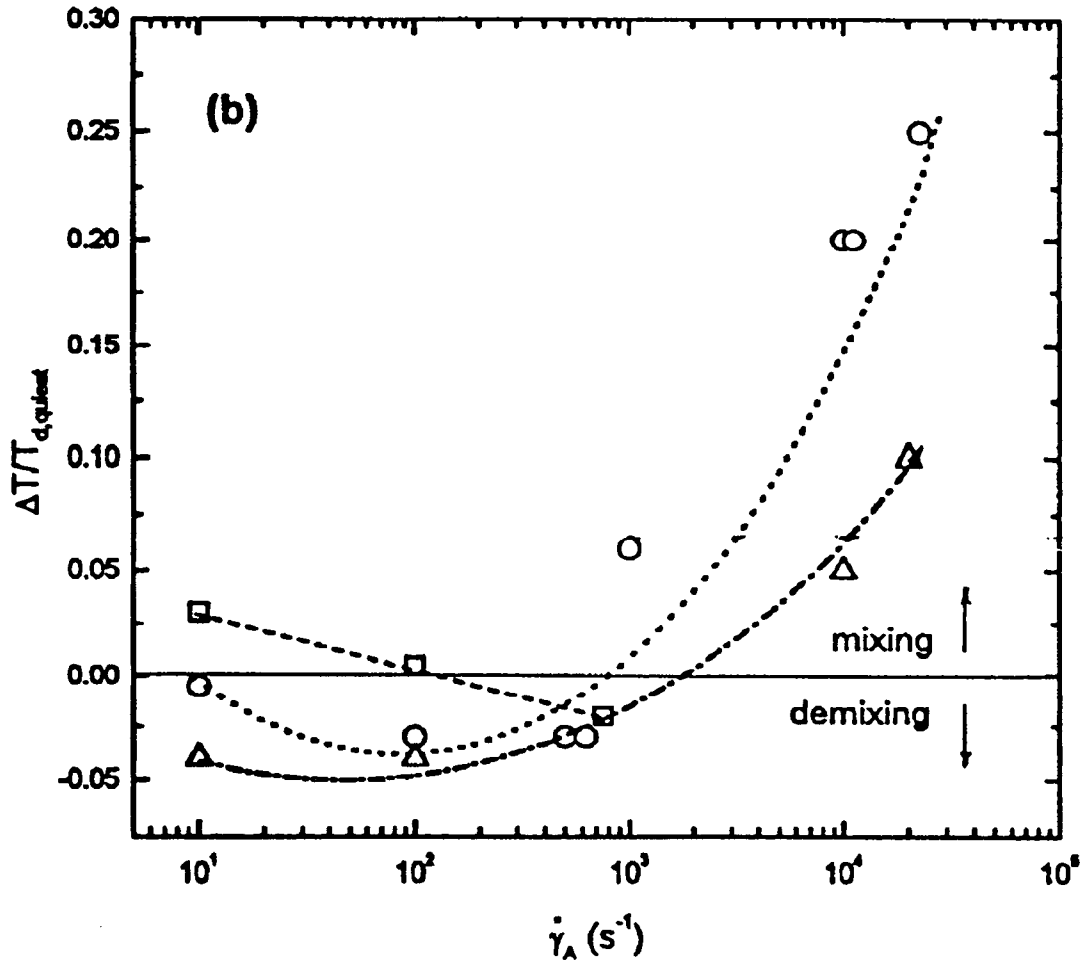


Figure 4.14. (a) Shear-phase diagram of 50/50 SMA/PMMA blend at various emperatures. Open squares indicate measurements corresponding to phase separated extrudates, and closed squares to homogeneous extrudates. The line is drawn to guide the eye. The high shear rate region shaded with dotted lines represents data corresponding to degraded extrudates (b) Representation of shear effects on phase state, as in (a), for different SMA/PMMA blends (50/50: ○ ; 25/75: Δ ; 40/60: ❑), in terms of deviation from the quiescent demixing temperature ($\Delta T=T_{d,shear}-T_{d,quiescent}$).

## 4.6. Dynamics

The SMA/PMMA 50/50 blend was kept at a constant temperature in a capillary rheometer, and was extruded after varied time intervals. Thus, the evolution of the two phases till the "dynamic" equilibrium was reached was examined. The shear stress decreased with increasing time (Figure 4.15a), apparently due to morphological changes and relaxations in the blend, which are especially evident in immiscible systems due to the on-going kinetics of spinodal decomposition. Increased fluctuations in shear stress during capillary extrusion at 240°C were observed in comparison to 220°C. The phase-separated domains at 240°C are apparently larger than at 220°C, and the corresponding difference in the viscosity of these domains is related to these fluctuations.

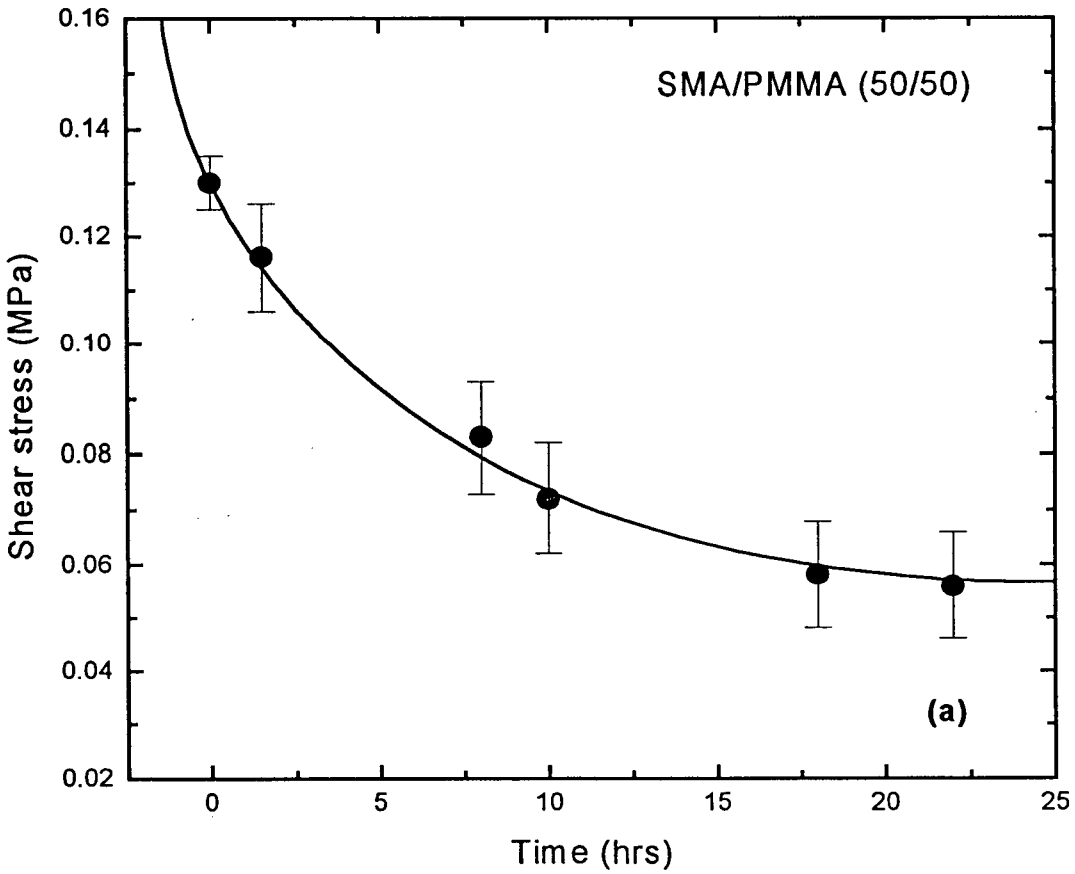

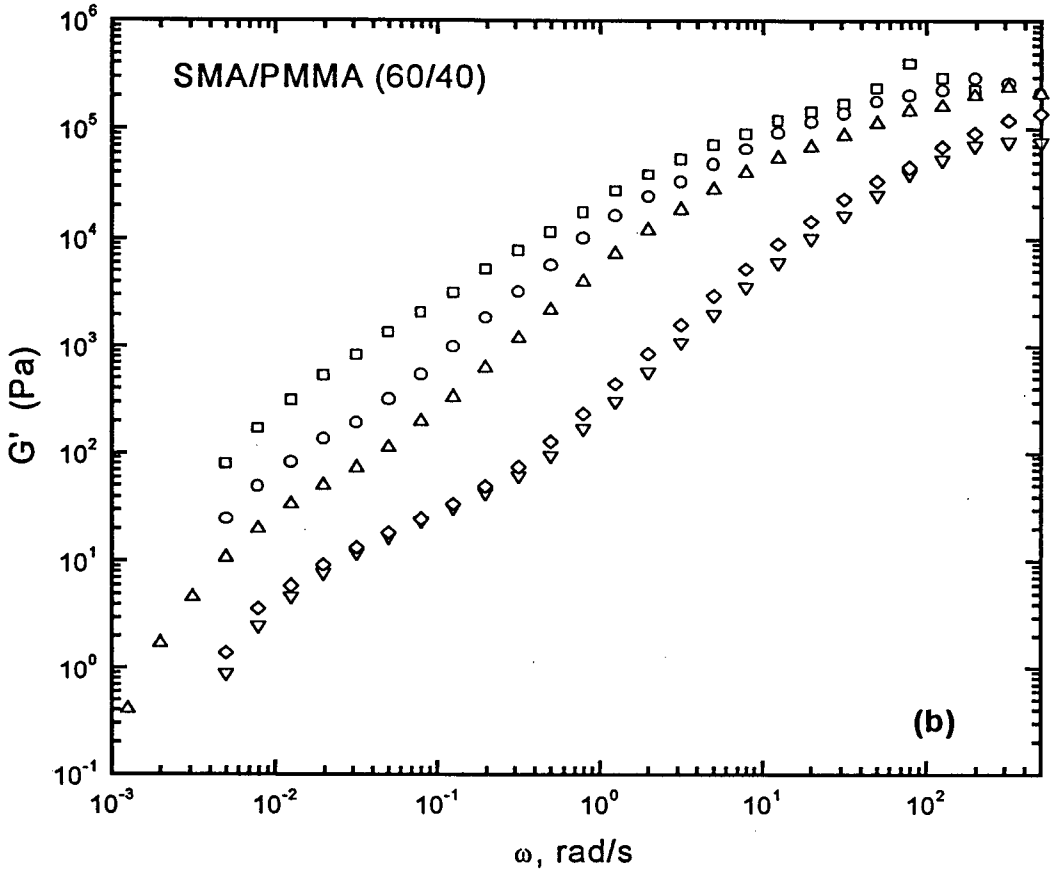


Figure 4.15. (a) Time evolution of shear stress in capillary rheometry for SMA/PMMA 50/50 at 240°C (●) ; line is drawn to guide the eye. (b) Time evolution of storage modulus in small-amplitude oscillatory shear data for SMA/PMMA 60/40 at 240°C (times: ❑: 0 s ; ○: 3 hrs ; Δ: 5 hrs ; ∇: 14 hrs ; ◊: 21 hrs).

On the other hand, DSC results of the phase-separated (opaque) extrudates, taken at different times, till the blend degrades, reveal two distinct $T_g$'s. The DSC study indicates that the composition of the two domains is independent of time. However, extrudates associated with a residence time of about 26 hours and above turn amber, showing single $T_g$. In such a case, a structural transformation in SMA has taken place, and in particular

degradation (chain scission). These results are consistent with the corresponding dynamic results from small-amplitude oscillatory shear measurements obtained at different times in phase-separated systems; a typical example for a SMA/PMMA 60/40 blend at 240°C is depicted in Figure 4.15b. The time for obtaining "dynamic steady state" is actually the same (about 20 hours), and the combination of the capillary and oscillatory shear results suggests that the reduction of stress with time is apparently due to a combination of degradation and morphological changes (spinodal decomposition); concerning the latter effect, analogous observations with dynamic frequency sweeps of PS/PVME blends were reported by Polios *et al.* (1997).

Concerning the effects of the phase diagram on the rheological properties, it has been already shown that the change in morphology occurring when the phase boundary is crossed, is manifested as a discontinuity in the slope of moduli versus temperature. Hence, one doesn't need to wait for steady state (as discussed above) to detect the temperature of phase separation in small amplitude oscillatory shear experiments. However, the two-phase rheology cannot be accurately quantified if the "dynamic" steady state is not reached.

# 5. THERMODYNAMIC MODELING OF SHEAR-INDUCED PHASE CHANGES

In this chapter, a simple general thermodynamic model is presented for predicting the shear-induced phase changes in polymer fluids. It is based on the established concept of generalized Gibbs free energy of mixing, with an extra entropic storage term due to flow. The latter term is related to the conformational changes of the polymer chains due to flow, via the first normal stress difference or the viscoelastic storage modulus. The general energy analysis is carried out within the framework of Flory's statistical mechanical lattice model. As such, this approach provides some insights with respect to the configurational changes of a polymer fluid subject to shear flow, and thus to the molecular origins of shear-induced structural changes. Moreover, the model is universal with respect to its applicability to different kinds of polymeric fluids, such as solutions and blends. Theoretical predictions of the phase diagrams under shear agree reasonably well with selected experiments with the systems polystyrene/dioctyl phthalate and poly(styrene-co-maleic anhydride)/poly(methyl methacrylate).

## 5.1. Development of the model

We consider a polymer mixture (solution or blend) containing $n_1$ moles of one component (polymer or solvent) and $n_2$ moles of the other component. The well-known Flory-

Huggins [Flory (1953)] equation for the Gibbs free energy of mixing polymer solution in the absence of flow, reads [Fast (1968), Strobl (1996)]:

$$\Delta G_M = \Delta H_M - T\Delta S_M = R\,T\,(n_1 \ln \phi_1 + n_2 \ln \phi_2 + \chi_{12}\,\phi_1\,\phi_2 N) \qquad (5.1)$$

with $\Delta S_M = k \ln \Omega_{12} - k \ln \Omega_1 - k \ln \Omega_2 = -R\,(n_1 \ln \phi_1 + n_2 \ln \phi_2)$

and $\Delta H_M = Vzm\phi_1\,\phi_2/v = \mathrm{RT}\chi_{12}\,\phi_1\,\phi_2$

Where $k$ is the Boltzmann constant, V is the total volume, z is the coordination number, m is the exchange energy, and v is the volume of one cell. The quantity zm/kT is often called the Flory interaction parameter $\chi_{12}$, but there are other definitions as well [Olabisis (1979)]. Careful experiments have shown $\chi_{12}$ to be a function of temperature, composition, and molecular weight distribution of the polymer; thus it has lost its simplistic classification of "parameter". However, PS/DOP system has been modeled in the past [Rangel-Nafaile *et al.* (1984)], taking into account only temperature dependent $\chi_{12}$.

For PS/DOP analysis $\chi_{12}$ is defined as $\chi_{12}=1/2+\psi\,(1-\theta/T)$ with $\psi$ and $\theta$ constants depending on the polymer system. In the above expressions defined by Eq. 1, $\Omega_1$ is the number of the possible configurations of $n_1$ moles, $\Omega_2$ is the number of the possible configurations of $n_2$ moles, and $\Omega_{12}$ is the total number of possible configurations of the polymer mixture. The volume fractions occupied by components 1 and 2 are $\phi_1$ and $\phi_2$ respectively. The expression for the spinodal temperature for a polymer solution can be

obtained by imposing condition given by Eq. (2.3) on Eq. (5.1) [Flory (1953), Rangel-Nafaile (1984)],

$$T = \frac{2\phi_2 \psi \theta}{\phi_2(2\psi - 1) + \frac{1}{\phi_1} - (1 - \frac{1}{r})}$$

where $r$ is the ratio of the molar volumes of polymer to solvent. It may be noted that a similar expression for polymer blends can also be derived [Bates (1991)] (Also see Eq.(5.20)).

### 5.1.1. The Gibbs Free Energy of Mixing in the Presence of Shear

Upon applying shear, it can be intuitively thought that some polymer configurations in a lattice are more preferred. In general, polymer chains will prefer to align in the direction of flow. Thus, an adjacent cell downstream of one containing a polymer segment is very likely to also contain a segment of the same chain. Therefore, a chain step in this direction should receive a weighting factor near unity. Similarly, it is unlikely that the chain will step against the flow field. Upstream steps therefore receive weighting factors near zero.

To better illustrate the main ideas of our approach, let's consider arranging $h^2$ non-identical balls in a square lattice of $h$ edge units, which has cells weighted in a random fashion (Figure 5.1).

| | | |
|---|---|---|
| 1 | ½ | 1 |
| 1/3 | ¼ | 1/8 |
| 1/2 | 1/6 | 1/5 |

Figure 5.1. Representation of the lattice model with randomly weighted cells.

It is assumed that some cells are more preferred. Despite the weighted asymmetry of the lattice, the manner in which the lattice is filled does not affect the total number of ways to arrange the particles in the lattice. Filling the lattice by rows or by columns yields the same number of possible configurations. We can now extend this result to a lattice of infinitely long edges containing a binary polymer solution. In a cubic lattice, a polymer molecule in a cell can move in any of the six directions, positive or negative, in a three dimensional space. The weight vector associated with the $n$th cell can therefore be written as, $w_n = [w_x, w_y, w_z]$, where $w_x$, $w_y$, $w_z$ are the components of the weight vector in $x$, $y$, and $z$ direction, respectively. The polymer in a particular cell tends to move in the direction of applied shear. The influence of the direction of the velocity on the weight vector needs to be considered. We can define a scalar quantity called the velocity-corrected weight of the cell ($w_v$), by taking the dot product of the weight vector with the unit vector ($\hat{n}$) in the

direction of the applied shear, $w_v = \underline{w_n}.\hat{n}$, where $\hat{n} = \frac{\underline{v}}{|\underline{v}|}$, and $\underline{v}$ is the velocity vector associated with the polymer solution under the application of shear. The multiplicity for such a lattice is then given by,

$$\Omega_{12}^{*} = \frac{N.w_{v1}.[(N-1).w_{v2}].[(N-2).w_{v3}].....[1.w_{vn}]}{m_1!rm_2!} \tag{5.2}$$

where, $\Omega^{*}_{12}$ is the total number of polymer chain configurations under shear, $N$ is the total number of cells in the lattice, $w_{vi}$ is the weight vector associated with the $i$th cell, $m_1$ and $m_2$ are the number of solvent and polymer molecules in the lattice, and $r$ is the number of repeating units in a polymer molecule. Eq. (2) can be rewritten as,

$$\Omega_{12}^{*} = \prod_{i=1}^{N} \frac{(N-i+1).w_{vi}}{m_1!rm_2!} \tag{5.3}$$

Since, $\Omega_{12} = \prod_{i=1}^{N} \frac{(N-i+1)}{m_1!rm_2!}$, where $\Omega_{12}$ is the total number of possible configurations in the absence of shear, the following simple result can then be obtained from Eqs. (5.2) and (5.3):

$$\frac{\Omega_{12}{}^{*}}{\Omega_{12}} = \prod_{i=1}^{N} w_{vi} \tag{5.4}$$

The product of the weighting factors in Eq. (5.4) yields a scalar quantity, which we call $w = \prod_{i=1}^{N} w_{vi}$, the total weight of the system or the lumped weighting factor in the presence of shear. Now, let us consider a square lattice of $h$ edge units. The $h$ units can be a properly normalized diameter in the case of flow in a pipe, or a properly normalized distance between parallel plates in case of planar Couette flow. The total number of configurations under shear, $\Omega^*_{12}$, is given by Eq. (5.4) written in terms of the lumped weighting factor $w$. Experimental observations place clear limits on the possible values that $w$ may take [Hobbie *et al.* (1994)]. These are the following:

(i) $w = 1$, for system under no shear.

(ii) $0 < w < 1$, in case of steady shear, with $w \to 0$, as the level of shear tends to infinity.

Flow inputs energy into the binary polymer solution. A part of this energy is dissipated due to the viscous nature of the polymer, and the rest is stored by the system components (mainly polymer chains). The stored energy, $E$, increases the end-to-end distance of the polymer molecules, as well as promotes orientation in the direction of the flow. Hence, there is an overall increase in order that results in a decrease of the system entropy. In terms of Eq. 5.4, shear causes a decrease in the total number of system configurations. Thus, if $\Omega$ represents the multiplicity under no shear, and $d\Omega$ the decrease in the multiplicity under the application of shear, then $\Omega$ - $d\Omega$ will be the new number of possible configurations. The stored energy restores the original state of the polymer upon removal of shear stress. For an incompressible lattice (i.e. no $pdV$ work), the change in the internal energy ($dE$) of the polymer solution under shear is given as,

$$dE = TN_0\, dS = kTN_0\, d\ln\Omega \tag{5.5}$$

where T is the absolute temperature, and $N_0$ is the Avogadro's number. Integrating Eq 5.5, one obtains the following result:

$$\int_{\Omega_{12}}^{\Omega_{12}^*} d\ln\Omega = \frac{1}{kTN_o}\int_{E_0}^{E} dE$$

$$\Omega_{12}^* = \Omega_{12} e^{\Delta E / kTN_o} = \Omega_{12} w \tag{5.6}$$

where $\Omega^*_{12}$ is the multiplicity in the presence of shear, $\Omega_{12}$ is the multiplicity in the absence of shear, and $\Delta E$ is the change in the internal energy of the system, which must be less than zero for the process to occur (chain orientation).

Eq. (5.6) gives the total number of configurations at steady state. It states that the decay in the total number of configurations is given by a Boltzmann-type distribution. Also, the lumped weighting factor $w$, is observed to be a state function that depends only on the temperature and the internal energy change of the system. A change in the total number of configurations that causes a change in the phase diagram, is possible only if the system is capable of changing its entropy. Finally, Eq (5.6) implies that as thermal energy ($kT$) tends to infinity, the total number of possible configurations will become insensitive to shear, while at increasingly lower temperatures, the total number of possible configurations under shear becomes much less than that in the absence of shear.

In the case of simple shear of a polymer solution or melt, where all the cells undergo equal deformation, the weight of each cell $w_n$ is the same. However, in the case of pipe flow, the weight of each cell is different because the shear rate is zero at the centerline and takes its highest value at the wall [Dealy and Wissbrun (1990)].

The dependence of weight on $\Delta E$ (change of the internal energy of the system) is shown in Figure 5.2. At high shear rates the total number of possible configurations is reduced significantly. The value of the weight increases for a particular value of $\Delta E$ as the temperature of the polymer solution is increased. In other words, at higher temperatures it becomes increasingly difficult to reduce the total number of possible configurations in the presence of shear.

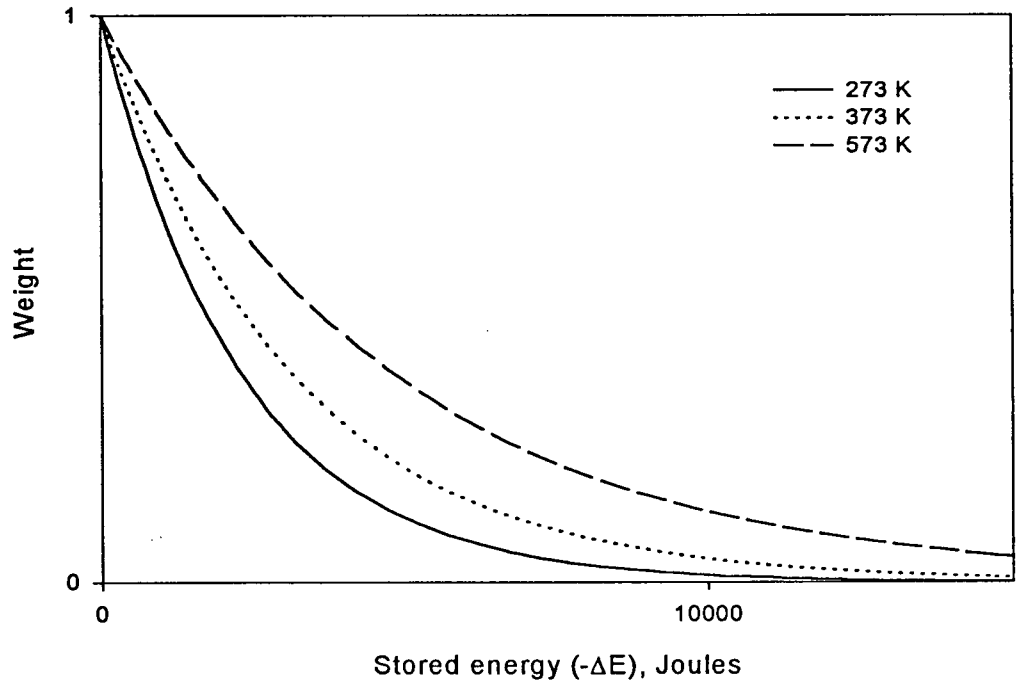


Figure 5.2 The dependence of the statistical weight of the unit cell (number of possible configurations) on the system internal energy, at different temperatures.

The dependence of weight on temperature (thermal energy) is shown in Figure 5.3. At a particular temperature, the value of weight decreases with increasing value of stored energy. Thus at constant temperature, increasing the shear reduces the total number of possible configurations. Both trends are consistent with the experimentally observed effects of shear on polymer solution morphology [Rangel-Nafaile *et al.* (1984)].

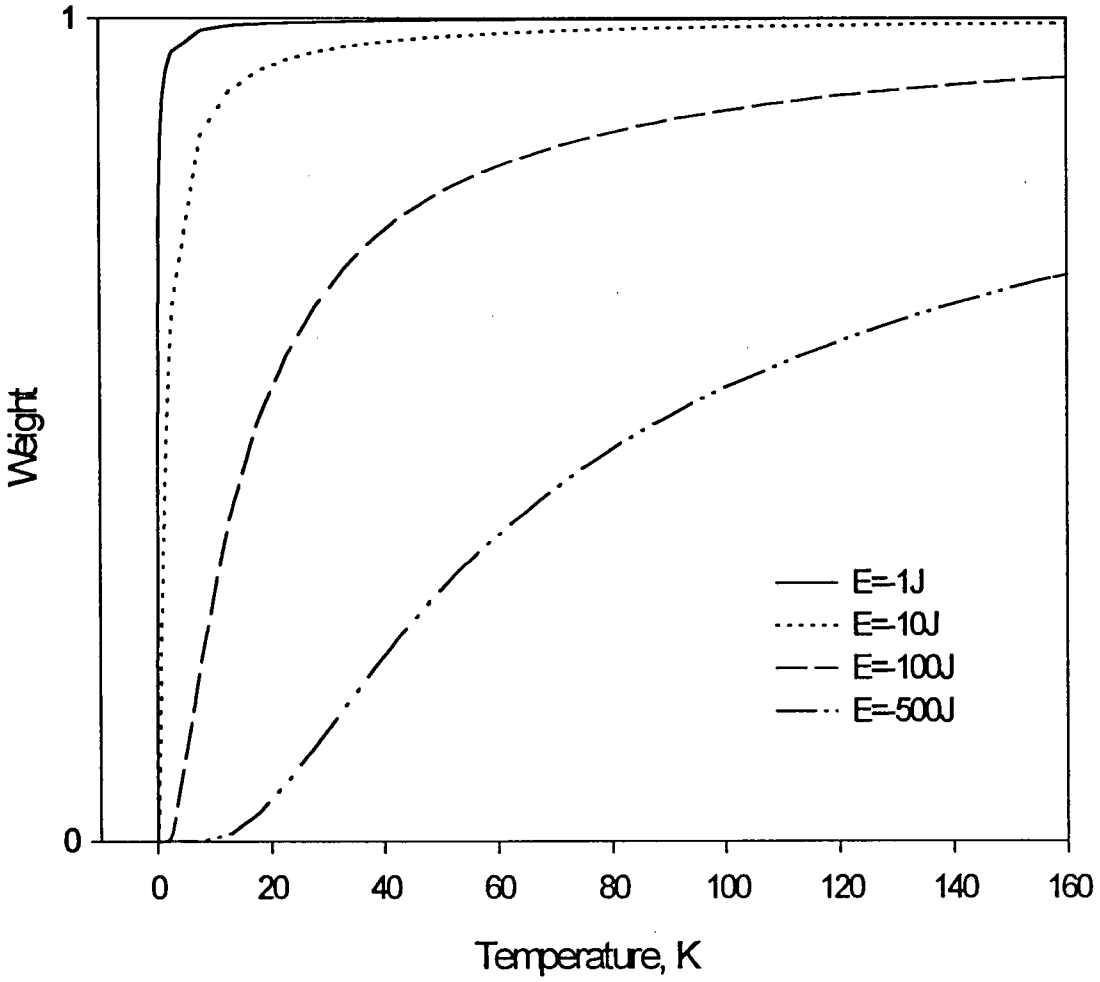


Figure 5.3 The dependence of the statistical weight of the unit cell (number of possible configurations) on the absolute temperature, at different values of the internal energy of the system.

### 5.1.2. The Energy analysis

It is known that shear introduces a velocity gradient into the system [Dealy and Wissbrun (1990)]. In its absence, the polymer molecules have an average end-to-end distance that is relatively small, and there is no preferred orientation of the polymer chains. When the solution undergoes deformation individual chain segments are dragged along in the direction of flow. Because of the relatively large size of a polymer molecule, chain segments are exposed to different solvent velocities. In other words, each chain is subject to forces that vary from segment to segment along the backbone. These forces change the conformation of the molecules, thereby increase their average end-to-end distance. A consequence of this is the promotion of some degree of orientation in the direction of flow; the latter in turn alters the rheological behavior of the fluid. At high shear rates, the shape of polymer molecules and the anisotropy of the system are different from that at low shear rates. This alters the solution's resistance to flow and thus its viscosity [Dealy and Wissbrun (1990)].

We assume here that the internal energy change of a polymer segment is proportional to a proper measure of the stress experienced by the segment multiplied by the volume of the lattice site. The internal energy change is then directly proportional to the stress associated with the orientation phenomena, that is

$$\Delta E \propto FvN \tag{5.7}$$

where, $v$ is the volume of a cell, $N$ is total number of cells in the lattice [Brannock *et al.* (1991)], and $F$ is a measure of the elasticity of the polymer, which in turn relates to the entropic conformational changes and orientation.

To complete our analysis, we are left with the problem of identifying the rheological property that best defines a proper measure of the asymmetric stress imposed on the lattice site due to shear. Several measurable rheological properties are related to this effect. However, the first normal stress difference $N_1$ seems most appropriate [Dealy and Wissbrun (1990), Rangel-Nafaile *et al.* (1984), Marrucci (1972)] as it takes into account the changes in elasticity under the application of shear flow. The deformation of a polymer chain from a random–coil configuration is known to generate a first normal stress difference [Dealy and Wissbrun (1990)]. In simple shear, say between a cone and a plate, the first normal stress difference defines those forces that push the cone apart from the plate when the polymer is flowing. Numerical simulations explaining the shear-induced phase changes taking into account only the first normal stress difference $N_1$ have been reported [Soontaranun et al. (1996a,b), Rangel-Nafaile *et al.* (1984), Marrucci (1972)]. Therefore, we assume that $F$ in Eq. (5.7) is proportional to $N_1$, as follows

$$\Delta E = -\zeta N_1 v N \tag{5.8}$$

where $\zeta$ is proportionality constant that is independent of temperature and it relates the change in the internal energy of the system with the elasticity of the system (first normal stress difference). The minus sign in Eq. (5.8) indicates that the change in the internal

energy of the system upon the application of shear (or any other type of deformation) is of entropic origin (see Eq. (5.5)). Eq. (5.8) provides the connection between the solution rheology (i.e., shear) and the observed changes in thermodynamic properties of the mixture. Provided that the value of $\zeta$ can be determined, this Equation allows calculation of the decrease in internal energy (and thus $w$) for systems for which $N_1$ has been determined experimentally.

It should be pointed out that the connection between a change in solution energetics and $N_1$ is not new. Marrucci (1972) used a simple Hookean-type dumbbell model (which can roughly approximate a dilute polymer solution) to relate $N_1$ to what he termed the elastic stored energy, $\Delta E_s$, of a polymer solution under shear. His result for simple shear flow in a lattice reduces to $\Delta E_s = N_1 \nu N/2$. Since this $\Delta E_s$ is always positive, it cannot be equivalent to the internal energy change $\Delta E$, which arose naturally from our statistical-thermodynamic development. Instead, $\Delta E_s$ is most likely related in some way to the Gibbs free energy change of the mixture resulting from the application of shear in analogous fashion to Wolf's (1984) phenomenological development. Assuming $\Delta E_s$ to be the Gibbs free energy change, both Rangel-Nafaile *et al.* (1984) and Soontaranun *et al.* (1996a,b) were able to qualitatively capture experimental shifts in cloud point temperature for polymer solutions and blends, respectively, under shear.

Although it provides validation that $N_1$ is an appropriate rheological parameter for describing the effect of shear on phase behavior, the result of Marrucci (1972) does not include a rigorous connection to the thermodynamic state of the system. The present

analysis indicates that the Gibbs free energy increases in a polymer mixture under shear. This results from the fact that the application of shear is directly related to the entropy loss of the oriented polymer chains. For example, we consider a binary system in which solvent (1) and polymer (2) are mixed under quiescent conditions and then the mixture is subject to shear. We assume, in accordance with Flory-Huggins theory that the enthalpy of mixing depends only on the interaction parameter, $\chi_{12}$, and the bulk volume fractions of the components. The total entropy of mixing $\Delta S^*$ for this process is then given by

$$\Delta S^*_M = k \ln \Omega^*_{12} - k \ln \Omega_1 - k \ln \Omega_2 \tag{5.9}$$

From our development, this leads directly to the following result for the molar entropy of mixing the polymer solution under shear, $\Delta S^*_M$

$$\Delta S^*_M = \Delta S_M - \frac{\zeta \nu N N_1}{T} \tag{5.10}$$

which relates the loss in polymer conformational (quiescent) entropy to the first normal stress difference. The change in Gibbs free energy of a polymer solution in the presence of shear is then given by

$$\Delta G^*_M = \Delta H^* - T\Delta S^*_M = \Delta H^* - T\Delta S_M + \frac{\zeta \nu N N_1}{N_o} \tag{5.11}$$

By combining Eq. (5.3) and (5.11) after assuming that the change in enthalpy for a polymer solution is independent of shear, which is a reasonable assumption for dilute polymer solutions, $\Delta G^*_M$ becomes $\Delta G^*_M = \Delta G_M + \frac{\zeta \nu N N_1}{N_o}$. Converting this expression to refer all quantities per mole, we end up with

$$\Delta G^*_M = \Delta G_M + \zeta \nu N N_1 = RT(n_1 \ln \phi_1 + n_2 \ln \phi_2 + \chi_{12} \phi_1 \phi_2 N) + \zeta \nu N N_1 \tag{5.12}$$

According to Eq. (5.12), the change in the Gibbs free energy of mixing of a polymer solution under shear is more than that in the absence of shear by the amount of $\zeta \nu N N_1$.

## 5.2 Model predictions

### 5.2.1. The Phase diagram shift of a polymer solution subject to shear

The reduced chemical potential, is obtained from Eq. (5.12):

$$\mu^*_1 = \frac{\mu_1}{RT} = \frac{\partial(\Delta G^*_M / RT)}{\partial n_1} = \ln(1-\phi_2) + \phi_2(1-\frac{1}{r}) + \chi_{12}\phi_2^{\,2} + \frac{\zeta \nu}{RT}(N_1 - \phi_2 \frac{\partial N_1}{\partial \phi_2}) \tag{5.13}$$

The first three terms in the right hand side of Eq. (5.13) consist the classic quiescent expression for $\mu_1^*$ and result in negative value, whereas the flow effects are included in the last term defined with the inclusion of the parameter $\zeta$. When the system subject to steady shear approaches equilibrium at longer times, the chemical potential of the polymer in the two phases is equal and constant. Determination of the critical points also requires that the first and second derivatives of the chemical potential with respect to $\phi_2$ are zero.

$$\frac{\partial \mu^*_1}{\partial \phi_2} = \frac{-1}{(1-\phi_2)} + (1-\frac{1}{r}) + 2\chi_{12}\phi_2 - \frac{\zeta v}{RT}(\phi_2 \frac{\partial^2 N_1}{\partial \phi_2^2}) = 0 \qquad (5.14)$$

$$\frac{\partial^2 \mu^*_1}{\partial \phi_2^2} = \frac{-1}{(1-\phi_2)^2} + 2\chi_{12} - \frac{\zeta v}{RT}\left(\phi_2 \frac{\partial^3 N_1}{\partial \phi_2^3} + \frac{\partial^2 N_1}{\partial \phi_2^2}\right) = 0 \qquad (5.15)$$

For systems exhibiting shear-induced demixing, the dependence of the first normal stress difference, $N_1$, on $\phi_2$ exhibits a maximum. Therefore, the rate of change of $N_1$ with respect to $\phi_2$ is always negative at relatively high values of $\phi_2$. No reliable expression for the dependence of the first normal stress difference on composition exists (it is based on experiments actually) [Dealy and Wissbrun (1990)]. However, experimentally a parabolic behavior of $N_1$ with respect to composition has been observed for the case of PS/DOP [Rangel-Nafaile *et al.* (1984)]. The fluid is Newtonian at zero concentration, so the normal forces are zero. Addition of polymer increases the normal force progressively and the curve rises. As higher concentrations are reached, the shear rate at which the experimental measurements are made progressively decreases (since the fluid viscosity

increases with concentration while the shearing stress is held constant). Consequently, as very high concentrations are reached, the deformation rate, and hence the normal forces, again goes to zero. In order to, best capture the concentration range in the vicinity of critical point, we assume a quadratic dependence of $N_1$ on $\phi_2$ of the following form [Rangel-Nafaile *et al.* (1984)]:

$$N_1 = a(\phi_2 - \phi_{2m})^2 + b\phi_2 + N_{1m} \tag{5.16}$$

where, $\phi_{2m}$, and $N_{1m}$ are empirical parameters, and $a$ and $b$ are the first and second coefficients of the quadratic polynomial respectively. Once, the dependence of the first normal stress difference on composition is known, the spinodal curve can be generated using the condition $(\partial^2 \Delta G_M / \partial \phi_2^2)_{T,P} = 0$. From Eq. (5.14) and (5.16) we get:

$$\frac{-1}{(1-\phi_2)} + (1 - \frac{1}{r}) + 2\chi_{12}\phi_2 - \frac{2a\zeta v\phi_2}{RT} = 0 \tag{5.17}$$

whereas from Eq. (5.15) and Eq. (5.16), we obtain:

$$\frac{-1}{(1-\phi_2)^2} + 2\chi_{12} - \frac{2a\zeta v}{RT} = 0 \tag{5.18}$$

To solve Eqs. (5.17) and (5.18) we assume, $\chi_{12} = \chi_0 + \frac{\zeta a v}{RT}$, where, $\chi_0$ is the interaction parameter under quiescent conditions. On substituting this value of $\chi_{12}$ in Eq. (5.17) and

Eq. (5.18), we obtain essentially the results of Tompa (1949). Hence, the value of $\chi_{12}$ above is the derived solution. Calculating the change in temperature using an empirical expression for $\chi_{12}$ [Rangel-Nafaile *et al.* (1984)] for PS/DOP, $\chi_{12}$ =0.5 + $\psi(\theta/T$ -1) one may obtain, $\Delta T = \frac{-T^2\Delta\chi}{\psi\theta}$. Substituting, $\Delta\chi = \frac{\zeta a v}{RT}$ yields $\Delta T = \frac{-T^2\zeta a v}{\psi\theta RT}$, where for $T$ $\approx$ 300K, $\theta$ = 288K, $\psi$ = 1.72, we obtain $\Delta T$ = 2.84055 x $10^{-6}$ $\zeta a$. By considering Eq. (5.16) for the dependence of $N_1$ on composition and the value of $\chi_{12}$ above, Eq. (5.14) yields:

$$T = \frac{\frac{\zeta v \phi_2}{R}\frac{\partial^2 N_1}{\partial \phi_2^2} - 2\phi_2\psi\theta}{\frac{-1}{(1-\phi_2)} + (1-\frac{1}{r}) + \phi_2(1-2\psi)} \qquad (5.19)$$

Eq. (5.19) can now be used to predict the phase diagram under shear of a polystyrene/dioctyl phthalate solution system reported by [Rangel-Nafaile *et al.* (1984)]. As will be shown later, this is a UCST system that exhibits shear-induced demixing behavior. For such a system, the necessary and sufficient condition is

$$(\partial^2 \Delta G^*_M / \partial \phi_2^2)_{T,P} \geq 0.$$

The value of the adjustable parameter $\zeta$ in Eq. (5.19) can be calculated by substituting the values of parameter $a$ (obtained from the quadratic dependence of $N_1$ on composition) and $\Delta T_{measured}$ (the measured temperature shift of the binodal curve under

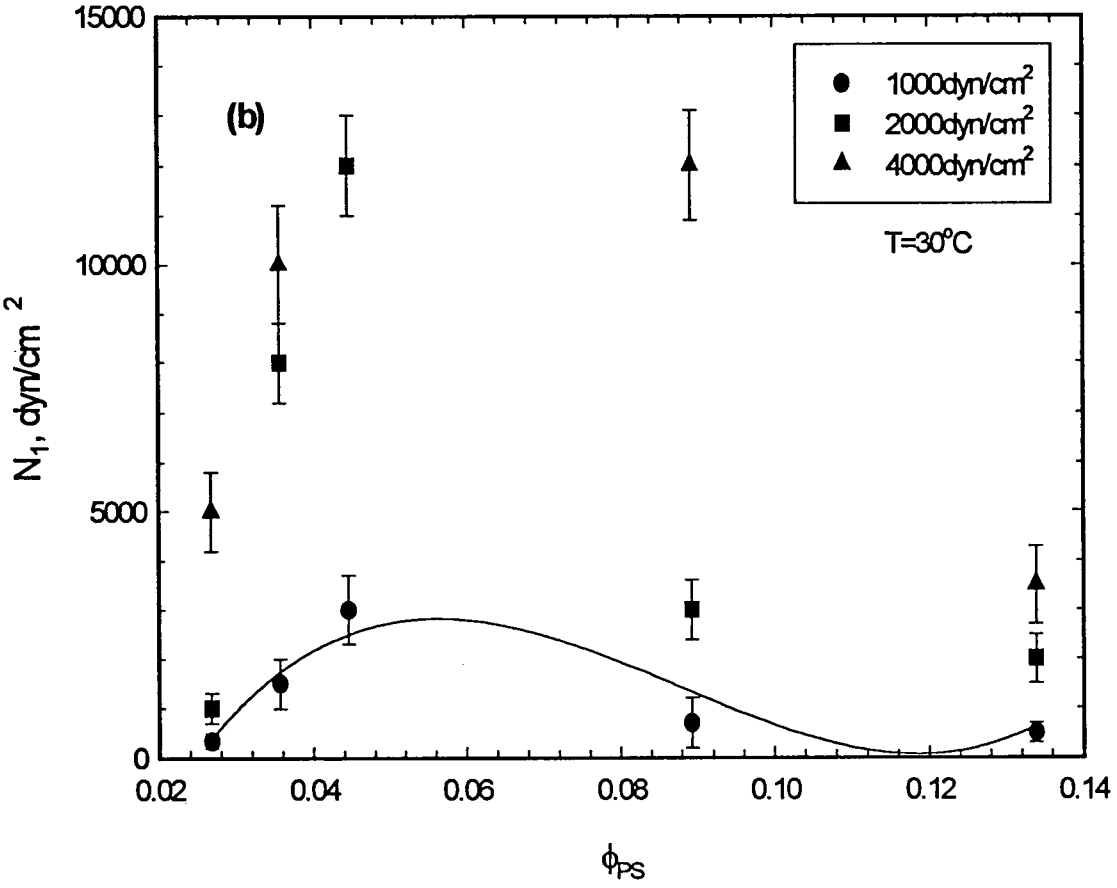


Figure 5.4. The (shear rate dependent) first normal stress difference of the PS/DOP solution, $N_1$, as a function of composition, $\phi_{PS}$, at (a) 25°C and (b) 30°C and three different levels of shear stress.

Figure 5.4 (a) and (b) depicts the dependence of $N_1$ on concentration of PS in DOP (g/ml) at 25°C and 30°C respectively for three different levels of shear stress. It can be seen that $N_1$ increases strongly with concentration, passes through a clear maximum and subsequently decreases mildly with further increase of concentration. The continuous lines are polynomial regression lines to guide the eye.

In view of Eq. (5.19) and Figure 5.4, one would expect that the phenomenon of shear-induced demixing will be more clear and dominant at small PS concentrations. The same dependence of $N_1$ on $\phi_{PS}$ was also found at 35°C. Figure 5.5 (a), (b) and (c) depict the dependence of $N_1$ on concentration of PS in DOP (g/ml) at the shear stress of 1000 dyn/cm$^2$, 2000 dyn/cm$^2$ and 4,000 dyn/cm$^2$ and two temperatures (25°C and 30°C) respectively. It can be seen again that $N_1$ increases strongly with concentration, passes through a maximum and subsequently decreases with further increase of concentration. It is noted that to derive Eq. (5.19), a quadratic polynomial was assumed for the dependence of $N_1$ on concentration. Such a polynomial is sufficient to represent the data plotted in Figures 5.4, and 5.5 up to concentrations of 0.1 g/ml. This is the range of concentrations (0-0.1 g/ml) that will be used in predicting the phase diagram as well as the range over which the phase diagram of PS/DOP under shear shows significant changes upon the application of shear.

The overlap concentration ($C^*$) for PS/DOP can be calculated using the following relation derived by Rudin *et al.* (1976).

$$C^* = 3\,\phi' / 4\,\pi\,N_0\,[\eta]_\Theta = (1.24 / [\eta]_\Theta)\ \text{g/cm}^3 \qquad (5.20)$$

Where $\phi' = 3.1\text{x}10^{24}$ [according to Flory (1953)]

$N_0 = 6.0\text{x}10^{23}$ [Avogadro's number]

$[\eta]_\Theta = K_\Theta\,M^{1/2}$

For PS/DOP used in this work the limiting viscosity number of Θ solution, $[\eta]_\Theta$ is equal to 113.6. Substituting appropriate values in Eq. (5.20), an overlap concentration of

0.011g/ml is obtained for the latter. Thus it can be noted in Figure 5.6 that the concentration of PS/DOP was always below the overlap concentration, thereby allowing maximum total number of configurations to the chains.

At higher concentrations where the maximum and the dramatic change of $N_1$ with concentration disappear, the thermodynamic phenomena (shear induced mixing or demixing) become of minor importance (Figure 5.4 and 5.5).

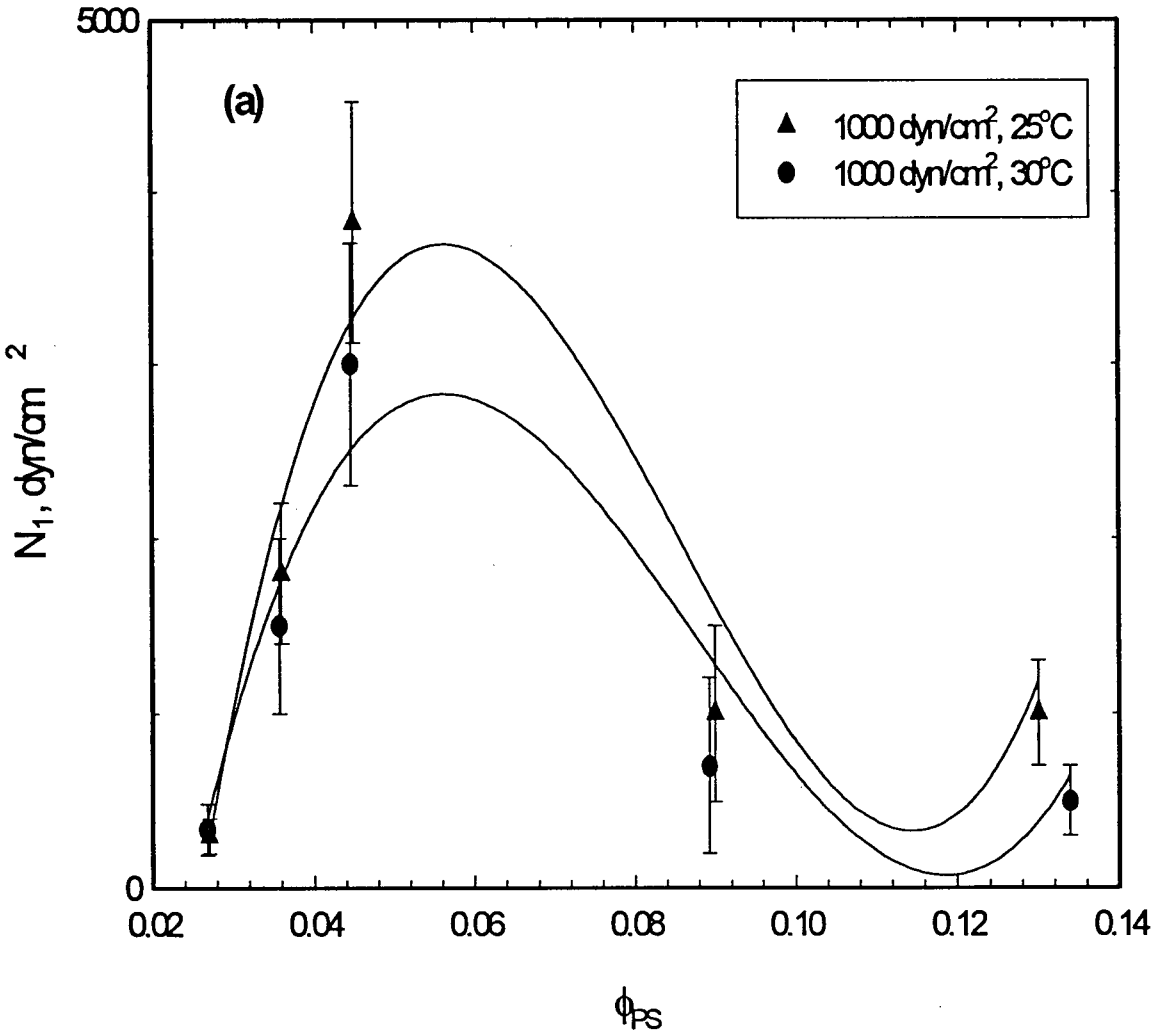

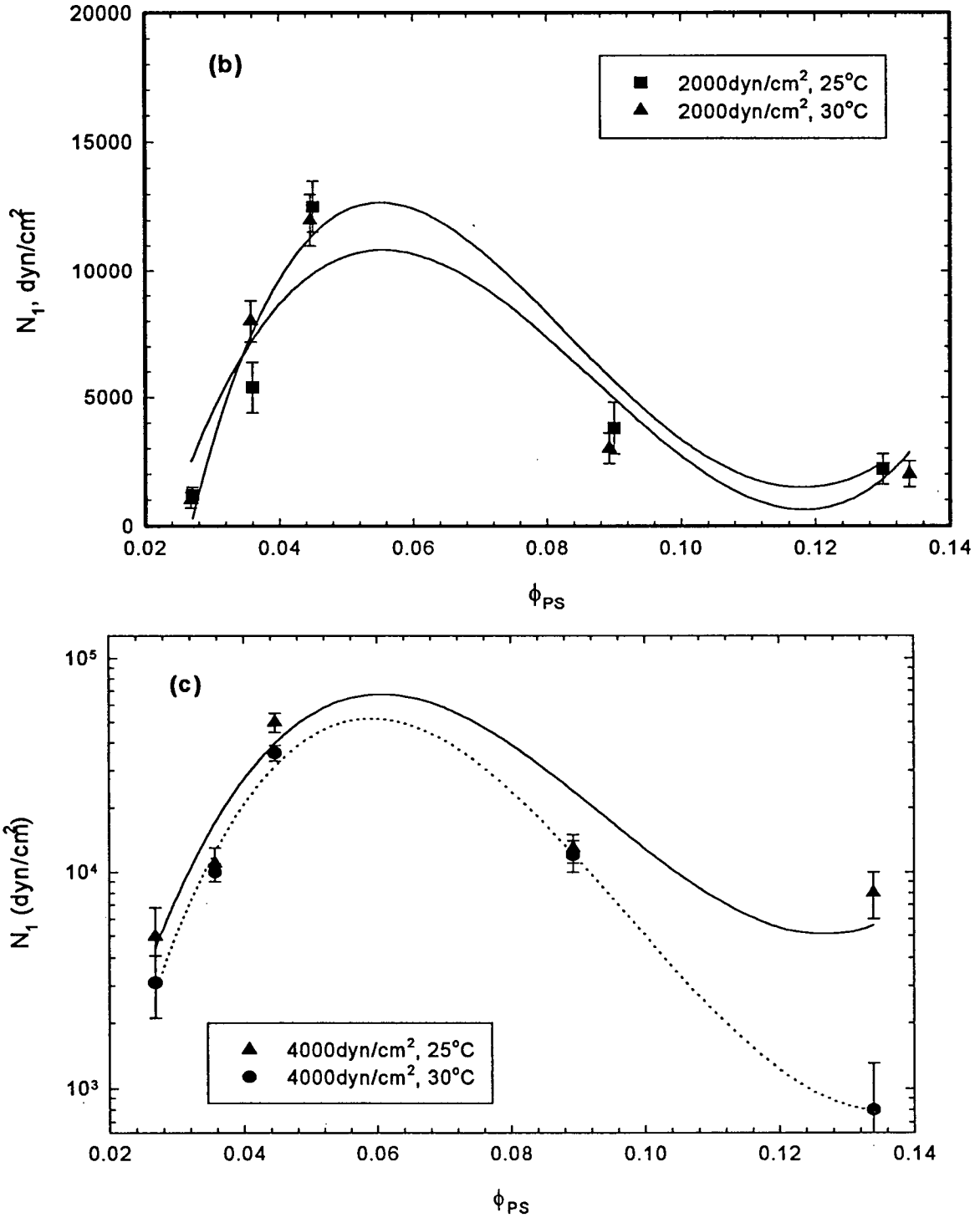


Figure 5.5. The (shear rate dependent) first normal stress difference of the PS/DOP solution, $N_1$, as a function of composition, $\phi_{PS}$, at the shear stress of (a) 1000 dyn/cm$^2$ (b) 2000 dyn/cm$^2$ (c) 4000 dyn/cm$^2$ and 25°C and 30°C.

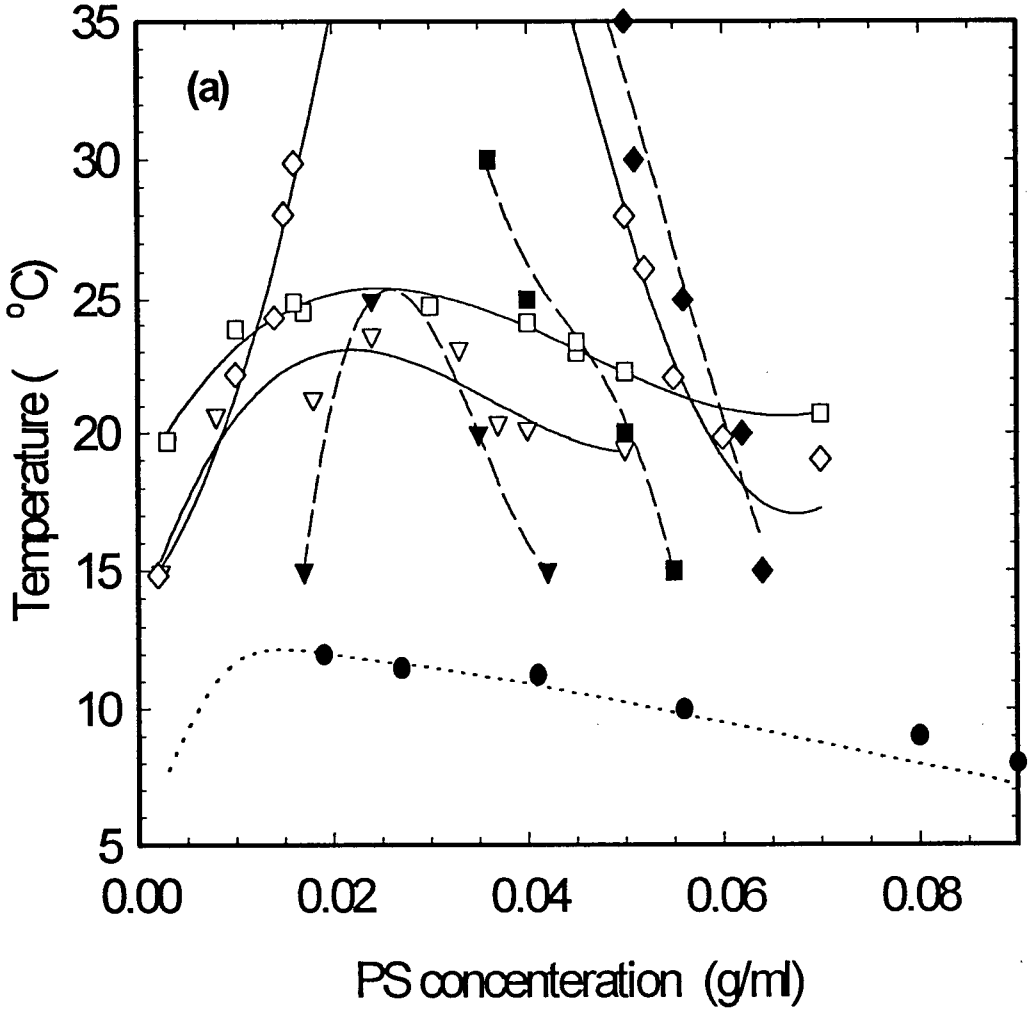


Figure 5.6.(a) The phase diagram of PS/DOP for quiescent and various flow conditions (data of Rangel-Nafaile et al[3]): comparison of theory and experiment. (●) experimental at quiescent conditions; (▼) experimental at $T_{12}$=1000 dyn/cm$^2$; (■) experimental at $T_{12}$=2000dyn/cm$^2$; (◆) experimental at $T_{12}$=4000 dyn/cm$^2$; (.....) predicted at quiescent conditions; (□) predicted at $T_{12}$=1000 dyn/cm$^2$ ($\zeta$=1); (❑) predicted at $T_{12}$=2000 dyn/cm$^2$ ($\zeta$=0.37); (◊) predicted at 4000 dyn/cm$^2$ ($\zeta$=0.13). Continuous and dashed lines represent regressions to guide the eye.

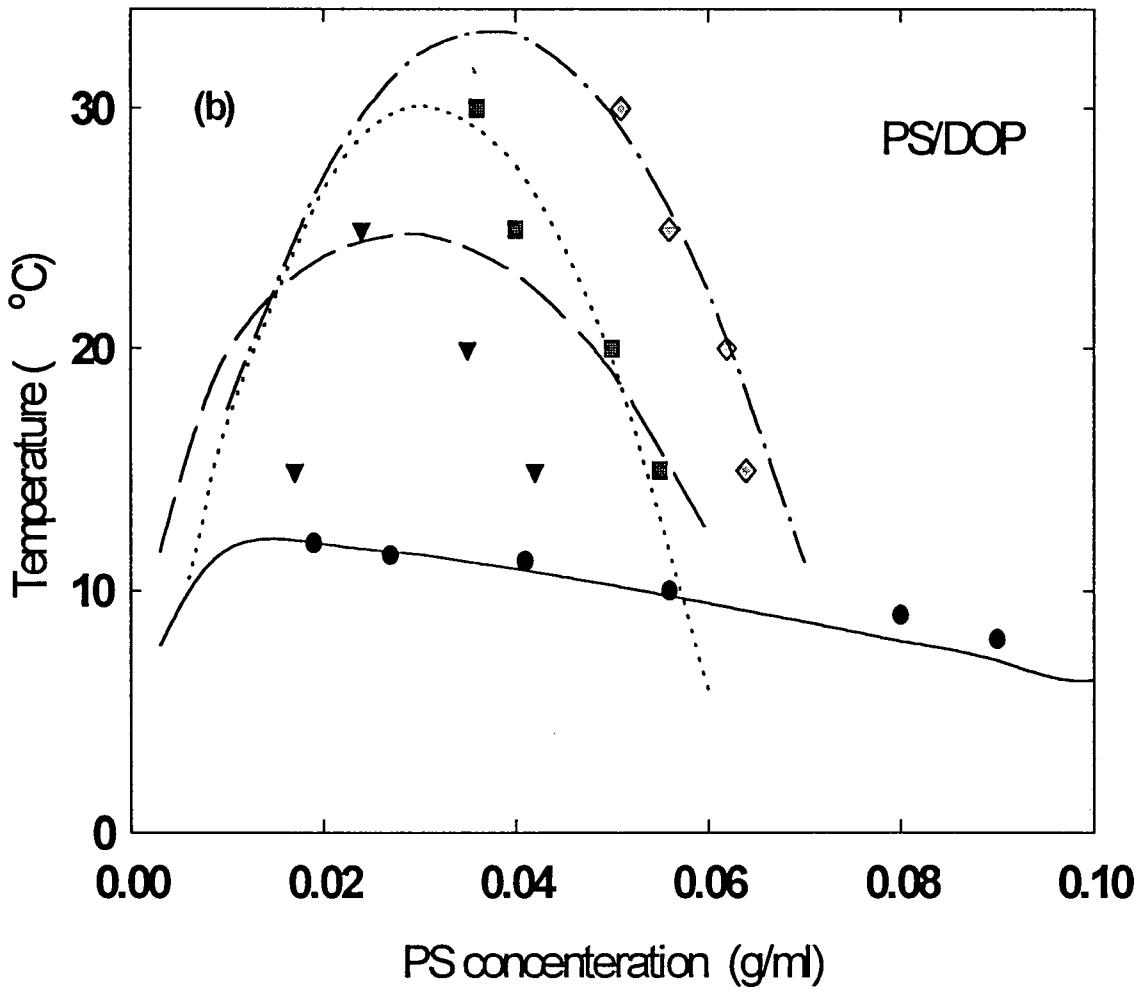


Figure 5.6.(b) The phase diagram of PS/DOP for quiescent and various flow conditions (data of Rangel-Nafaile et al[3]): comparison of theory and experiment. (●) experimental at quiescent conditions; (▼) experimental at $T_{12}$=1000 dyn/cm$^2$; (■) experimental at $T_{12}$=2000dyn/cm$^2$; (◆) experimental at $T_{12}$=4000 dyn/cm$^2$; (—) predicted at quiescent conditions; (-----) predicted at $T_{12}$=1000 dyn/cm$^2$ ($\zeta$=0.9); (.....) predicted at $T_{12}$=2000 dyn/cm$^2$ ($\zeta$=0.37); (— · —) predicted at 4000 dyn/cm$^2$ ($\zeta$=0.1). Continuous and dashed lines represent regressions to guide the eye.

Figure 5.6.(a) shows the experimental data reported by [Rangel-Nafaile *et al.* (1984)] for the PS/DOP system at quiescent conditions as well as at three different levels of shear stress, namely 1000, 2000 and 4000dyn/cm$^2$. The experimental data points are indicated by the closed symbols. It can be seen that this system exhibits an upper critical solution temperature (UCST) as well as a shear-induced demixing behavior. The data corresponding to quiescent conditions were obtained by using dynamic temperature ramp experiments [Kapnistos *et al.* (1996a,b), Wolf (1996)].

The corresponding open symbols represent the model predictions. The model predictions under quiescent conditions are represented by a continuous dotted line. The continuous lines are regression lines through the experimental points (closed symbols) while the dashed ones represent regression lines through the calculated points (open symbols) to guide the eye. The predictions were performed as follows. Once the quadratic form of the dependence of $N_1$ on concentration for various stress values and temperatures are known (only the coefficient of the quadratic term is actually needed, listed in Table 5.1), the value of $\zeta$ can be calculated using Eq (5.19) as discussed above. The values of $\zeta$ are also listed in Table 5.1 for all three cases. These values show a decay in $\zeta$ with increasing shear stress, indicating that the portion of $N_1$ responsible for the loss in entropy decays with increasing shear stress. The lumped weighting factor can be calculated by substituting the value of $\Delta E$ in Eq. 5.6 as given by the following equation,

$$w = e^{-\frac{\zeta N \nu N_1}{RT}} \tag{5.21}$$

Since, $N_1$ is dependent on $\phi_{PS}$ as seen in Figures 5.4a,b and 5.5a,b,c, $w$ should also be dependent on $\phi_{PS}$ (Eq. (5.21). The $w_{max}$ values in Table 5.1 refer to the maximum values of the lumped weighting factor obtained by using the $N_1$ values corresponding to the maximum in the $N_1$ vs $\phi_{PS}$ plots (Figures 5.4a,b) for the specified shear stress.

Figure 5.6.(b) shows the fit of the proposed model to the data of Rangel-Nafaile *et al.* (1984) taking into account a polynomial best fitting the $N_1$ vs. $\phi_{PS}$ data. The values of $\zeta$ remain almost unchanged while the fit is much more convinving than the discrete point fit in Figure 5.6.(a) obtained after considering a different $N_1$ vs. $\phi_{PS}$ polynomial for each temperature and shear stress. This is possible because the values of $N_1$ for the range of composition, temperature, and stress studied behave qualitatively in the same manner.

It can be seen from Figure 5.6 that the model confirms qualitatively and semi quantitatively (at least for the cases of 1,000 and 4,000 dyn/cm$^2$) the observed shift in the critical temperature. The differences between experiment and theoretical predictions can be attributed to a number of reasons. First, it is noted that the determined $N_1$ data differed from the limited data reported by [Rangel-Nafaile *et al.* (1984)] by about one order of magnitude. This can be attributed to differences in the solution (molecular weight and polydispersity of PS) as well as to the advancement and accuracy of modern rheometrical equipment. Moreover, the $N_1$ data were represented by polynomials in order to be able to derive the analytical solution of Eq. (5.9). A more accurate method could be to consider the exact dependence of $N_1$ on concentration and subsequently solve the problem numerically. However the aim of this exercise was to compare predictions of Rangel-

Nafaile *et al.* (1984) Finally, the assumption that $\zeta$ is independent of composition may not be true.

| | $T_{12}$ (dyn/cm$^2$) | | |
|---|---|---|---|
| | 1000 | 2000 | 4000 |
| a (25°C) | $-3.96 \times 10^6$ | $-1.25 \times 10^7$ | $-3.50 \times 10^7$ |
| a (30°C) | $-3.10 \times 10^6$ | $-1.32 \times 10^7$ | $-4.54 \times 10^7$ |
| a (35°C) | $-2.20 \times 10^6$ | $-1.28 \times 10^7$ | $-5.60 \times 10^7$ |
| $\zeta$ | 1.1 | 0.37 | 0.13 |
| $\Delta T_{calculated}$* | 12.3 | 13.03 | 12.83 |
| $\Delta T_{measured}$* | 13 | 14 | 14 |
| $w_{max}$ | 0.86 | 0.85 | 0.75 |

**Table 5.1.** Comparison of the value of $\zeta$ fitted to the measured change in temperature at different shear stress levels [data from Rangel-Nafaile *et al.* (1984)]. The first coefficient of $N_1$ vs $\phi_{PS}$ quadratic relationship is denoted by 'a'. *These values refer to 25°C, while the values of $\zeta$ are independent of temperature.

Both G' (storage modulus) and $N_1$ exhibit the same qualitative behavior at low shear rates, as discussed in detail later in section 5.2.2. Although, G' is more reliable and an easier quantity to measure, $N_1$ was used in the stored energy term in the present simulation for two reasons. First, stresses of 1000 dyn/cm$^2$, 2000 dyn/cm$^2$ and 4000 dyn/cm$^2$ correspond to very high shear rates (above 300s$^{-1}$) in PS/DOP system. It is experimentally noted that at such high shear rates, the qualitative behavior of G' may be

not as exact as $N_1$, but there is an experimental limitation in obtaining $N_1$ at high shear rates. Secondly, by using $N_1$, the value of $\zeta$ can be compared to that of Hookean dumbbells (equal to 0.5) [Marrucci (1972)], thereby providing some insight into the macromolecular response of real polymeric systems to shear. However, in the absence of $N_1$ one may reasonably use G' data as will be done below for the case of polymer blends.

### 5.2.2. The case of Polymer Blends

Flow does not only shift the quiescent phase boundary of a blend but also deforms domains of different composition in either component to create fine anisotropic structures [Vinckier *et al.* (1996), Nakatani *et al.* (1990), Hobbie *et al.* (1994), Vlassopoulos *et al.* (1997), Vlassopoulos (1996)] . Both flow-induced mixing and flow-induced demixing (phase separation) depending on composition, temperature and shear rates have been reported as already mentioned in the introduction, and the challenge lies in predicting these effects using the developed approach based on the entropic changes due to shearing deformation.

Since the proposed model is based on minimal assumptions, the same expression used for the change in the internal energy of a polymer solution can be employed to explain the thermodynamics of phase separation in polymer blends under the application of flow. In the case of polymer blends, the change in entropy can be calculated by using a simple mean field theory, i.e. the lattice treatment of mixture of two polymers originally proposed by Flory and Huggins [Flory (1953), Fast (1968), Strobl (1996)]. Using Eq.

(5.1), now $n_1$ and $n_2$ refer to the two polymer constituents, whereas $\chi_{12}=A-B/T$. The values of parameters A and B are obtained after fitting the quiescent spinodal data with Eq. (5.20) for the specific example of poly(styrene-co-maleic anhydride)/poly(methyl methacrylate), SMA/PMMA with $N_1 = 0$ (no shear); $g_1 = 1000$ and $g_2 = 650$ [Vlassopoulos *et al.* (1997)], where 1=SMA, 2=PMMA, and $g$ is the degree of polymerization; this procedure yielded $A$=0.084 and $B$=39.9K.

Figure 5.7(a) and (b) depicts the experimental (obtained by shear rheological measurements using a Rheometric Scientific ARES 2KFRTN1 rheometer as in the previous case of PS/DOP) and the predicted (after fitting the empirical parameters) binodal curves are plotted.

Under the application of shear, the generalized Gibbs free energy of mixing expression Eq. (5.12) yields at the spinodal limit, $(\partial^2 \Delta G_M / \partial \phi_1^2)_{T,P} = 0$,

$$T = \frac{2B + (\zeta \nu N \frac{\partial^2 N_1}{\partial \phi_1^2} / R)}{2A - \frac{1}{\phi_1 P_1} + \frac{1}{\phi_2 P_2}} \qquad (5.22)$$

In the present case of polymer blends, the volume of one cell in the lattice, $\nu$ is given as, $\nu = \phi_1 \frac{\rho_1}{M_1} + \phi_2 \frac{\rho_2}{M_2}$, where $\rho_1$ and $\rho_2$ represent the densities of polymer 1 and 2, respectively, and $N$ is the total number of cells in the lattice ($N = n_1 M_1 + n_2 M_2$). Eq.

(5.22) clearly shows that the second derivative of $N_1$ with respect to $\phi_1$ governs the mixing and demixing phenomena observed.

The experimental and calculated spinodal curves corresponding to 10 $s^{-1}$ are shown along with the quiescent phase diagram in Figure 5.7(a). At lower compositions, shear-induced mixing and at higher compositions ($\phi_1$ above 0.5) shear-induced demixing is observed. Note that for the case of 10 $s^{-1}$ only two experimental points are available, since at lower compositions shear-induced demixing occurs at very high temperatures where the blend degrades fast, while at higher compositions shear-induced mixing occurs at low temperatures where flow becomes almost impossible (due to high $T_g$'s [Vlassopoulos *et al.* (1997)]).

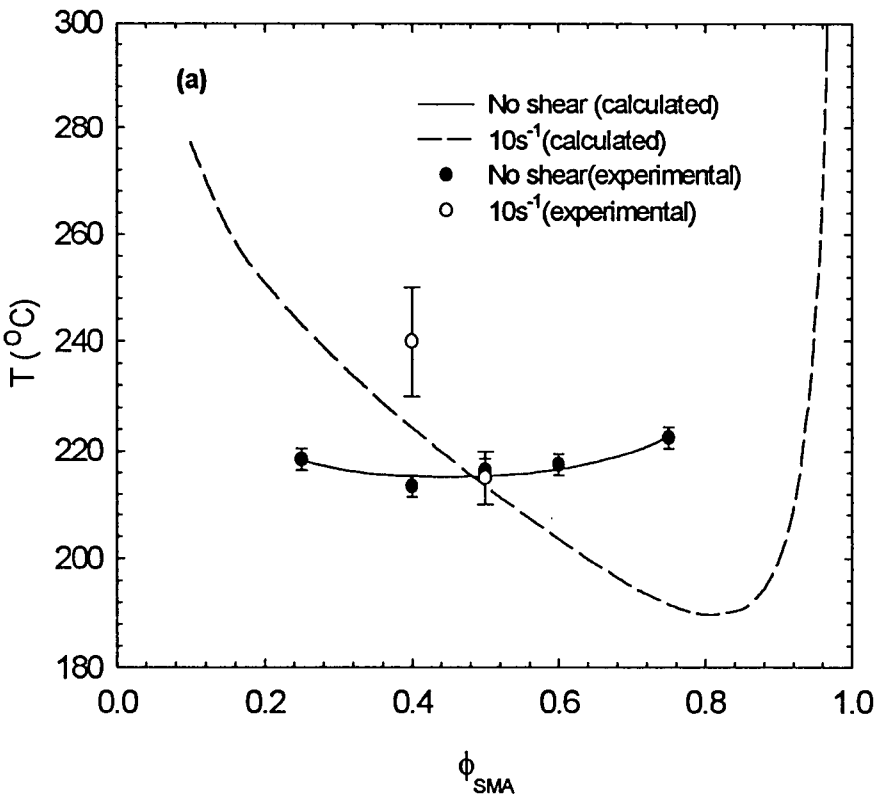


Figure 5.7(a). The phase diagram of the SMA/PMMA blend at quiescent conditions (from Figure 4.5) and at flow conditions of 10 $s^{-1}$. Note the shear induced mixing at small concentrations of SMA and the shear induced demixing at higher ones. Lines represent fits to models, as explained in the text.

The first normal stress difference decreases with increasing temperature [Chopra *et al.* (1998)]. Owing to high viscosity of the SMA/PMMA blend (plotted in Figure 5.8 at 220°C), $N_1$ data corresponding to high shear rates could not be easily obtained. The slope ($dN_1/d\dot{\gamma}$) is approximately the same (0.75 –1) for all the compositions (viz. 25/75, 50/50, 75/25) at 210°C, when all the blends are in the miscible region for shear rates less than 1 $s^{-1}$. However, this observation does not always hold true in the immiscible region. Also, in the low deformation rate region, $\frac{dN_1}{d\dot{\gamma}} \approx \frac{dG'}{d\omega} \approx 1$ (the Cox-Mertz rule assumed to be valid), for a particular temperature both in miscible and immiscible region [Chopra *et al.* (1998)]. For this reason G' may be used instead of $N_1$ at low deformation rates; the former can be obtained experimentally much more easily [Vlassopoulos *et al.* (1997), Vlassopoulos (1996)]. Thus, one may replace $dN_1/d\varphi_{2(SMA)}$ with $dG'/d\varphi_{2(SMA)}$ in Eq. (5.22) in predicting the phase diagram of the blend at various shear rate/stress levels. Since G' and $N_1$ indicate the degree of elasticity of a polymer such an assumption seems reasonable, particularly in view of the validity of the Cox-Merz rule at relatively small shear rates.

It may be noted that the fit for phase diagram associated with 10 $s^{-1}$ in Figure 5.7(a) is obtained after assuming a single polynomial for the G' vs. $\phi_{SMA}$ curve shown in Figure 5.9(b) at $10s^{-1}$. The idea is to show that negative deviation of G' from additivity results in mixing while positive deviation leads to demixing. The fact that the limited experimental data is in qualitative agreement with this simulation confirms that the assumed polynomial can reasonably model the phase diagram in the concerned temperature

window. On the other hand Figure 5.7(b) consists of simulated points, each point referring to a different polynomial characterized by a specific temperature. These points provide the fit to the shear-induced phase diagram associated with $100s^{-1}$ obtained by Lever's rule (Figure 4.13). The dotted line is just to guide the eye. The simulated points were generated by inputting the polynomial for $N_1$, the values of the parameters, and the cloud point temperature obtained from Figure 4.13 into Eq. (5.22) in order to obtain the values of $\phi_1$ and $\phi_2$.

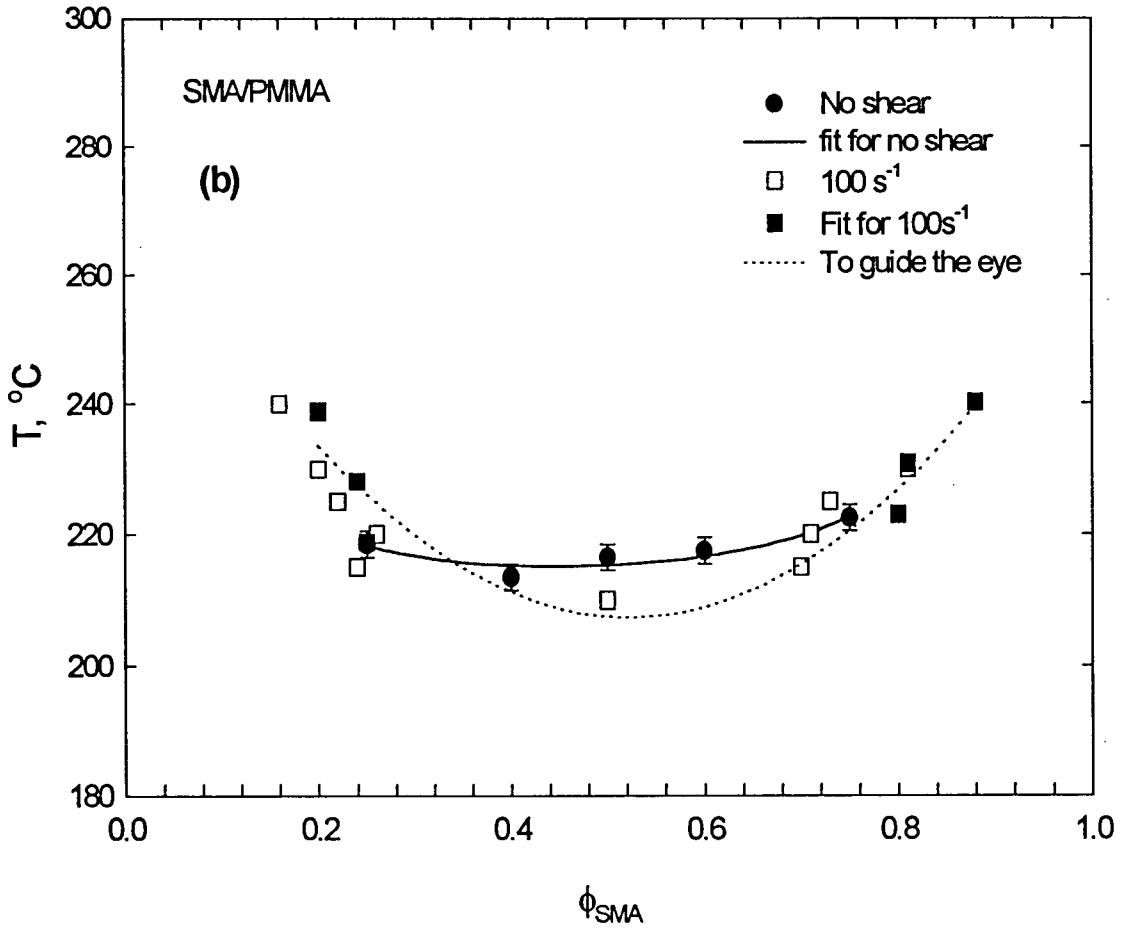


Figure 5.7(b). The phase diagram of the PSA/PMMA blend at quiescent conditions (from Figure 4.5) and at flow conditions of 100 $s^{-1}$.

The shear-induced mixing and demixing phenomena observed experimentally can be associated to the negative deviation of elasticity (here G') at lower compositions followed by positive deviation at higher compositions as depicted in Figure 5.9a and b for the SMA/PMMA blend. In these Figures, G' is plotted as a function of composition at 220°C and 240°C and various frequencies ($0.05s^{-1}$, $10s^{-1}$, $100s^{-1}$).

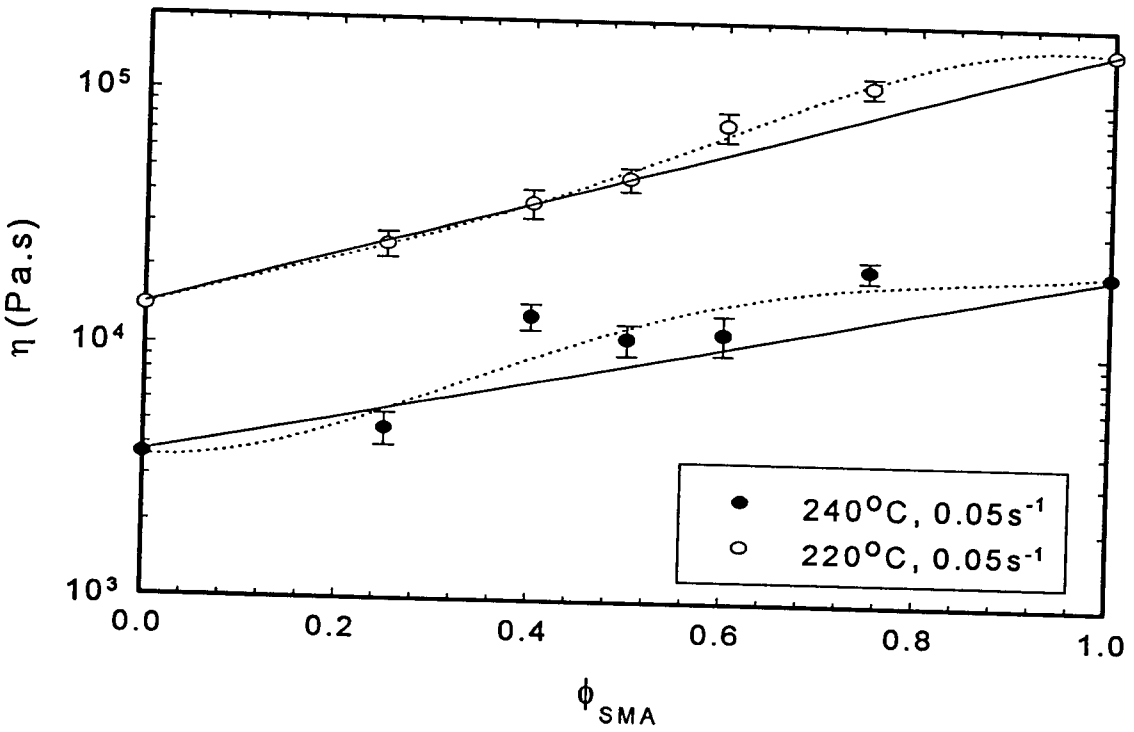


Figure 5.8. The viscosity of the PSA/PMMA blend, η, as a function of composition, $\phi_{SMA}$, at the shear rate of 0.05 $s^{-1}$ and two temperatures of 220 and 240°C. Dotted straight lines represent the linear mixing rule, whereas the curved solid lines represent nonlinear fits to the data.

The simulated spinodal curve plotted in Figure 5.7(a) and (b) provides a fairly good fit to the limited data for ζ equal to 3. This indicates that the loss in internal energy (due to the

imposed deformation leading to some kind of domain or chain orientation [Vlassopoulos *et al.* (1997), Vlassopoulos (1996), Chopra *et al.* (1998)] of the system upon the application of flow is as much as three times the elastic modulus attributed to the whole system.

At a certain temperature in the immiscible region and relatively low shear rates (typically 0.05 $s^{-1}$ to 100 $s^{-1}$), the values of *G'* exhibit an increasingly parabolic dependence (opening downwards) with $\phi_{SMA}$ (with shear rate), as seen in Figures 5.9a and 5.9b for SMA/PMMA blend. With increasing temperatures in the immiscible region, this kind of shear rate pattern is less distinct, and eventually disappears [Chopra *et al.* (1998)]. Such an uneven pattern leads to a unique shape of G' vs. $\phi_{SMA}$ at different temperature and shear rates and is thought to be responsible for the islands of immiscibility reported earlier [Vlassopoulos *et al.* (1997), Vlassopoulos (1996), Wu *et al.* (1991), van Egmond *et al.* (1993), Jian *et al.* (1996), Yanase *et al.* (1991), Kume *et al.* (1997)].

It should be pointed out that in this analysis the behavior (slope) of G' vs. $\phi_{SMA}$ is assumed to depend only on the shear rate, whereas the magnitude of G' depends of course on both shear rate and temperature. Based on the above analysis, as well as the experimental evidence, the fact that during flow-induced demixing (phase separation) the loss in internal energy (due to the growing "order" in the system) is responsible for an increase in Gibbs energy of mixing seems quite plausible. These findings are in good qualitative agreement with the recent theoretical investigation of Balazs and co-workers [Sun *et al.* (1998)] on the phase behavior of sheared polymer blends. They have

concluded that a nonlinear dependence of the shear modulus of the blend on the volume fraction of one of the species is crucial for the shift in the stability line to be induced by shear flow.

In order to compare the efficiency of G' with respect to the stored energy term used to date [Soontaranun *et al.* (1996a,b), Rangel-Nafaile *et al.* (1984), Marrucci (1972), Wolf (1984, 1996), Nakatani *et al.* (1990), Hobbie *et al.* (1994)], the latter was calculated for different compositions of $\phi_{SMA}$ in Figure 5.10 using Marrucci's (1972) stored energy term [Soontaranun *et al.* (1996a,b)] for simple shear, $E_s = \frac{(\eta\dot{\gamma})^2}{G}$. Since, the blends are in miscible region at 205°C and 210°C respectively, a positive deviation from additivity is seen for both viscosity (Figure 5.8) and stored energy (Figure 5.10), for 220 and 240°C. This is in agreement with the fact that both viscosity and stored energy show the same deviation [Soontaranun *et al.* (1996a,b)]. However, viscosity and stored energy are obtained by empirical relations [Soontaranun *et al.* (1996a,b), Marrucci (1972)]. Based on our approach, the elasticity seems to capture the main physics of the flow-induced conformation (and thus) structural changes and this is confirmed by experiments [Vinckier *et al.* (1996), Kapnistos *et al.* (1996a,b), Marrucci (1972), Vlassopoulos (1996), Vlassopoulos *et al.* (1997), Chopra *et al.* (1998), Sun *et al.* (1998)]. We already noted that G' is more convenient to use for viscous blends than $N_1$, especially in the regime of validity of the Cox-Merz rule. It is noted here that G' shows a greater deviation than viscosity or stored energy at these temperatures. Similarly, at 240°C and 0.05$s^{-1}$ (Figure 5.9b), G' shows positive deviation from additivity thereby explaining

immiscibilty more clearly than the stored energy term (Figure 5.10), which shows a negative deviation for $\phi_{SMA}$ below 0.2. Based on these results, and the unavailability of $N_1$ data at high shear rates for SMA/PMMA blends [Kapnistos *et al.* (1996a,b)], we propose G' as an equivalent expression of $E_s$. G' is a reasonable choice because it relates essentially to the elastic energy of the polymer fluid under shear [Chopra *et al.* (1998)], and it is of entropic origin. Therefore, we consider only G' as the rheological quantity responsible for the complex thermorheological behavior of the polymer fluid. The proposed model predicts the shift in the phase diagram only on the basis of G' vs $\phi_{SMA}$ dependence.

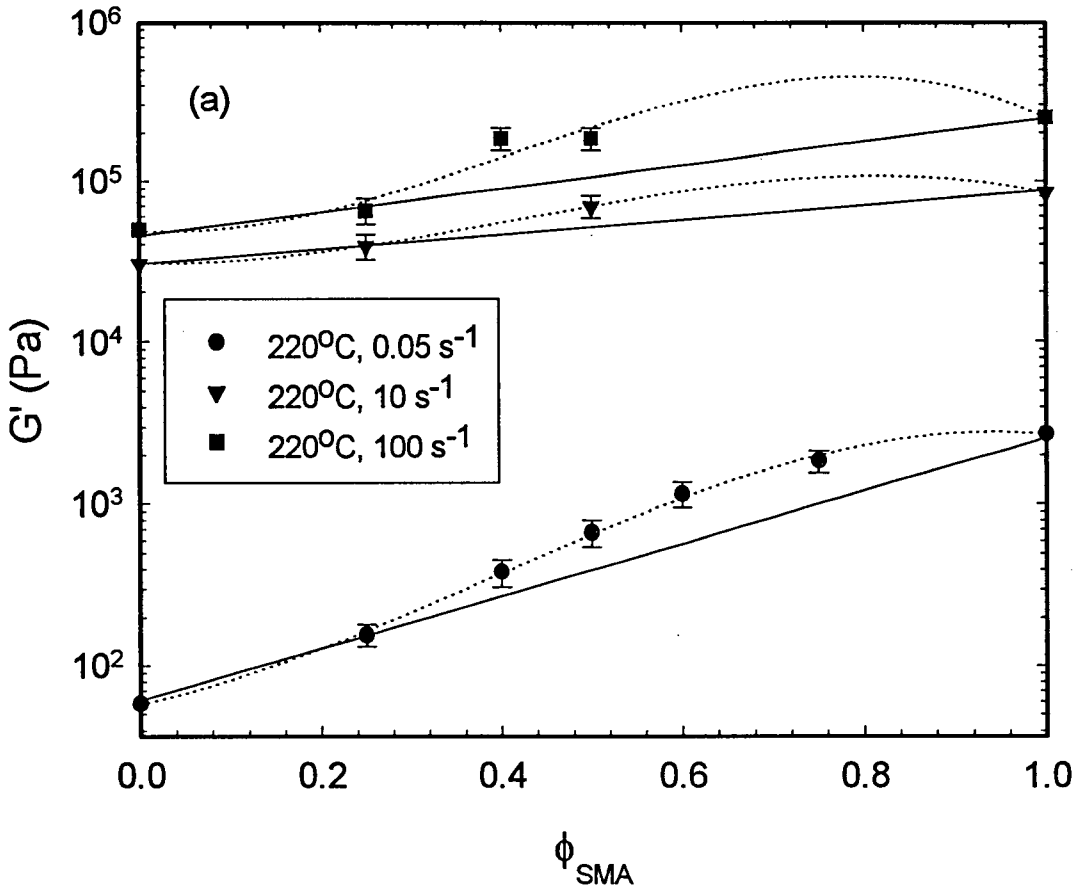

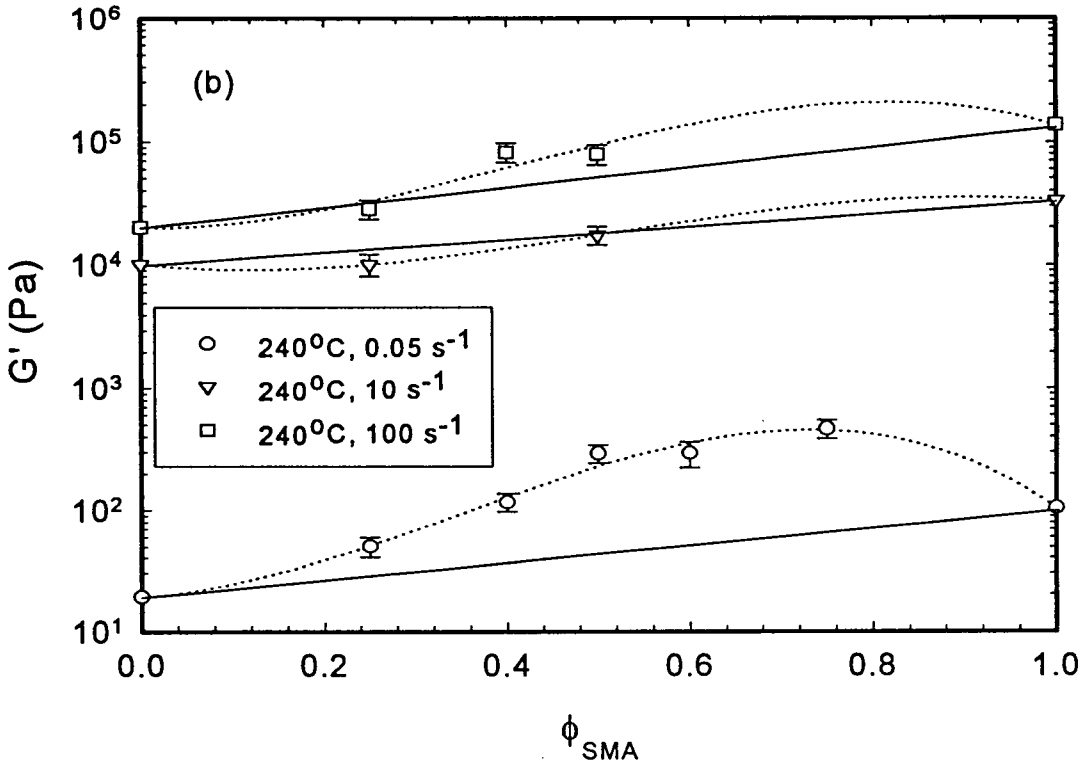


Figure 5.9. **(a)** The storage modulus of the PSA/PMMA blend, G', as a function of composition, $\phi_{SMA}$, and shear rate at 220°C; **(b)** The storage modulus of the PSA/PMMA blend, G', as a function of composition, $\phi_{SMA}$, and shear rate at 240°C. Dotted straight lines represent the linear mixing rule, whereas the curved solid lines represent nonlinear fits to the data. Note that negative deviation from linearity corresponds to mixing while positive one corresponds to demixing (as indicated in Figure 5.7(a))

An uneven increase in G', at lower frequencies, apparently due to form relaxation of the soft domains is observed and experimentally established [Vlassopoulos (1996), Vlassopoulos *et al.* (1997), Chopra *et al.* (1998)]. A negative deviation in G' at 240°C

and 10 $s^{-1}$ (see Figure 5.9b) for $\phi_{SMA}$ below 0.5, confirms the experimental observation of mixing exhibited by SMA/PMMA(40/60) [Vlassopoulos (1996), Vlassopoulos *et al.* (1997)]. On the other hand, a positive deviation of G' from additivity corresponds to demixing. Thus by following the experimental behavior of the blend elasticity vs. $\phi_{SMA}$ (G' or $N_1$) this model can predict shear-induced structural changes, in good agreement with experimental observations (see Figure 5.7).

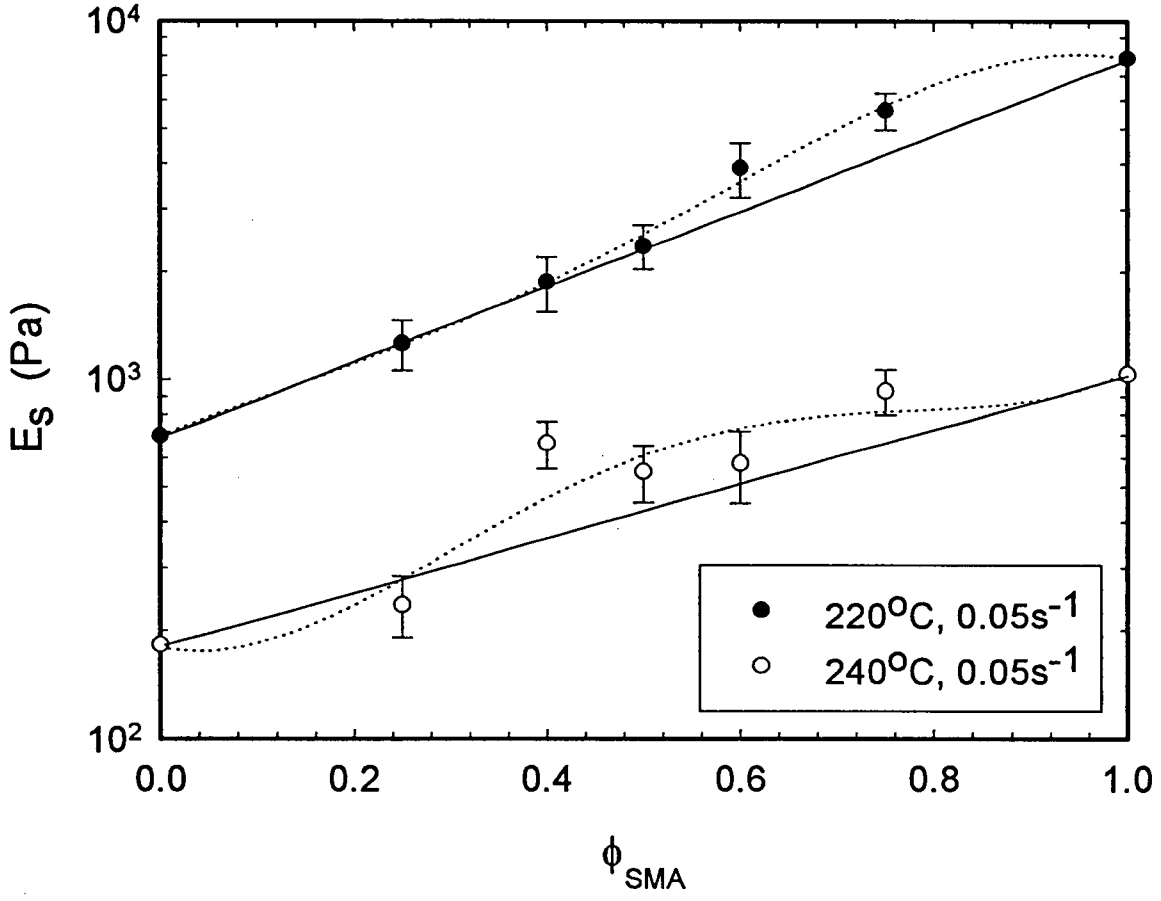


Figure 5.10. The stored energy of the PSA/PMMA blend, $E_S$, as a function of composition, $\phi_{SMA}$, at the shear rate of 0.05 $s^{-1}$ and two temperatures of 220 and 240°C.

# 6. CONCLUSIONS AND RECOMMENDATIONS FOR FUTURE WORK

## 6.1 CONCLUSIONS

In this work the effects of shear flow on the phase behavior of a lower critical solution temperature mixture of a random copolymer of styrene and maleic anhydride, SMA, and poly(methyl methacrylate), PMMA were investigated using shear and capillary rheometry, complemented by differential scanning calorimetry and analysis of the extrudates. Both shear-induced mixing, at low and very high shear rates, and shear-induced demixing, at moderate shear rates, were observed. In the former case, extrudes were optically transparent, yielded one $T_g$ and were thermorheologically simple at all temperatures up to the capillary extrusion one; on the other hand, extrudates related to shear-induced demixing were opaque, yielded two $T_g$'s and were thermorheologically complex up to the extrusion temperature. Particular emphasis was placed on the strong shear effects, which have not been studied in the past. We showed how to detect and isolate the degradation effects, which are predominant in SMA at high temperatures, and result in opaque but not necessarily phase-separated samples. The physical mechanism of the shear-induced structural changes was attributed to different amounts of stored elastic energy in the deformed domains of different glass transition and viscosity. This idea is different from the mechanism of droplet break up and coalescence, which is relevant to blends of low viscosity and elasticity materials, even at high shear rates and temperatures.

The methodology presented here for the determination of the shear-phase diagram in a flowing polymer blend is proposed for any industrial mixture, and it is of particular value for assessing the effects of strong shear flow, relevant in processing applications. The method of solution preparation, i.e., solution-cast versus melt-mixed samples, did not affect the rheologically determined demixing temperatures, although some differences were observed in the magnitudes of linear rheological material functions.

To explain these shear-induced phase changes we developed a model based on the change in the total number of configurations (thus the entropy) of a polymer fluid under the application of shear flow, thereby providing additional insight into the observed phase mixing or separation phenomena observed experimentally. This approach does not imply a dumbbell model, but it is rather general through the introduction of the parameter $\zeta$. The latter makes the model flexible, as convenient expressions best explaining the energy term can be used along by adjusting it, being independent of temperature but possibly dependent on composition. Thus, the parameter $\zeta$ accounts for the complex thermorheological behavior of entropic origin, whereas the interaction parameter, $\chi_{12}$ accounts for enthalpy changes. The proposed expression for the stored energy can explain both shear-induced mixing and demixing in polymeric mixtures. The choice of the first normal stress difference, $N_1$, or the storage modulus, G', as a representation of the internal energy change of the system works reasonably well. However, it is recognized that physical parameters associated with the mechanism of orientation such as birefringence, or structure factor may lead to more physical insights and better correspondence to experiments.

Other important conclusions are summarized as follows:

1. It was demonstrated that capillary rheometry can be efficiently used to study the effect of shear on the thermodynamics of polymer blends.
2. The composition dependence of the glass transition of SMA/PMMA blends follow Gordon-Taylor-Kwei equation.
3. Phase separated SMA/PMMA blends result in two transitions when subjected to Differential Scanning Calorimetry while single-phase samples show only one transition.
4. It was shown that the shear-induced phase diagram of SMA/PMMA blend can be assessed by applying Levers rule to the DSC results of the extruded samples.
5. Phase separation in SMA/PMMA blends was detected rheologically, both by failure of time-temperature superposition in dynamic frequency sweeps and change in slope in dynamic temperature ramps.
6. It was confirmed by shear rheology that degradation does not effect the phase separation kinetics in SMA/PMMA blend.
7. Both shear-induced mixing and demixing was found in the same blend viz. SMA/PMMA depending on the level of shear and temperature of extrusion.
8. Dynamic study of the SMA/PMMA blends confirmed that the morphological evolution is also time dependent.
9. The second derivative of the first normal stress difference with respect to composition governs the observed mixing and demixing effects.
10. The use of G' in place of $N_1$ in the proposed model fits the shear-induced phase diagram sufficiently well.

## 6.2. Recommendations for future work

Considerable efforts are required to understand and predict the rheological behavior of both miscible and immiscible polymer blends. This effort is important as it will serve as a foundation for the development of polymer blends with controlled morphology. The following recommendations for future work fall out as a consequence of this thesis.

1. Apply self-consistent field theory to directly calculate the weight associated with each cell in the lattice. This would throw some light on the response of polymer chains to shear under constraints such as entanglements and enthalpic interactions.
2. Perform experiments to find out the first normal stress difference as a function of temperature and composition for a polymer blend having high $T_g$ constituents.
3. Develop a high speed photography visualization technique (Laser-speckle velocimetry) [Binnington *et al.* (1983)] to directly detect the onset of phase separation at various locations along the die. This will also give us an indication as to the effect of L/D (residence time) on the phase separation kinetics.
4. Try to improve the model by incorporating other measures of anisotropy like birefringence. This would give way to the problems associated with the determination of $N_1$ at high shear rates. Also it would help in confirming that mixing and demixing in the same blend are primarily of entropic origin.
5. Rheological study of phase separated systems can help us in better understanding the instabilities, droplet break-up and coalescence associated with the thermo-rheologically complex behavior of the phase-separated systems.

# REFERENCES

Aelmans, N. J. J. and V. M. C. Reid, "Shear-induced (de)mixing of SMA/PMMA blends at high shear rates", *Proceedings of the Fifth European Symposium on Polymer Blends*, Maastricht, The Netherlands, **1996**.

Baird, D.G.; Collias, D.I., *Polymer Processing Principles and Design*, Butterworth-Heinemann, Newton, MA 02158, **1995**.

Bates, F.S., "Polymer-Polymer Phase Behavior", *Science*, vol. 251, **1991**

Billmeyer Jr., F.W., *Textbook of Polymer Science*, Third edition, John Wiley & sons, NY, **1984**.

Binningto, R.J., Troup, G.J., Boger, D.V., A low cost laser-speckle photographic technique for velocity measurement in slow flows, J. Non-Newtonian Fluid Mech., 12, 255-267, **1983**.

Brannock, G. R., J. W. Barlow and . R. Paul, "Blends of styrene/maleic anhydrite Copolymers with polymethacrylates", *J. Polym. Sci.: Part B: Polym. Phys.*, **29**:413-429 **1991**.

Brochard, F.; de Gennes, P.G. *Macromolecules* 10, 1157, **1977**.

Brochard, F. *J.Phys.* (France), 44, 39, **1983**.

Cahn, J.W. *J. Chem. Phys.* 42, 93, **1965**.

Chen, Z. J., M. T. Shaw and R. A. Weiss, *Macromolecules*, **28**:648, **1995**.

Chopra, D.; Vlassopoulos, D.; Hatzikiriakos, S.G., *manuscript in preparation.*

Coleman, B.D., Noll, W.: Foundations of linear viscoelasticity. *Rev Mod. Phys.* 33, 239-249, **1961**.

Coleman, B.D., Markovitz, H: Normal stress effects in second-order fluids. *J.Appl. Phys.* 35, 1-9, **1964**.

Cong G, Huang Y, Mac Knight WJ, Karasz FE *Macromolecules* 19:2765, **1986**.

De Gennes, P. *Scaling Concepts in Polymer Physics* Cornell University Press, N.Y., **1979**.

Dealy, J.M. and K.F. Wissbrun, *Melt rheology and its role in plastics processing – theory and applications*, Van Nostrand Reinhold, New York , **1990**.

Doi, M. *Introduction to Polymer Physics* Oxford Science Publications, **1996**.

Fast, J.D. *"Entropy of Mixing of Polymer Solutions"*, **1968**

Strobl, G. *The Physics of Polymers*, 2nd Ed., Springer: Berlin, **1996.**

Feng, H., L. Shen and Z. Feng, "Miscibility of homopolymer/random copolymer blends – 2. SMA/PMMA blends", *Eur. Polym. J.*, **31**:243-247, **1995**.

Fernandez, M. L., J. S. Higgins, R. Horst and B. A. Wolf, *Polymer*, **36**:149, **1995**.

Ferry, J.D. *Viscoelastic properties of polymers*, 2nd ed. New York: Wiley **1970**.

Flory, P.J., Principles of Polymer Chemistry, Cornell Univ. Press, Ithaca, N.Y., **1953**.

Friedrich, C., C. Schwarzwalder and R.-E. Riemann, *Polymer*, **37**:2499-2507, **1996**.

Gross, B.: Mathematical structure of the theories of viscoelasticity. Paris: Herman et Cie. **1953**.

Hashimoto, T., K. Matsuzaka, E. Moses and A. Onuki, "String phase in phase-separating fluids under shear flow", *Phys. Rev. Lett.*, **74**:126-129, **1995**.

Hatzikiriakos, S. G. and J. M. Dealy, "Wall slip of molten high density polyethylenes II. Capillary rheometer studies", *J. Rheol.*, **36**: 703-741, **1992**.

Helfand, E.; Frederickson, G.H. *Phys. Rev. Lett.*, 62, 2468, **1989**.

Doi, M.; Onuki, A. *J. Phys. II.*, 59, 3423, **1990**.

Milner, S.T. *Phys. Rev. E*, 48, 3674, **1993**.

Hindawi, A., J. S. Higgins and R. A. Weiss, "Flow-induced mixing and demixing in a polymer blend", *Polymer*, **33**:2522-2530, **1992**.

Hobbie, E. K., A. I. Nakatani and C. C .Han, "Shear-induced mixing in polymer blends", *Modern Phys. Lett. B*, **8**:1143-1161, **1994**.

Hobbie, E.K.; Nakatani, A.I.; Han, C.C. *Modern Phys. Lett B*, 8, 1143, **1994**.

Horst, R; Wolf, B.A. *Macromolecules* **1992**, 25, 5291; **1993**, 26, 5676.

Horst, R; Wolf, B.A. *Polymer*, 38, 4697, **1997**.

Horst, R. *Macromol. Theory Simul.*, 4, 449, **1995**.

Jian, T.; Vlassopoulos, D.; Fytas, G.; Pakula, T.; Brown, *W. Colloid Polym. Sci.*, 274, 1033, **1996**.

Kammer HW, Inoue T, Ougizawa T *Polymer* 30:888, **1989**.

Kapnistos, M., A. Hinrichs, D. Vlassopoulos, S. H. Anastasiadis, A. Stammer and B. A. Wolf, *Macromolecules*, **29**:7155-7163, **1996a**.

Kapnistos, M., D. Vlassopoulos and S. H. Anastasiadis, *Europhys. Lett.*, **34**:513-518 **1996b**.

Kapnistos, M., Vlassopoulos, D., Anastasiadis, S.H., *Europhys. Lett.*, 34 (7), **1996**.

Karatasos, K., G. Vlachos, D. Vlassopoulos, G. Fytas, G. Meier and A. DuChesne, *J. Chem. Phys.*, **108**:2028-2037, **1998**.

Katsaros, J.D., M.F. Malone and H. H. Winter, "The effects of flow on miscibility in a blend of polystyrene and poly (vinyl methyl ether)", *Polym. Eng. Sci.*, **29**:1434-1445 **1989**.

Kazatchkov, I. B., S.G. Hatzikiriakos, and C.W. Stewart "Extrudate distortion in the capillary / slit extrusion of a molten polypropylene," *Polym. Eng. Sci.*, **35**: 1864-1871 **1995**.

Kim, s., E. K. Hobbie, J-W. Yu and C. C. Han, "Droplet breakup and shear-induced mixing in critical polymer blends", *Macromolecules*, **30**:8245-8253, **1997**.

Krämer-Lucas, H.; Schenk, H.; Wolf, B.A; *Makromol. Chem.*, 189, 1613; 189, 1627, **1988**.

Kumar, S. K., R. H. Colby, S. H. Anastasiadis and G. Fytas, *J. Chem. Phys.*, **105**:3777-3788, **1996**.

Kume, T.; Hashimoto, T.; Takahashi, T.; Fuller G.G. *Macromolecules,* 30, 7232, **1997**.

Larson, R,G., "Flow induced mixing, demixing, and phase transitions in polymeric fluids", *Rheol. Acta*, **31**:497-520, **1992**.

Mani, s., M.F. Malone and H. H. Winter, "Shear-induced demixing in a polystyrene / poly (vinyl methyl ether) blend: In-situ fluorescence and rheometry", *Macromolecules*, **25**:5671-5676, **1992**.

Marrucci, G. *Trans. Soc. Rheol.* 16:2, 321-330, **1972**.

Meier, G., D. Vlassopoulos and G. Fytas *Europhys. Lett.*, **30**:325-330, **1998**.

Nakatani, A.I.; Kim, H.; Takahashi, Y.; Matsushita, Y.; Takano, A.; Bauer, B.J.; Han, C.C., J. *Chem. Phys.*, 93, 795, **1990**.

Olabisi O., Robeson L.M., and Shaw M.T. *Polymer-Polymer miscibility*, Academic Press, NY, 1979

Onuki, A., *Int. J. Thermophys.*, 10: 293-308, **1989**.

Ougizawa T, Inoue, T., Kammer, H.W., *Macromolecules* 18:2089, **1985**.

Ougizawa T, Inoue, T., *Polymer J* (Tokyo) 19:405, **1986**.

Polios, I. S., M. Soliman, C. Lee, S. P. Guido, K. Schmidt-Rohr and H. H. Winter, *Macromolecules*, **30**:4470-4480, **1997**.

Rangel-Nafaile, C.; Metzner, A.B.; Wissbrun, K.F. *Macromolecules* 17, 1187, **1984**.

Remediakis, N. G., R. A. Weiss and M. T. Shaw, *Rubber Chem. & Techn.*, **70**:71 **1997**.

Saito, H., Fujita, Y., Inoue, T., *Polymer J* (Tokyo) 18:521, **1987**.

Schmidt, J.R.; Wolf, B.A. *Colloid Polym. Sci.* 257, 1188, **1979**.

Schwahn, D. Chapter II, Polymer Blends and Phase separation, Neutron and Synchrotron Radiation for Condensed Matter Studies Volume III, Springer-Verlag NY, **1994**.

Silberberg, A; Kuhn, W. *J. Polym. Sci.: Polym. Phys.* **1954**, 13, 21

Silberberg, A.; Kuhn W. *Nature* 170, 450, **1952**.

Soontaranun, W., J. S. Higgins and T.D. Papathanasiou, "Shear flow and the phase behavior of polymer blends", *Fluid Phase Equilibria*, **121**:273-292 , **1996a**.

Soontaranun, W., J. S. Higgins and T.D. Papathanasiou, "Rheology and thermodynamics in partially miscible polymer blends", *J. Non-Newtonian Fluid Mech.*, **67**:191-212, **1996b**.

Sun, T.; Balazs, A.C.; Jasnow, D. *"Dynamics of phase behavior of a polymer blend under shear flow"*. Paper S*.4 presented at the General Meeting of the American Physical Society, Los Angeles, CA, March **1998**.

Takebe, T., R. sawaoka and T. Hashimoto, "Shear-induced homogenization of semidilute solution of polymer mixture and unmixing after cessation of the shear", *J. Chem. Phys.*, 91:4369-4379.

Tanner, R. I., *Engineering Rheology*, Oxford University Press, Oxford, **1985**.

Tompa, H., Trans. Faraday Soc., 45, 1142, **1949**.

Utracki, L. A., Polymer Alloys and Blends. Thermodynamics and Rheology, Hanser, New York **1990**.

van Egmond, J.W.; Fuller, G.G. *Macromolecules*, 26, 7182, **1993**.

van Egmond, J.W. *Macromolecules*, 30, 8045, **1997**.

Vinckier, I., P. Moldenaers and J. Mewis, "Relationship between rheology and morphology in model blends in steady shear flow", *J. Rheol.*, **40**:613-631, **1996**.

Vlassopoulos, D. *Rheol. Acta*, **35**:556-566, **1996**.

Vlassopoulos, D., A. Koumoutsakos, S. H. Anastasiadis, S. G. Hatzikiriakos and P. Englezos, *J. Rheol.*, **41**:739-755, **1997**.

Vrahopoulou-Gilbert E.; McHugh, A. J. *Macromolecules*, 17, 2657, **1984**.

Williams, M.L.; Landel, R.F.; Ferry, J.D., "The temperature dependence of Relaxation Mechanisms in Amorphous Polymers and other Glass-Forming Liquids", *J. Am. Chem. Soc.* 77, 3701-3707, **1955**.

Wolf, B.A. *Macromol. Chem. Rapid Commun.* 1, 231, **1980**.

Wolf, B.A. *Macromolecules* 17, 615, **1984**.

Wolf, B. A. *Macromolecules* 29,7155, **1996**.

Wu, X.L.; Pine, D.J.; Dixon, P.K. *Phys. Rev. Lett.* 66, 2408, **1991**.

Yanase, H.; Moldenaers, P; Abetz, V.; van Egmond, J.W.; Fuller G.G. *Rheol. Acta* 30, 89, **1991**.

# NOTATION

| | |
|---|---|
| $a_T$ | shift factor |
| $b$ | Rabinowitsch correction |
| $D$ | capillary diameter, m |
| $g_i$ | Degree of polymerization of polymer in a solution or polymers in a blend (i = 1,2) |
| G' | elastic modulus, Pa |
| $L$ | capillary or slit length, m |
| $M_i$ | molecular weight of the components in polymer solution or blend (i = 1,2), kg/kmol |
| $n_i$ | moles of component i in the polymer solution or blend |
| $N$ | total number of cells in the lattice |
| $N_0$ | Avogadro's number |
| $N_1$ | first normal stress difference, Pa |
| $P_d$ | driving pressure, Pa |
| $P_{end}$ | Bagley correction, Pa |
| $Q$ | volumetric flow rate, $m^3/s$ |
| $r$ | ratio of molar volume of polymer to the molar volume of solvent |
| $R$ | capillary radius, m |
| $T$ | absolute temperature, K |
| $T_c$ | critical temperature, K |
| $T_g$ | glass transition temperature, K |
| $u$ | melt velocity, m/s |
| $V$ | segment volume, $m^3$ |
| $v$ | volume of a cell in the lattice, $m^3$ |

$\underline{w_i}$ weight vector for cell *i*

$w_{vi}$ velocity corrected weight vector for cell *i*

$w$ lumped weighting factor

**Greek Letters**

$\chi_{ij}$ interaction parameter

$\Delta E$ change in the internal energy of the system, J

$\Delta G_m$ molar Gibbs energy of mixing, J

$\Delta H_M$ enthalpy of mixing, J

$\Delta S_C$ combinatorial entropy of mixing, J/K

$\Delta S_{NC}$ non-combinatorial entropy of mixing, J/K

$\dot{\gamma}_A$ apparent shear rate, $s^{-1}$

$\dot{\gamma}_w$ wall shear rate, $s^{-1}$

$\eta$ viscosity, Pa · s

$\eta_0$ zero-shear viscosity, Pa · s

$\phi_c$ critical concentration

$\phi_i$ volume fraction of the components of the polymer solution or blend (i = 1, 2)

$\rho$ polymer density, $kg/m^3$

$\sigma_w$ wall shear stress, MPa

$\Omega_{12}$ total number of configurations in the absence of shear

$\Omega^*_{12}$ total number of configurations in the presence of shear

$\Omega$ multiplicity of the system